A STATIC MODEL OF DIRECT AND TRANSVERSE IMPACT MODULATORS

By

SILAS KATZ

Bachelor of Mechanical Engineering
City College of New York
New York, New York
1949

Master of Science
University of Maryland
College Park, Maryland
1957

Submitted to the Faculty of the Graduate College
of the Oklahoma State University
in partial fulfillment of the requirements
for the Degree of
DOCTOR OF PHILOSOPHY
July, 1970

A STATIC MODEL OF DIRECT AND TRANSVERSE IMPACT MODULATORS

Thesis Approved:

Karl N. Reid
Thesis Adviser

William A. Iiederman, Jr.

Don F Kincannon

Ladislaus J Fila

D. Durham
Dean of the Graduate College

ACKNOWLEDGEMENTS

I would like to express my appreciation for the help given me by the following people:

Professor Karl N. Reid, my thesis adviser, who began it all by friendly persuasion and then devoted so much of his time assisting me along the way. His stimulation and counsel was invaluable.

Professors L. J. Fila, Don F. Kincannon, and William G. Tiederman, the members of my committee, whose suggestions and criticisms guided me throughout the program. Their patience, interest, and cooperation was a great help to me.

Mr. Joseph M. Kirshner, Chief, Fluidics Research Branch, Harry Diamond Laboratories, who shared with me some of his physical insight and extraordinary knowledge.

Mr. Fred Ravilious, Research Physicist, Fluidics Research Branch, Harry Diamond Laboratories, who assisted me with the mathematical formulation of the superposition integral.

I would also like to acknowledge the following organizations:

The Harry Diamond Laboratories, Department of the Army, for providing me with a full time fellowship for the 1967-68 school year.

The National Science Foundation for its support (under GU-3160) of the Center for Systems Science which funded the research phase of my doctoral program.

In addition, I would like to thank Velda Davis, Margaret Estes, and Marilynn Bond for their typing excellence and advice.

Finally I want to thank Estella for devotion above and beyond the call of marital duty, my children, Joan and Eliot, for the many sacrifices they have made, and my father for his encouragement.

TABLE OF CONTENTS

LIST OF TABLES

LIST OF FIGURES

NOMENCLATURE

A	Throat Area, $in.^2$
A_{ca}	Area of annular auxiliary nozzle, $in.^2$
A_{ct}	Area of transverse auxiliary nozzle, $in.^2$
A_e	Area of emitter or primary nozzle, $in.^2$
C	Decay factor
C_e	Corrected decay factor
C_f	Decay factor change due to feedback
C_p	Decay factor for jet impinging on flat plate
D	Source and emitter nozzle diameter, in.
D_a	Diameter of annular control nozzle, in.
D_c	Diameter of transverse control nozzle, in.
D_r	Reference diameter, in.
E	Parameter equal to $4C^2 X^2/D^2$
$f(r)$	Velocity profile function, $in.^{-2}$
G_p	Pressure gain
G_{pa}	Annular modulator pressure gain
G_{pe}	Emitter modulator pressure gain
G_{pt}	Transverse modulator pressure gain
H	Distance from impingement surface to end of free jet region, in.
K	Scale factor, $in.^{-2}$
K_a	Annular modulation constant
K_f	Feedback constant
K_s	Shape constant

K_t	Transverse modulation constant
K_q	Flow constant
K_x	Constant in general
L	Nozzle spacing, in.
P	Centerline total pressure, psig
P_a	Atmospheric pressure, psig
P_{ca}	Annular control total pressure, psig
P_{ct}	Transverse control total pressure, psig
P_e	Emitter total pressure, psig
P_n	Nozzle chamber total pressure, psig
P_o	Output total pressure, psig
P_p	Centerline total pressure on flat plate, psig
P_s	Source total pressure, psig
Q_m	Maximum source flow, scfm
Q_s	Modulated source flow, scfm
r	Radial dimension, in.
R	Nozzle radius, in.
S	Setback, in.
S_K^G	Sensitivity
u(X,r)	Instantaneous velocity in axial direction, ft/sec.
$\overline{u^2}$	Time average of the square of the instantaneous axial velocity, ft^2/sec^2
u_{ca}	Initial annular velocity, ft/sec.
u'	Velocity fluctuation in axial direction, ft/sec.
U_c	Centerline velocity, ft/sec.
U_o	Initial velocity at nozzle exit, ft/sec.
v'	Velocity fluctuation in transverse direction, ft/sec.

X	Axial dimension, in.
X_p	Axial distance to impingement surface, in.
Z	Axial dimension from source nozzle, in.
$Z(O)$	Centerline distance from source nozzle to streamsurface, in.
$Z(R)$	Curtain distance from source nozzle to streamsurface, in.
α	Dummy variable, in.
δ	Boundary layer thickness, in.
$\theta(\alpha,r)$	Angle of equal contribution, radians
ρ	Fluid density, $lbf\text{-}sec^2/in^4$
φ	Displacement angle, degrees
β	Oblique angle, degrees
$\Lambda(x)$	Proportionality parameter-momentum transfer length, in.

Subscripts for Bracketed Variables

a	Annular modulation
b	Boundary layer
e	Emitter modulation
i	Infinitesimal hold
t	Transverse modulation
ea	Emitter in the annular modulator with $P_{ca} = 0$
et	Emitter in the transverse modulator with $P_{ct} = 0$

CHAPTER I

INTRODUCTION

In 1959, the announcement of fluid control components, without mechanical moving parts, focused attention on a promising new area for research. These components produced signal amplification through the interaction of jets or the flow field changes caused by walls in proximity to jets. The components became known as fluid amplifiers or "fluidic" devices. Since 1959, many different types of proportional and digital fluid amplifiers have been developed.

The impact modulator is a type of fluid amplifier with high pressure gain in proportional operation and large fan-out capability in digital operation. Although experimental input-output characteristics are established for particular geometries, there have not been any analytical descriptions of impact modulators. The objective of this investigation is to provide an analytical model for the static performance of impact modulators.

The Impact Modulator

Figure 1 shows a schematic drawing of the impact modulator. Two round nozzles, an 'emitter' and a 'source,' are on a common axis. An annular output chamber surrounds the source nozzle. Under normal conditions of operation, jet flow from the emitter totally or partially blocks flow from the source. Modulation or control of the emitter jet

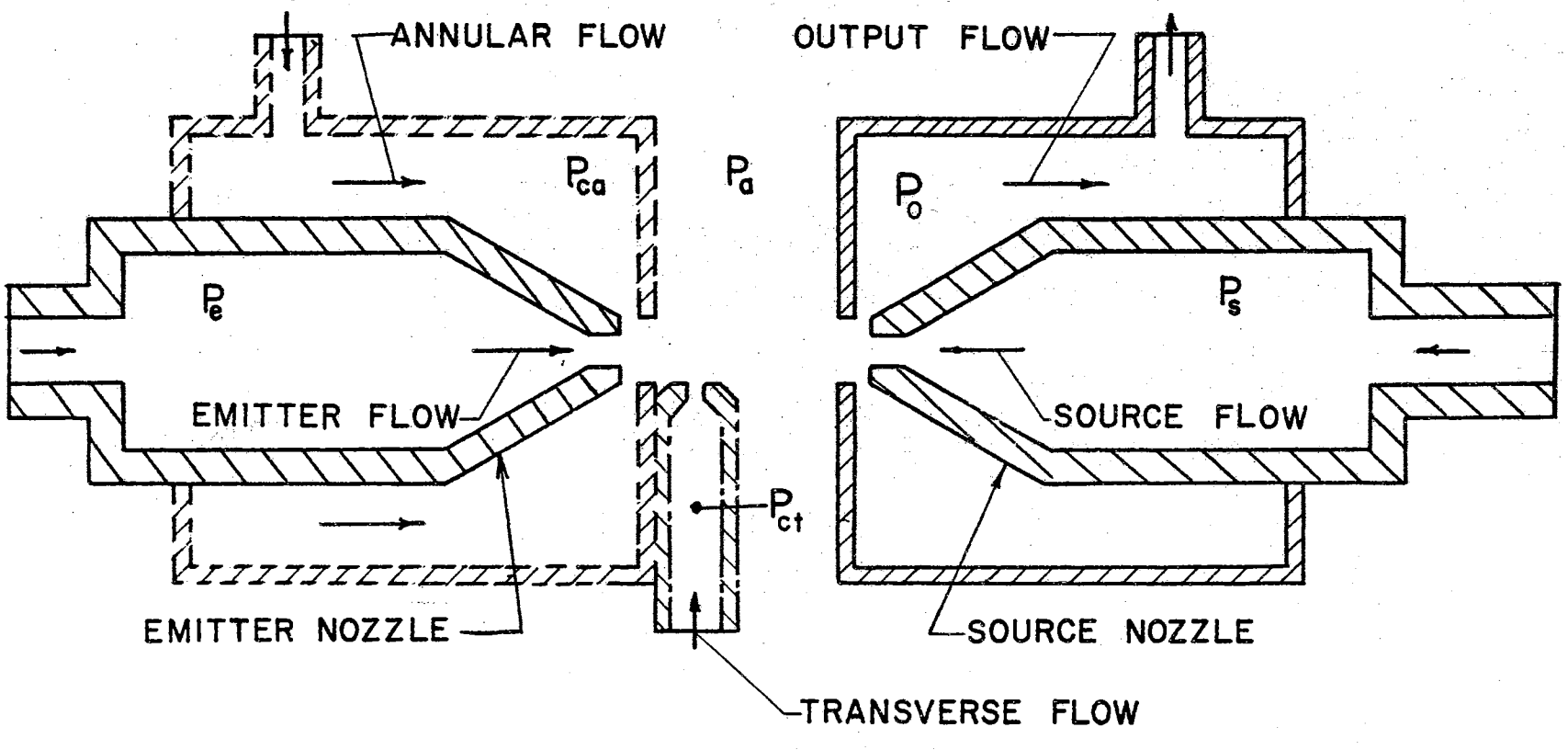

IMPACT MODULATOR

Figure 1. Impact Modulator Schematic

may occur in one of three ways:

1. By changing the emitter flow --- emitter modulation (direct).
2. By introducing flow into an annular chamber surrounding the emitter nozzle (dashed lines in Figure 1) --- annular modulation (direct).
3. By introducing flow into a transverse control nozzle (dot-dash lines in Figure 1) --- transverse modulation.

In the absence of control flow, the flow field is similar to that of coaxial opposing jets, except that the impact region is in close proximity to the source nozzle exit plane. The addition of control flow alters the characteristics of the emitter jet and causes the impact position to move slightly towards or away from the source. As a consequence, the pressure in the output chamber (P_o) increases or decreases. Since the output pressure change normally exceeds the control pressure change, the device is an amplifier. The pressure gain is defined as the ratio of the change in output total pressure to the change in control total pressure.

Previous Work

Direct and transverse impact modulators were introduced in 1964. Bjornsen (1) provided a qualitative description and experimental results. Lechner and Sorenson (2) considered impedance matching and cascading techniques. Both of these papers emphasized the characteristics of complete devices. Misevich (3) introduced an empirical model for the balance position of axisymmetric impacting jets. The basis of the model was some centerline decay experiments on 0.007, 0.016, and 0.025 in. diameter jets. Subsequently the jet balance position was

calculated by equating the "average" total pressure of the opposing jets. In this case the average was taken over the area of the nozzles. Katz (4) found the balance point from a force balance on a round disk the size of the nozzles. The disk position then determined the pressure gain for emitter modulation. Desai and McGregor (5) performed a parametric study of annular impact modulators. Their experimental device produced pressure gains which were two orders of magnitude lower than the values given by Bjornsen (1) and Lechner and Sorenson (2). Fenger (6) presented an inviscid analysis of coaxial impacting jets. The results were, to some extent, in agreement with experimental data.

Statement of the Problem

In general, most of the previous work considers the complete impact modulator as a 'black box' or concentrates on the impact of axisymmetric jets. The black box approach is a very useful practical method. However, it does not indicate the internal flow processes and is time consuming. On the other hand, the study of impacting jets alone provides no information about the modeling of impact modulators. One reason for this is that the actual modulator operates with one jet and one obstructed flow rather than with two impacting jets.

The purposes of this thesis are therefore:

1. To identify the basic fluid flow processes that occur within impact modulators.
2. To indicate the important parameters that underly modulator static performance.
3. To develop a generalized static model that can be used to predict input-output characteristics.

Treatment of the Problem

The flow phenomena in impact modulators is too complex to solve from first principles. Therefore, separation of the phenomena into distinct flow processes that are amenable to analysis or to simple experiment is necessary. In this investigation the selected processes are:

1. Modulation of emitter jet by control jet.
2. Submerged jet impinging on the streamsurface.
3. Source flow modulation.
4. Conversion of energy (breakdown of source total pressure into static and dynamic pressures).

The initial process (No. 1) is a function of the input signal and the final process (No. 4) relates to the output signal. The position and shape of a hypothetical dividing streamsurface within the modulator provides the connection between Processes No. 2 and No. 3.

Initially, each process is described in functional form. Then, empirical expressions, determined from experiment and analysis, replace the function forms. Finally the expressions taken together yield the input-output characteristics of impact modulators.

Results

A static model for predicting the input-output characteristics of direct and transverse impact modulators is developed. The input-output characteristics depend on eight distinct parameters. The most sensitive parameters are the nozzle spacing and the rate of jet centerline decay. Experimental data are presented for two large-scale impact modulators. The results show that the pressure gain varies with the operating

point. The pressure gain is highest when the output pressure is near mid-range ($P_o/P_s \approx 0.5$). The average experimental pressure gain throughout the linear operating range ($0.2 \leq P_o/P_s \leq 0.8$) is within 25 per cent of the gain predicted by the model.

The model consists of four distinct flow processes and their interconnections. A description of one of these processes requires the continuous characterization of an axisymmetric turbulent jet throughout the transition and fully developed regions. An analytical formulation is presented here to provide this description. The analysis, based on Reichardt's theory of turbulence (7) and the superposition principle, allows the introduction of any arbitrary nozzle exit velocity profile. Experimental jet data are presented to verify the adequacy of the analytical formulation with and without auxiliary flows superimposed on the primary jet flow. The results of the analysis are also applied to the case of a jet impinging on a flat plate.

Turbulence intensity measurements are presented for a jet with auxiliary flows. A small annular auxiliary flow, reduces the axial turbulence intensity in the jet two or more nozzle diameters downstream. As a consequence, there is a decrease in jet spread. When the annular flow exceeds one third of the primary flow the downstream turbulence intensity is increased. In the case of transverse auxiliary flow the turbulence intensity of the control jet appears to supplement the turbulence intensity of the primary jet. The result is an increase in the turbulence intensity downstream and an increase in jet spread.

CHAPTER II

FORMULATION OF THE PROBLEM

The problem is the development of a model to predict the input-output characteristics of impact modulators. The structure of the model should consist of a set of logically connected fundamental processes that are amenable to analysis or simple experiment.

Basic Concepts

To provide the logical separation of fundamental processes, the concept of a "dividing streamsurface" is adopted. The dividing streamsurface is an apparent barrier that separates emitter flow from source flow. Two hypothetical dividing streamsurfaces are shown in Figure 2 for the extreme operating conditions of an impact modulator. At the "beginning of flow modulation" (Figure 2a), the source flow is not restricted by the dividing streamsurface. In this condition, the source flow is independent of emitter flow. An appropriate change in control signal moves the dividing streamsurface towards the source and causes a reduction of source flow. In the limiting condition, the streamsurface comes into contact with the source nozzle and the source flow is "cutoff" (Figure 2b). At this condition, a portion of the dividing streamsurface is concave and lies within the source nozzle. The concave curvature is necessary at cutoff so that the radial static pressure distribution along the concave portion of the streamsurface

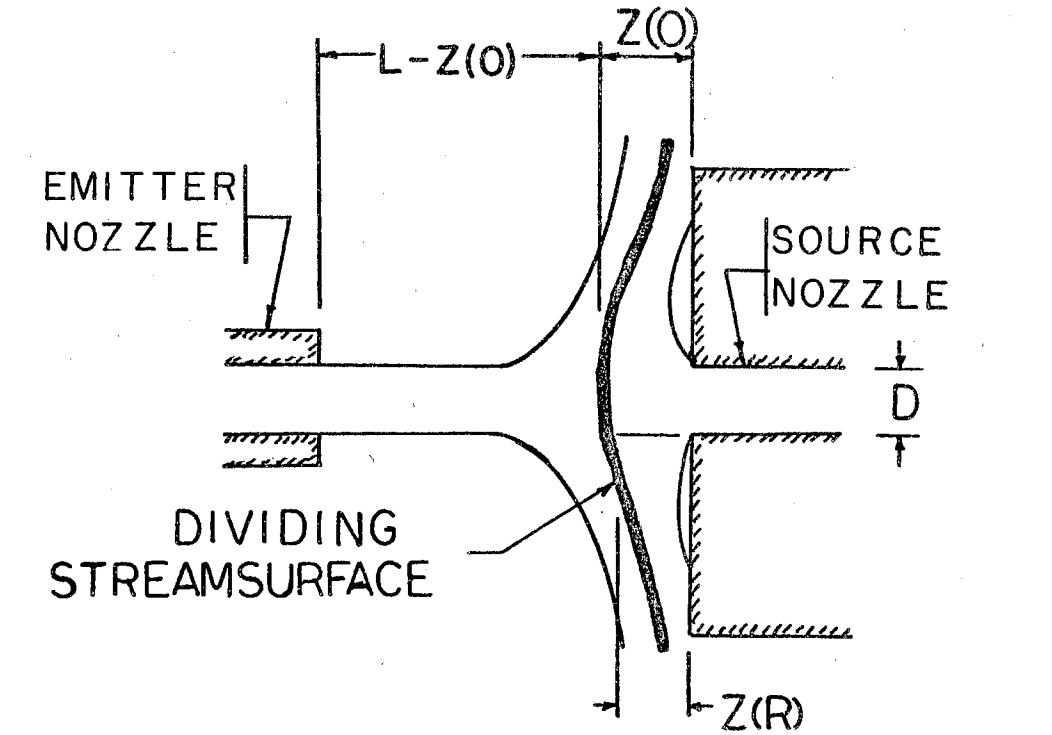

a) BEGINNING OF FLOW MODULATION

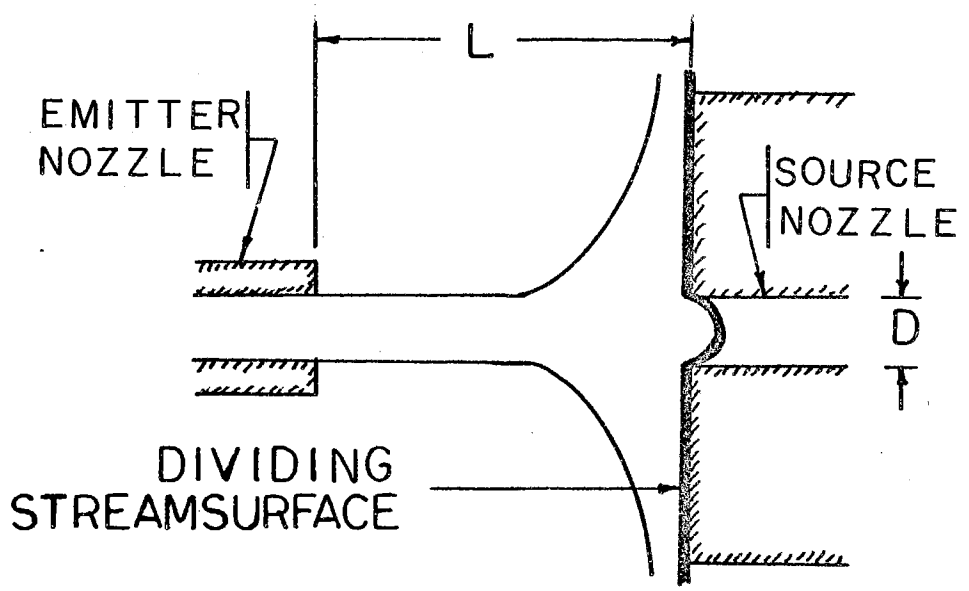

b) CUTOFF

Figure 2. Hypothetical Representation of Dividing Streamsurface

will balance the uniform pressure of the source. An infinite number of operating conditions exist between the beginning of flow modulation and cutoff. There is a different streamsurface shape and position for each operating condition. Thus, the streamsurface controls the impact modulator source flow similar to the way a flapper controls a flapper-nozzle flow. For this reason, the position and shape of the dividing streamsurface are important factors in an impact modulator model. To reduce complexity, the streamsurface is represented by only the centerline and curtain distances from the source nozzle (Z(O) and Z(R), respectively).

The centerline distance, Z(O), is colinear with the stagnation streamline and can be approximated from a centerline total pressure balance. Figure 3 shows the concept of a centerline pressure balance schematically. The centerline total pressure distributions for the emitter and source jets (measured separately) are superimposed. Since the jets (spaced a distance, L, apart) oppose each other, the slopes of the centerline pressure distributions have an opposite sign. A balance point occurs at the point of intersection or where the pressures are equal. In the operating region the balance point is close to the source nozzle. Thus, the source total pressure is equal to the balance point total pressure in a typical modulator. Since the centerline total pressure distribution depends on the streamsurface shape, the value of Z(O) determined from probe or flat plate centerline data is only a first approximation.

The curtain distance, Z(R), is determined experimentally since it is difficult to approximate without a knowledge of the streamsurface

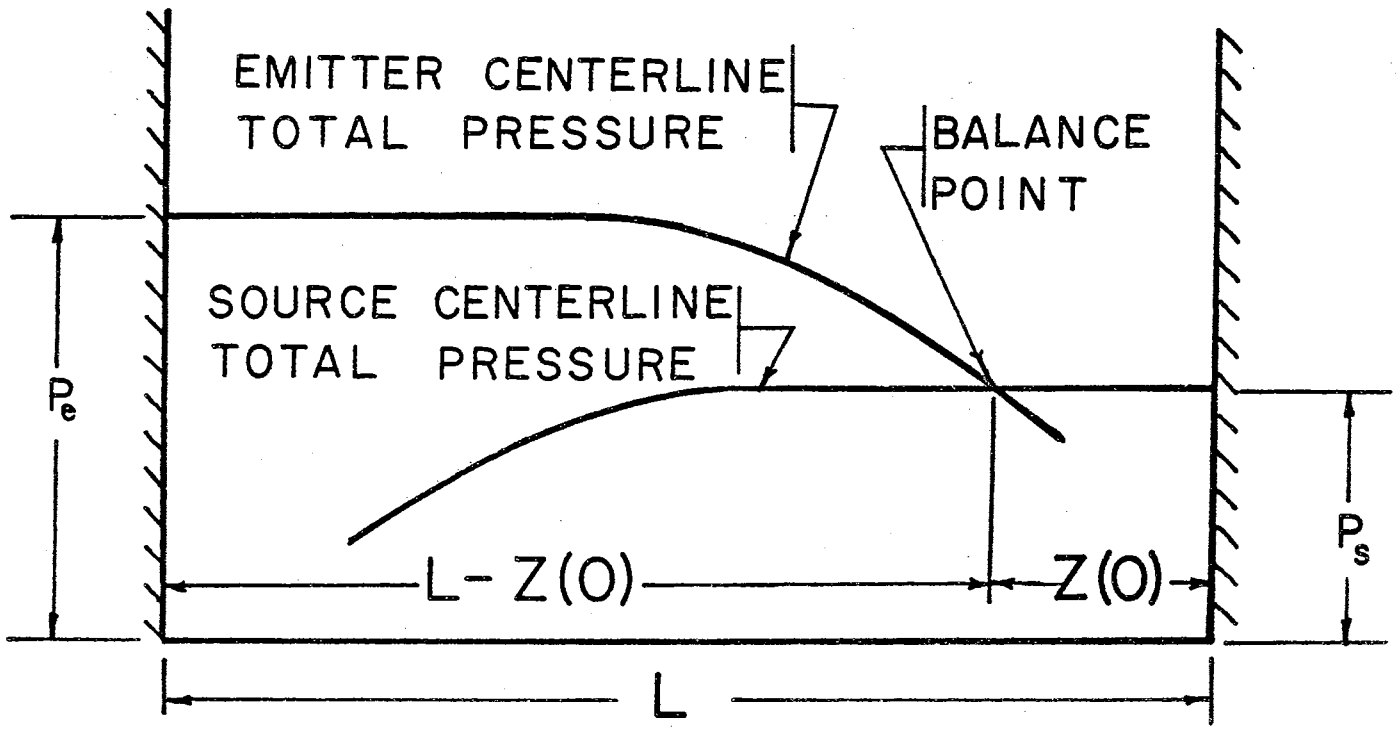

Figure 3. Superposition of Centerline Total Pressure Distributions

curvature. This distance is important in the impact modulator because it defines the area that controls the source flow.

Fundamental Processes

Figure 4 illustrates a convenient separation of the fundamental flow processes which govern impact modulators. These processes are:

1. Emitter Jet Modulation. Control jets act on the emitter jet in a region near the emitter nozzle exit.
2. Impinging Jet Flow. The modulated emitter jet passes into a zone of free shear flow and then impinges on the dividing streamsurface.
3. Source Flow Modulation. The dividing streamsurface regulates the source flow.
4. Energy Conversion. The output pressure signal is the static pressure portion of the source total pressure near the exit of the source nozzle. In effect, the modulating signal at the input of the impact modulator changes the proportion of dynamic and static source pressure that exists at the output position.

The position and shape of the dividing streamsurface provide the connection between the impinging jet (Process No. 2) and the source flow modulation (Process No. 3).

Assumptions

In the course of this investigation the following assumptions are made:

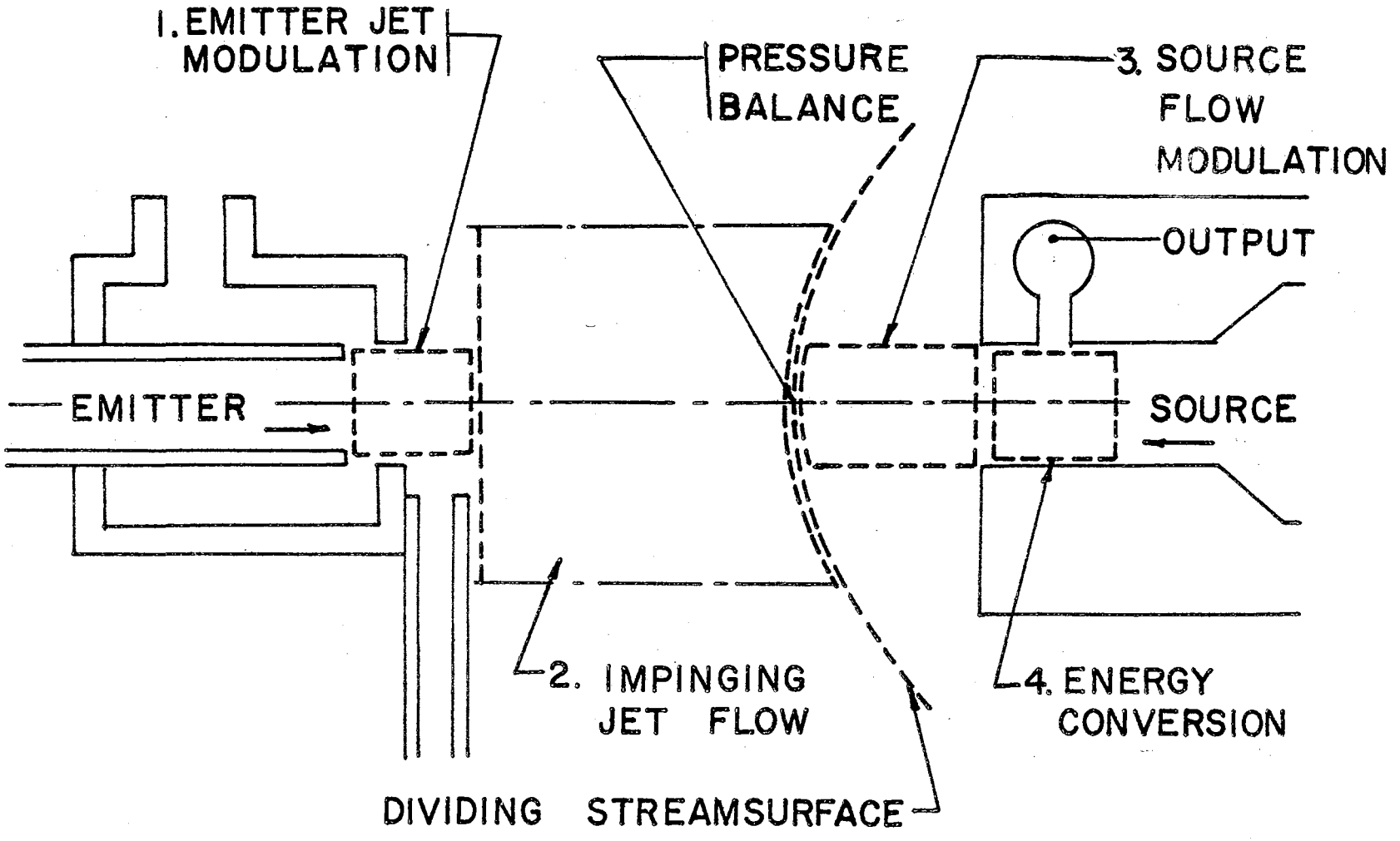

Figure 4. Fundamental Processes

1. The predominant effect of annular or transverse control flow is to alter the turbulence intensity in the axial direction. (Appendix A shows that the effect of jet deflection is negligible).
2. The impinging jet flow process is describable by the free jet analysis method of Alexander, Baron, and Comings (9), with a suitable change in the method of determining the single experimental constant which accounts for the jet spread (jet decay factor).
3. The centerline position, Z(O), is calculable from a centerline total pressure balance when the centerline total pressure distribution is corrected to account for the shape of the streamsurface.
4. The correction to the centerline total pressure distribution depends on nozzle spacing, streamsurface shape and the centerline total pressure distribution as measured on a flat plate.
5. The curtain position Z(R) is only a function of the centerline position, Z(O).
6. The controlling area for source flow is the curtain area, $\pi DZ(R)$.
7. The flow within the source nozzle is inviscid and Bernoulli's equation applies.
8. The source flow emanates from a zero impedance supply.
9. The flow is incompressible.
10. The output chamber is equivalent to a static pressure tap at the source nozzle exit.

11. The output flow (see Figure 1) is zero; this condition is referred to as "blocked load."

The Model

The conceptual model in Figure 5 illustrates the assumed relations between the flow processes. The control signals (entering on the left side of Figure 5) alter the turbulence intensity of the emitter jet and, in turn, change the centerline total pressure distribution. This distribution, which is assumed to depend on the streamsurface shape, is represented by a jet spread or jet decay factor. Since the position and shape of the actual dividing streamsurface change with operating point, a quantitative description is difficult. In the proposed model, a flat plate represents the initial shape of the dividing streamsurface and a flat plate decay factor, C_p, represents the initial centerline total pressure distribution. A centerline total pressure balance (using C_p) determines an approximate centerline position. The actual streamsurface centerline depends on the streamsurface shape which, in general, is not flat. A feedback circuit corrects the approximate decay factor (C_p) and produces an effective decay factor ($C_e = C_p + C_f$). The input to the feedback circuit is the plate decay factor, C_p, and the output is the corrected streamsurface curtain position, Z(R). In the next process, the curtain position determines the source flow (source flow modulation on Figure 5). To complete the model the source flow controls the magnitude of the output pressure signal (Energy conversion on Figure 5).

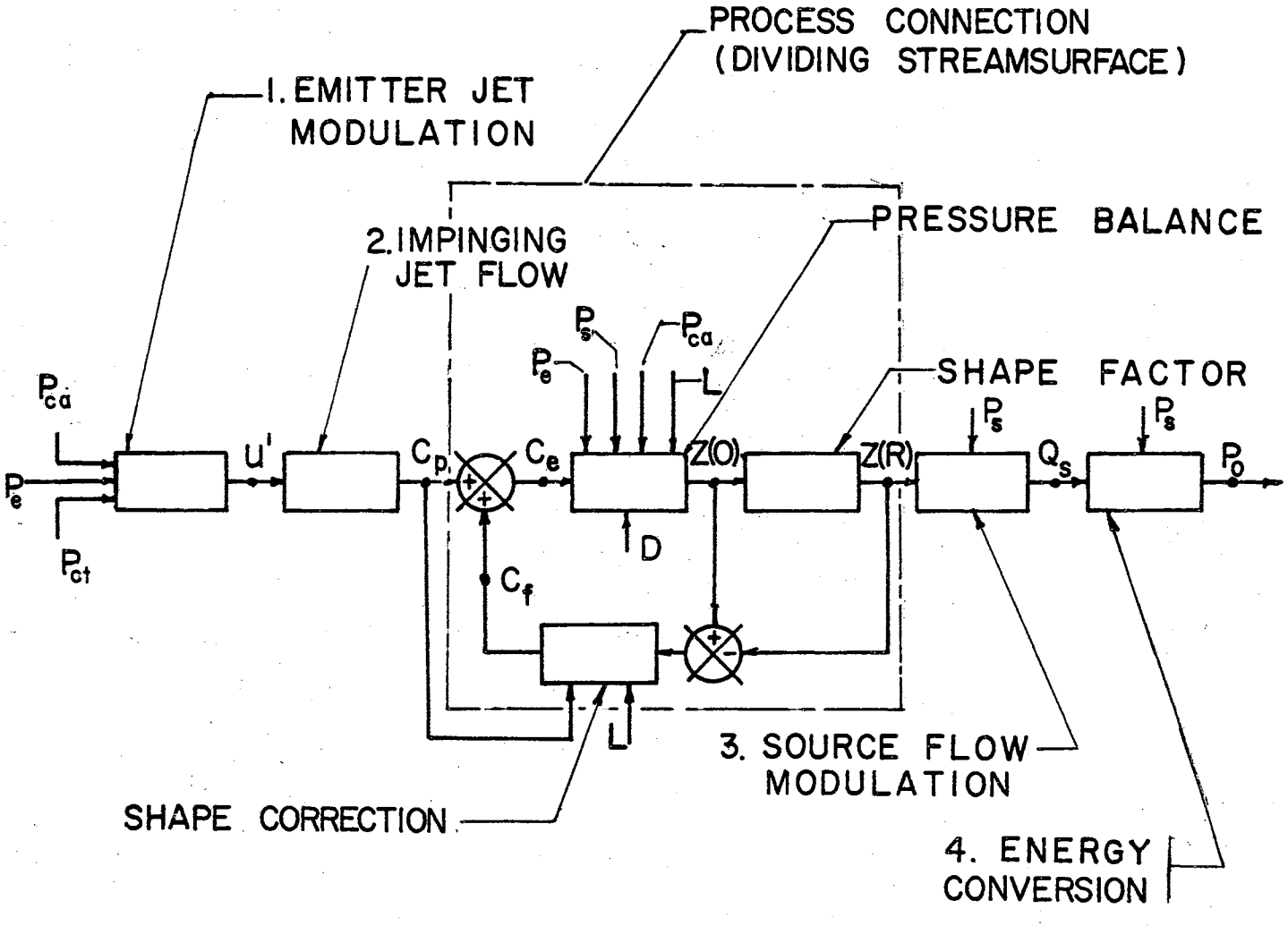

Figure 5. Conceptual Model

Functional Relations

Functional relations for each portion of the model are presented below.

Emitter Jet Modulation and Impinging Jet Flow

For convenience, fundamental processes No. 1 and No. 2 are combined into a single functional relation between control pressure signal and the jet decay factor as determined from flat plate measurements. In functional form (see Assumption No. 1) this is:

$$C_p = C_p \left[P_e, P_{ca}, P_{ct}, \text{geometry}\right] \tag{1}$$

where P_e, P_{ca}, and P_{ct} are the control pressures for emitter, annular, and transverse modulation, respectively.

Streamsurface Centerline Position

The location of the stream surface on the jet centerline occurs where the total pressure in the emitter jet equals the source pressure (Figure 3); this is the balance point. From Assumption No. 3, the centerline position is:

$$Z(0) = Z(0) \left[P_e, P_{ca}, P_s, C_e, \text{geometry}\right] \tag{2}$$

where C_e is the corrected decay factor. The transverse control pressure does not appear in Equation (2) since the emitter deflection is small (typically < 2 degrees -- see Appendix A) and no momentum is added in the axial direction by the transverse control flow.

Streamsurface Shape

In this investigation, two points on the streamsurface (the curtain position and the centerline position) represent the streamsurface shape. From Assumption No. 5, the dividing streamsurface shape has the form:

$$Z(R) = Z(R)\ [Z(0)] \tag{3}$$

Source Flow Modulation

The source flow depends on the geometry of the source nozzle, the curtain distance (Assumption No. 6) and the source pressure. The impedance of the supply to the source chamber is not considered here (Assumption No. 8). Thus, the relation for the source flow is:

$$Q_s = Q_s\ [P_s,\ Z(R),\ \text{geometry}] \tag{4}$$

Energy Conversion

The total pressure at the output is the static pressure portion of the source total pressure. From Assumptions Nos. 7 and 11, the functional form is:

$$P_O = P_O\ [Q_s,\ P_s,\ \text{geometry}] \tag{5}$$

Shape Correction

The feedback decay factor, C_f, provides a correction to the flat plate decay factor, C_p; C_f depends on the nozzle spacing, streamsurface shape, and the plate decay factor (Assumption No. 4). Thus:

$$C_f = C_f\ [(Z(0) - Z(R)),\ L,\ C_p] \tag{6}$$

where the difference between the centerline and curtain distances represent the streamsurface shape.

The Proposed Investigation

Four fundamental flow processes separate the impact modulator into distinct units. The processes, connected by the dividing streamsurface and an associated feedback circuit, form a conceptual model of impact modulators. The functional relations of the previous section follow directly from the conceptual model and a set of assumptions.

The objective of the presentations in Chapters III to VI is to find empirical relations for the functional forms given in Equations (1) through (6). A reference back to the appropriate functional form follows the derivation of each empirical relation.

In later chapters (Chapters VII and VIII), the empirical expressions are combined to indicate the input-output characteristics and the pressure gains of emitter, annular, and transverse impact modulators. The model indicates the relative importance of operational and geometrical parameters.

CHAPTER III

THE AXISYMMETRIC FREE JET

The conceptual model for impact modulators requires the time-average characteristics of impinging axisymmetric turbulent jets. To obtain these characteristics, expressions are derived in this chapter for the free jet. Then, in the following chapter, the expressions are modified to apply to impinging jets.

Free jets have been the subject of a large number of investigations. In this chapter, only a few directly applicable papers are cited.

Goertler (7) provides a similarity solution that describes the free turbulent jet in the fully developed region. Albertson et al. (8) separate the free jet flow field into a "zone of flow establishment" and a "zone of established flow." This formulation does not account for the continuous transition from one zone to the other. An analytical formulation for the entire flow field is derived by Alexander, Baron, and Comings (9) for axisymmetric jets and by Kirshner (10) for two-dimensional jets. These latter papers linearize the equations of motion with Reichardt's turbulence hypothesis and then apply the superposition principle. This is the method followed here.

Free Jet Analysis

Alexander, Baron, and Comings (9) present axial velocity profiles determined both analytically and experimentally for the axisymmetric turbulent jet. This investigation presents a detailed development of an expression for the axial velocity as a function of x and r. The results are equivalent to those of Alexander et al.

The inductive theory of Reichardt (11) and the equation of motion combine to yield:

$$\frac{\partial(\overline{u^2})}{\partial X} = \Lambda(X)\left[\frac{\partial^2(\overline{u^2})}{\partial r^2} + \frac{1}{r}\frac{\partial(\overline{u^2})}{\partial r}\right] \tag{7}$$

where $\Lambda(X)$ is a proportionality parameter called the momentum transfer length. If $\Lambda(X) = C^2X/2$, a solution of Equation (7) has the form assumed by Albertson et al. (8); that is:

$$[\overline{u^2}(X,r)]_i = \frac{U_o^2 D_r^2}{4C^2X^2}\exp\left[-r^2/C^2X^2\right] \tag{8}$$

where the subscript $\underline{i}$ refers to flow originating from an infinitesimal hole, C is an experimentally determined constant, U_o is a reference velocity and D_r is a reference diameter. Since Equation (7) is a linear differential equation in the variable $\overline{u^2}$, superposition applies. This follows the calculation of the axial velocity at any location and for any arbitrary velocity profile at the nozzle exit.

The convolution of the solution given in Equation (8) and an arbitrary nozzle exit velocity profile function, f(r), for a finite nozzle diameter, D, yields:

$$\overline{u^2}(X, r) = \int_a^b f^2(\alpha)\,[\overline{u^2}(X, r+\alpha)]_i\,\theta(\alpha, r)\,[r+\alpha]d\alpha \tag{9}$$

where $f(r) = \sqrt{K}u(0,r)/U_0$, K is a scale factor, $\theta(\alpha,r)$ defines the angle of equal contribution, α is a dummy variable and the limits depend on the radial position.

Figure 6 gives a graphical representation of the angle, $\theta(\alpha,r)$. The views show the cross section of the jet nozzle. Figure 6a indicates the interior points of the flow field ($r \leq D/2$) and Figure 6b indicates the exterior points ($r \geq D/2$). The angle of equal contribution for interior points is:

$$\theta(\alpha,\ r) = 2\pi,\ -r \leq \alpha \leq (D/2 - 2r) \tag{10a}$$

$$\theta(\alpha,\ r) = 2\cos^{-1}\ \frac{r^2 + (r+\alpha)^2 - D^2/4}{2r(r+\alpha)},\ (D/2 - 2r) \leq \alpha \leq D/2 \tag{10b}$$

The angle of equal contribution for the exterior points has the same form as Equation (10b) except that the limits change to $-D/2 \leq \alpha \leq D/2$.

For a uniform velocity profile at the nozzle exit ($f(r) = K$) Equation (9) becomes:

$$\left[\frac{\overline{u^2}(X,r)}{U_0^2}\right]_{r\leq D/2} = 1 - \exp\left[-\frac{(D/2 - r)^2}{c^2X^2}\right] + \int_{D/2-2r}^{D/2} F(\alpha)\,d\alpha \tag{11a}$$

and

$$\left[\frac{\overline{u^2}(X,r)}{U_0^2}\right]_{r\geq D/2} = \int_{-D/2}^{D/2} F(\alpha)\,d\alpha \tag{11b}$$

where

$$F(\alpha) = \frac{2(r+\alpha)}{\pi c^2X^2}\ \exp\left[-\frac{(r+\alpha)^2}{c^2X^2}\right]\cos^{-1}\left[\frac{r^2 + (r+\alpha)^2 - D^2/4}{2r(r+\alpha)}\right]$$

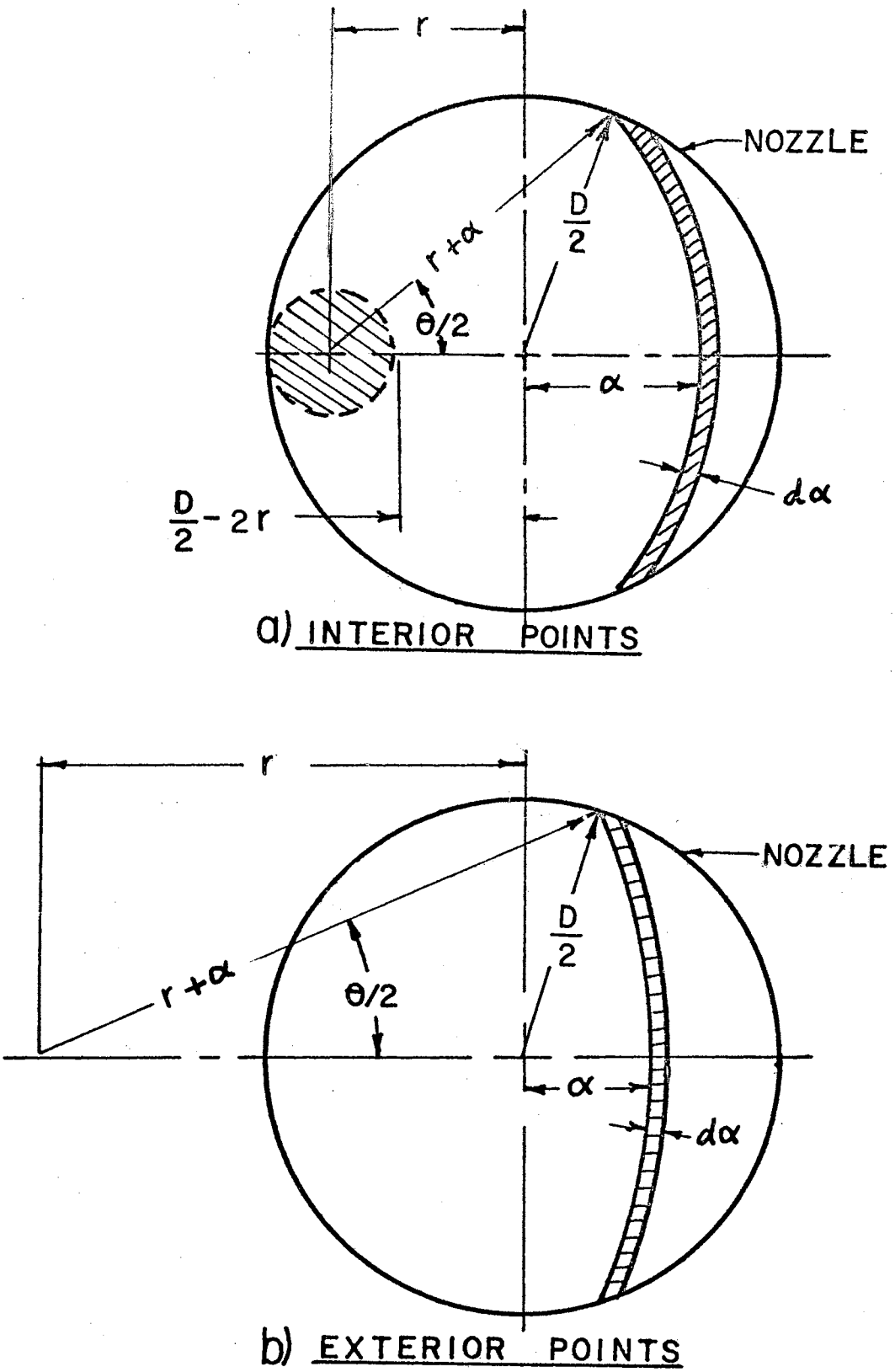

Figure 6. Areas of Equal Contribution to the Velocity

and

$$K = 4/\pi D^2, \text{ so that } u(0,0) = U_o$$

Evaluation of the integrals in Equation (11) requires numerical methods. Figure 7 shows the results of a numerical integration of Equation (11) with Simpson's rule. In this case the experimental constant is arbitrarily selected as 0.070. The formulation given in Equation (11) differs from those of Goertler (7), Albertson et al. (8), and others in that it provides a continuous characterization of the jet throughout the transition and fully developed regions.

Centerline Total Pressure Decay of Free Jet

The centerline balance point (Figure 3) depends on the analytical functions that represent the centerline total pressure distribution of the impinging jet. This distribution is called the "centerline decay." The procedure presented in the previous section leads to an analytical expression for the centerline decay of a free jet. The derivation of the expression follows below.

On the jet axis the convolution of Equation (8) and an arbitrary nozzle exit profile function, f(r) yields:

$$\overline{u^2}(X,0) = 2\pi \int_o^\infty f^2(\alpha) \left[\overline{u^2}(X,\alpha)\right]_i \alpha d\alpha \qquad (12)$$

As examples of the application of Equation (12), Figure 8 shows some assumed boundary layer exit profiles.

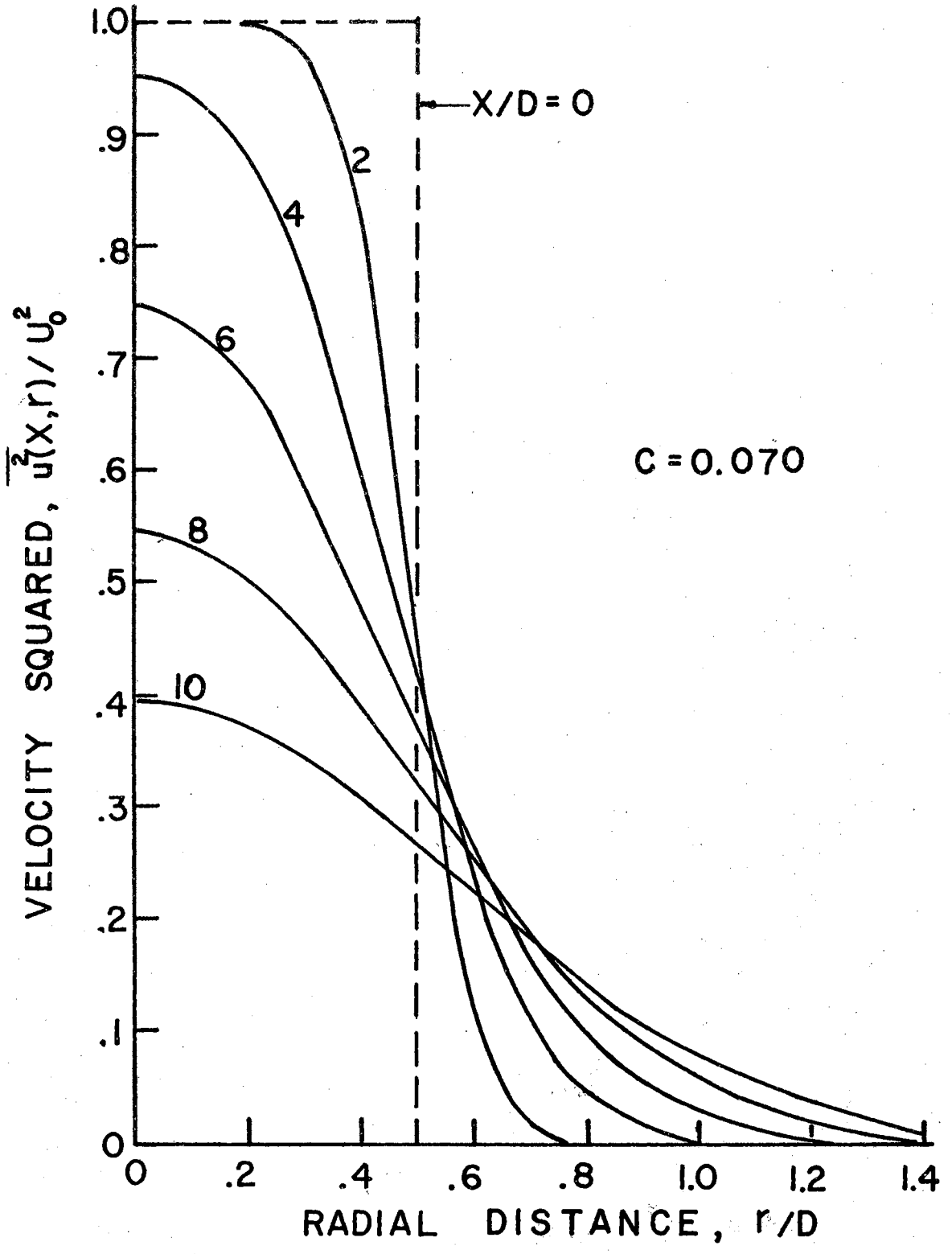

Figure 7. Downstream Distribution for a Uniform Exit Profile

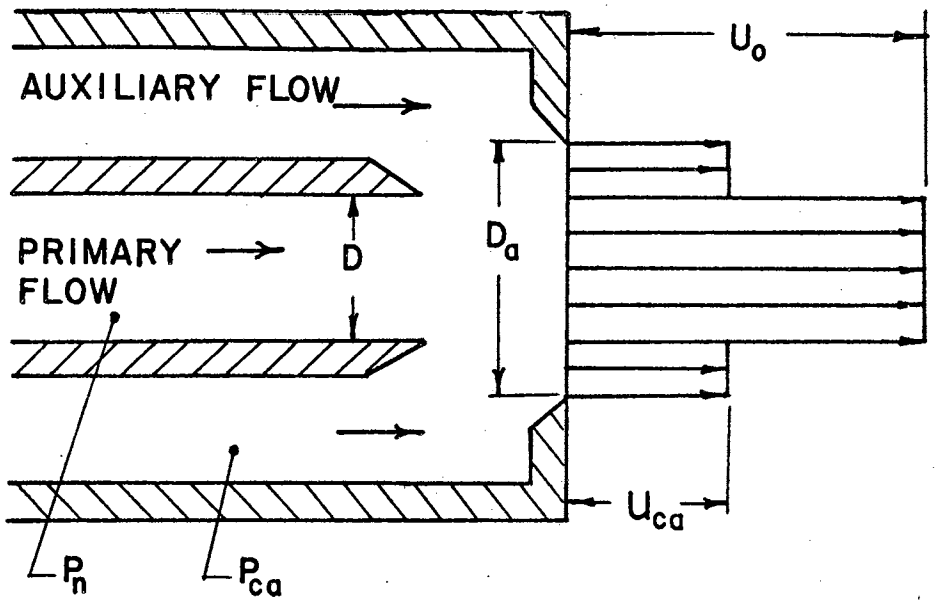

a) ANNULAR

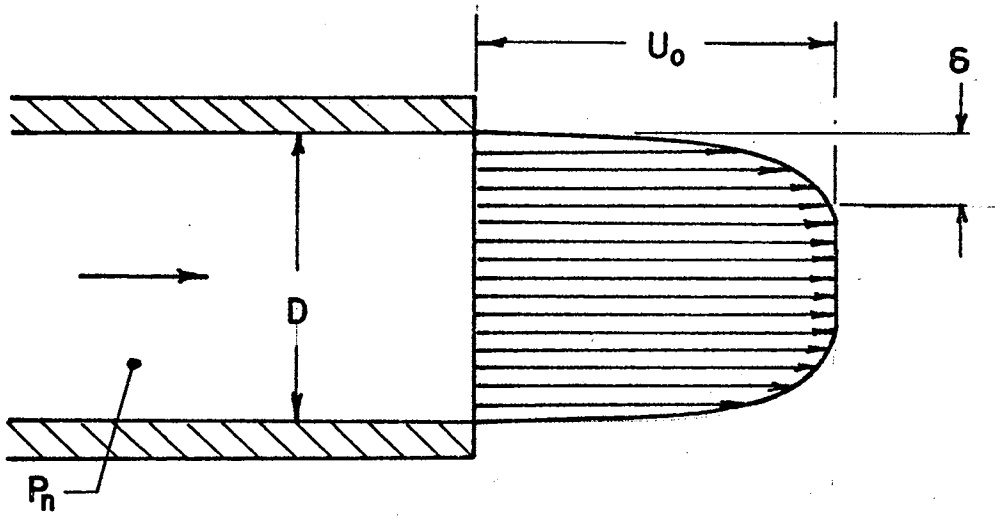

b) BOUNDARY LAYER

Figure 8. Assumed Exit Profiles

1. Annular Exit Profile

The annular velocity profile shown in Figure 8a is similar to the case of an annular auxiliary flow superimposed on a primary jet flow (emitter). The central region up to the radius of the inner nozzle has the uniform velocity, U_o. The surrounding annular flow has the uniform velocity, u_{ca}. The velocity profile function for this shape is:

$$[f(r)]_a = \sqrt{K}, \quad o \leq r \leq D/2 \tag{13a}$$

$$[f(r)]_a = \sqrt{K}u_{ca}/U_o, \quad D/2 \leq r \leq D_a/2 \tag{13b}$$

If Equation (13) is substituted into Equation (12) and the integration performed, the result is:

$$\left[\frac{\overline{u^2}(X,O)}{U_o^2}\right]_a = 1 - \exp\left[-\frac{1}{E}\right] + \frac{u_{ca}^2}{U_o^2}\left[\exp\left(-\frac{1}{E}\right) - \exp\left(-\frac{D_a^2/D^2}{E}\right)\right] \tag{14}$$

where $E = 4C^2X^2/D^2$ and $K = 4/\pi D^2$ so that $u(0,0) = U_o$. In incompressible flow the relation between total pressure at any point and dynamic pressure (12) is:

$$P = \frac{\rho\overline{u^2}}{2}\left[1 + \frac{\overline{u'}^2}{u^2}\right] \tag{15}$$

The contribution of the turbulent fluctuations is usually small. If these are neglected, Equations (14) and (15) combine to give:

$$\left[\frac{P}{P_n}\right]_a = 1 - \exp\left[-\frac{1}{E}\right] + \frac{P_{ca}}{P_n}\left[\exp\left(-\frac{1}{E}\right) - \exp\left(-\frac{D_a^2/D^2}{E}\right)\right] \tag{16}$$

where P is the total pressure on the centerline, P_n is the total pressure in the primary flow chamber and P_{ca} is the total pressure in

the auxiliary flow chamber. Without auxiliary flow, $P_{oa} = 0$, and Equation (16) reduces to:

$$\frac{P}{P_n} = 1 - \exp\left[-D^2/4C^2X^2\right] \tag{17}$$

Figure 9 represents Equation (17) for several values of the decay factor, C. The magnitude of C is a measure of both the spread and decay of the jet; the larger the value of C, the greater the jet spread and the more rapid the decay of centerline total pressure.

The centerline decay given in Equation (17) and the centerline decay proposed by Albertson et al. (8) are different. Figure 10 shows both representations. In the Albertson model, the centerline total pressure remains at the nozzle exit value until the parameter E equals 1. For greater values of the parameter, the centerline pressure decreases and is equal to 1/E. The centerline pressure decay presented in Equation (17) decreases continuously from the nozzle exit. It approaches the Albertson model asymptotically for both small and large values of the parameter E.

2. Exit Profile with Boundary Layer

Figure 8b shows the exit velocity profile with boundary layer buildup. The velocity profile function for this shape consists of a central region at uniform velocity surrounded by a curved region that lowers the velocity to zero at the walls. A precise representation of the boundary layer shape is not necessary here since the convolution integral is relatively insensitive to shape. The objective is rather to illustrate the effect of a nonuniform exit velocity profile. For convenience in obtaining a closed form expression from the integration

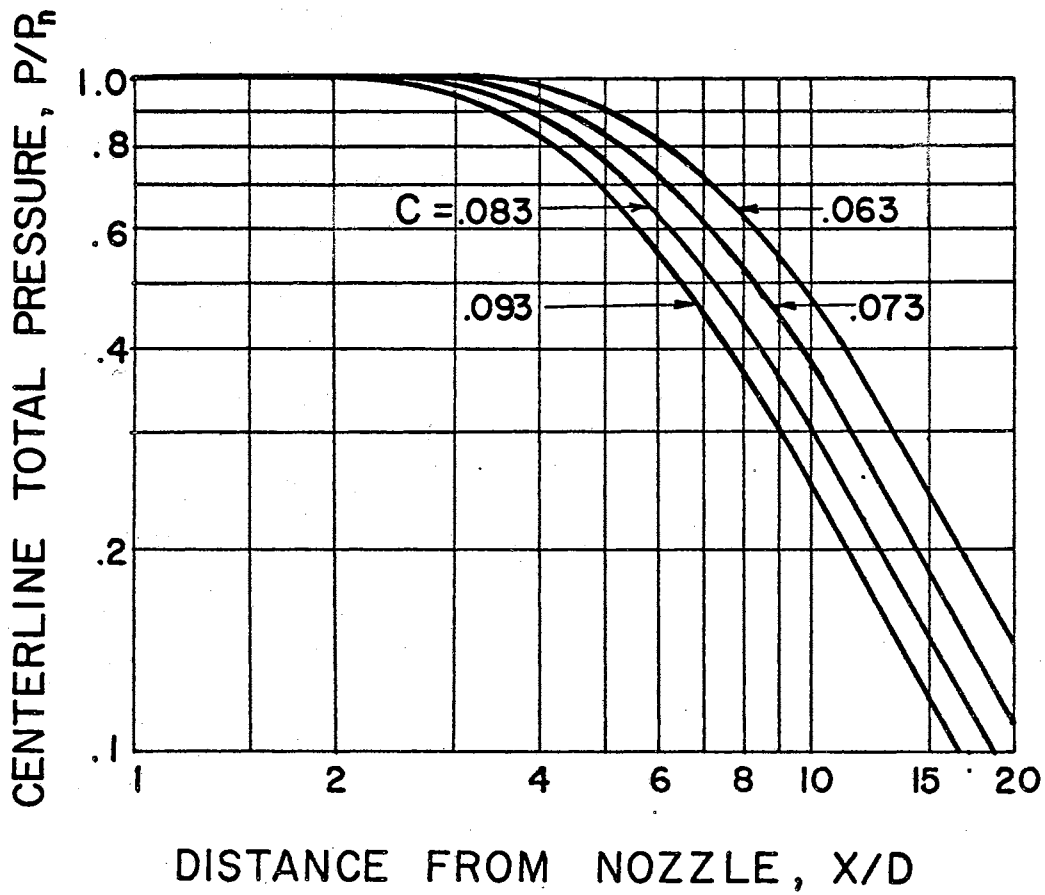

Figure 9. The Effect of Spread Parameter on the Centerline Pressure Distribution

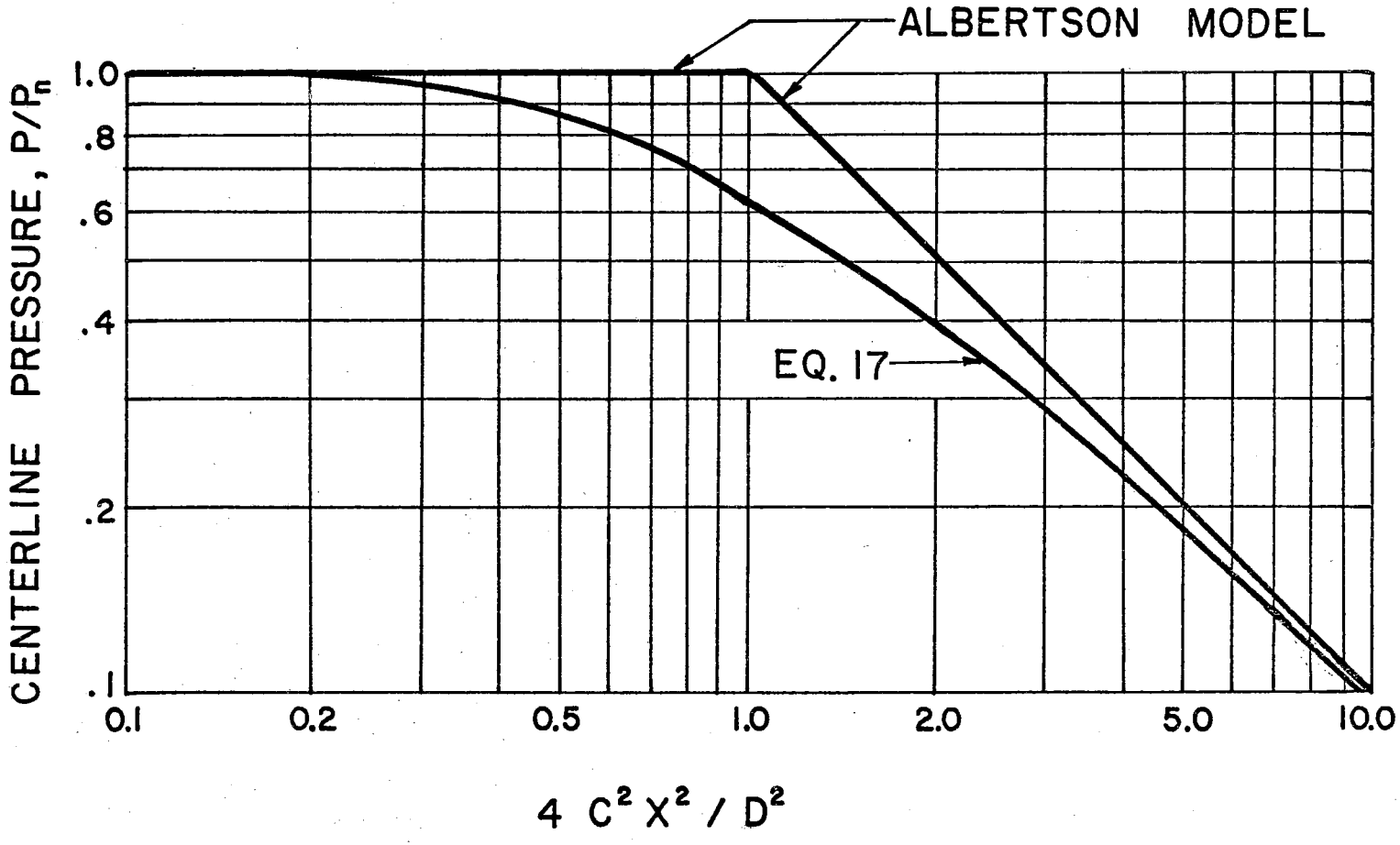

Figure 10. Centerline Pressure Distributions

of Equation (12), a parabolic velocity profile is selected. The velocity profile function for the shape shown in Figure 8b becomes:

$$[f(r)]_b = \sqrt{K}, \quad 0 \leq r \leq (D/2 - \delta) \tag{18a}$$

$$[f(r)]_b = \sqrt{K}\left[1 - \left(\frac{r - D/2 + \delta}{\delta}\right)^2\right]^{1/2}, \quad (D/2 - \delta) \leq r \leq D/2 \tag{18b}$$

where δ is the boundary layer thickness. The procedure followed for the annular exit profile is now repeated. Equation (18), in conjunction with Equation (12) yields:

$$\left[\frac{\overline{u^2}(X,0)}{U_o^2}\right]_b = 1 + \frac{c^2X^2}{\delta^2}\left[\exp\left(-\frac{1}{E}\right) - \exp\left(-\frac{[1 - 2\delta/D]^2}{E}\right)\right] +$$

$$\sqrt{\pi}\left(\frac{cX}{\delta}\right)\left[\frac{D/2 - \delta}{\delta}\right]\left[\operatorname{erf}\left(\frac{1}{\sqrt{E}}\right) - \operatorname{erf}\left(\frac{1 - 2\delta/D}{\sqrt{E}}\right)\right] \tag{19}$$

When the boundary layer thickness is zero, Equation (19) is indeterminate. However, evaluation by differentiation shows that Equation (19) is equivalent to Equation (14) with $u_{cs} = 0$. Figure 11 shows Equation (19) for various values of the boundary layer thickness. The boundary layer always effects the centerline decay. However, when the boundary layer-diameter ratio (δ/D) is between 0 and 0.1, there is only a small difference in the decay curves. Thereafter, the effect becomes progressively larger until the boundary layer extends to the nozzle axis.

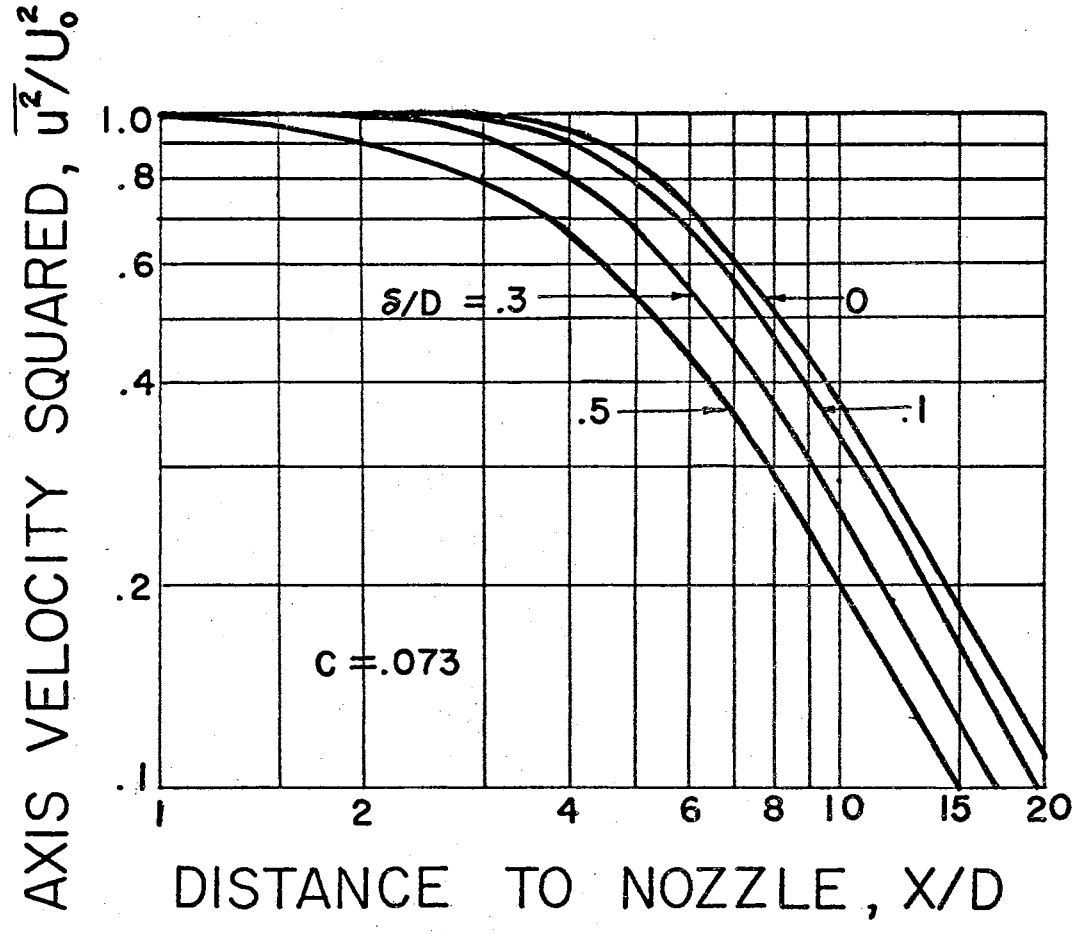

Figure 11. The Effect of Boundary Layer Thickness on Centerline Distribution

Experiments on Free Jets

The emitter nozzles in the experiments are 0.125 in. diameter and 0.500 in. diameter. Figure 12 shows the configurations of the nozzles and supply chambers. The 0.125 in. diameter nozzle (Figure 12a) has a 0.500 in. diameter plennum chamber and a 0.125 in. supply tube perpendicular to the nozzle axis. The 0.500 in. diameter nozzle (Figure 12b) is supplied through an 0.500 in. in-line tube at the end of a 1.750 in. diameter plennum chamber. In addition, the 0.500 in. nozzle has a screen in the plennum to make the flow more uniform. A 0.012 in. O.D. total-pressure probe measures the free jet total pressure of the 0.125 in. diameter jet and a 0.031 in. O.D. total pressure probe measures the 0.500 in. diameter jet. Each probe is mounted on a three-axis traversing mechanism. The pressure readings are taken on precision inclined manometers.

Figure 13 shows some typical centerline decay data for the 0.125 in. and 0.500 in. free jets. Equation (17), with values of the decay factors determined by a least squares fit to the data, is also plotted on Figure 13. The calculated decay factors are 0.075 for the 0.500 in. jet and 0.082 for the 0.125 in. jet. Equation (17) provides a good fit to the data from both jets. The difference between the data and Equation (17) is always less than 3 per cent. Variations in nozzle pressure, P_n, from 4 to 30 in. H_2O, result in a decay factor change of less than 5 per cent.

Figure 14 shows some free jet axial velocity profiles measured 2, 6, and 10 diameters downstream from the nozzle exit. Equation (11) with $C = 0.075$ is plotted on Figure 14 for comparison. The agreement between experiment and theory varies with downstream distance and

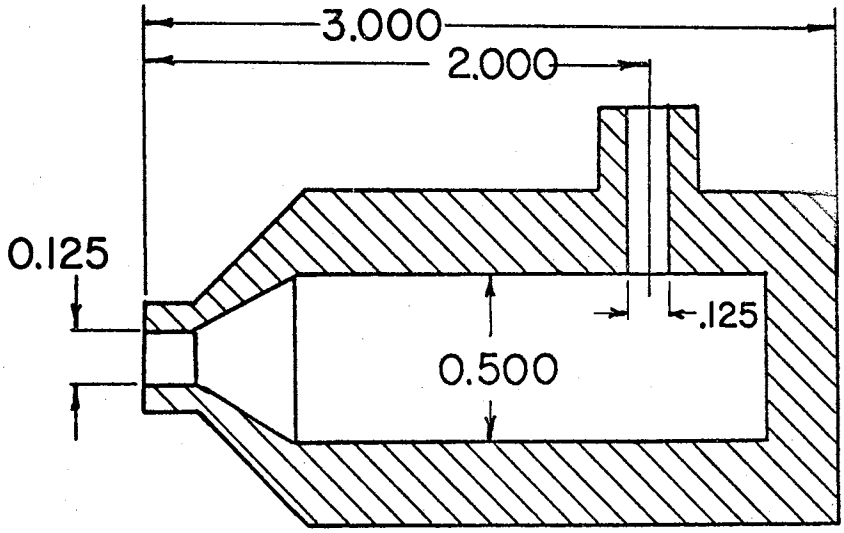

a) 0.125 in. NOZZLE

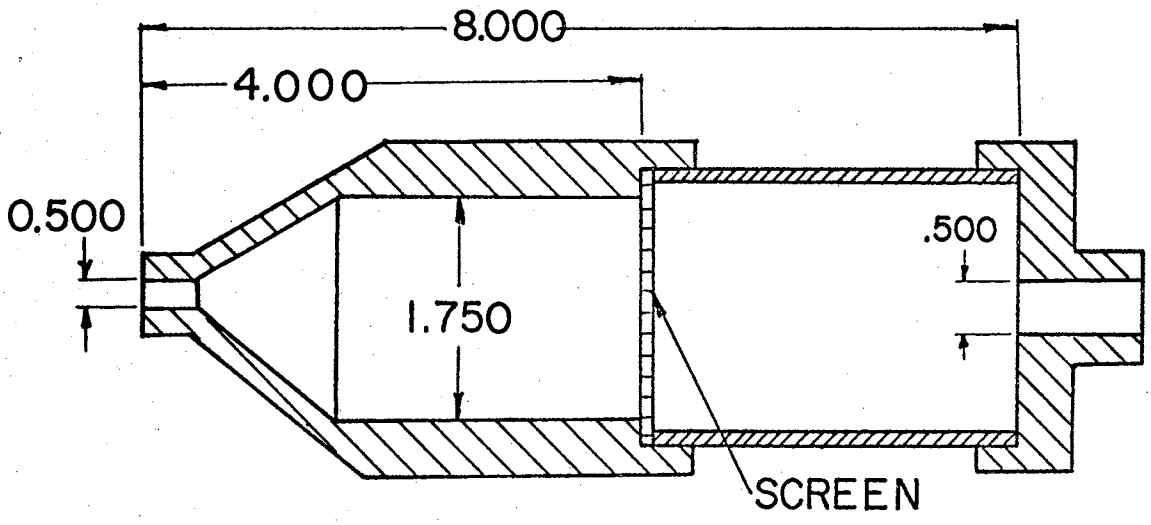

b) 0.500 in. NOZZLE

Figure 12. Experimental Nozzles

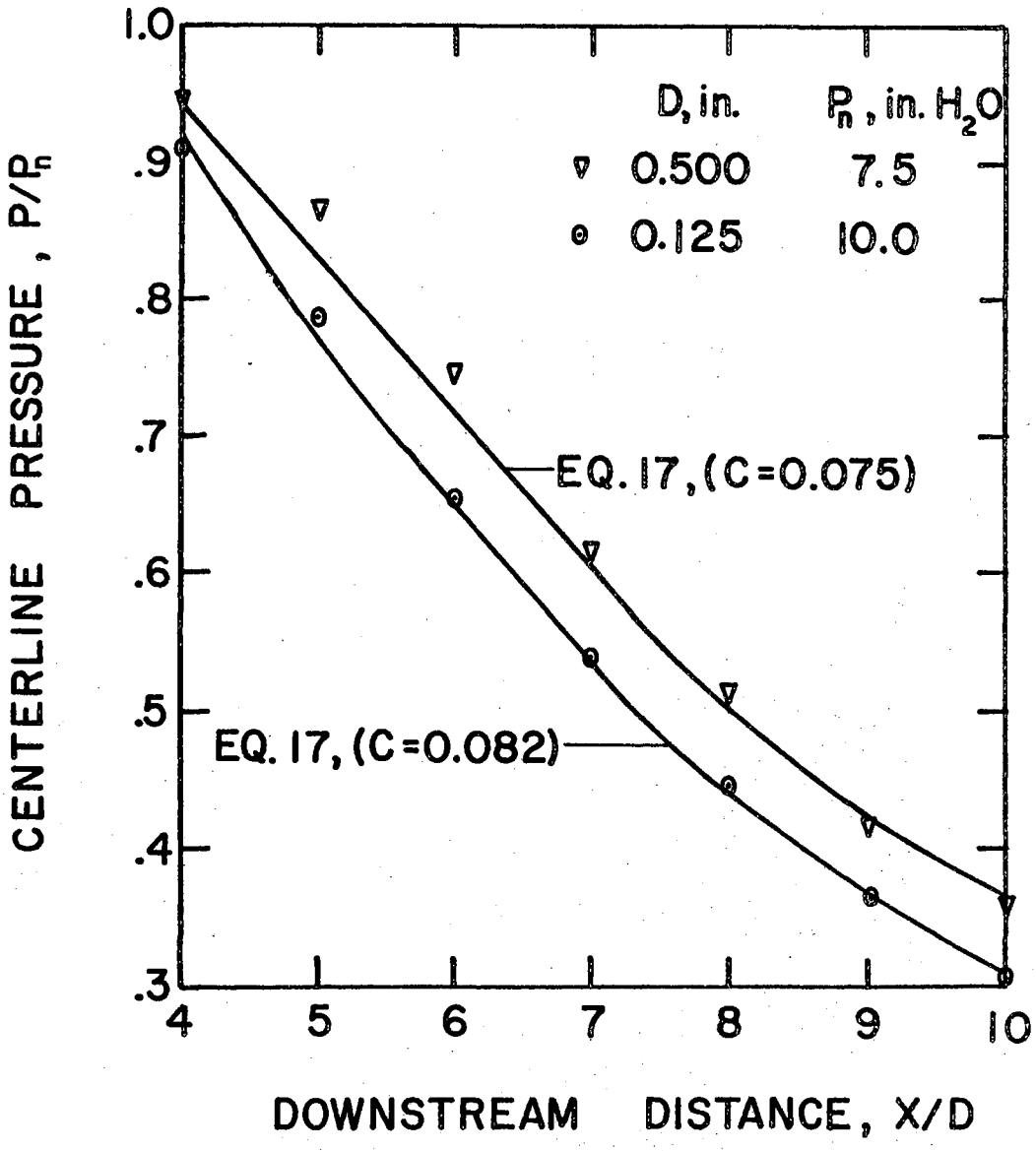

Figure 13. Free Jet Centerline Total Pressure Distribution

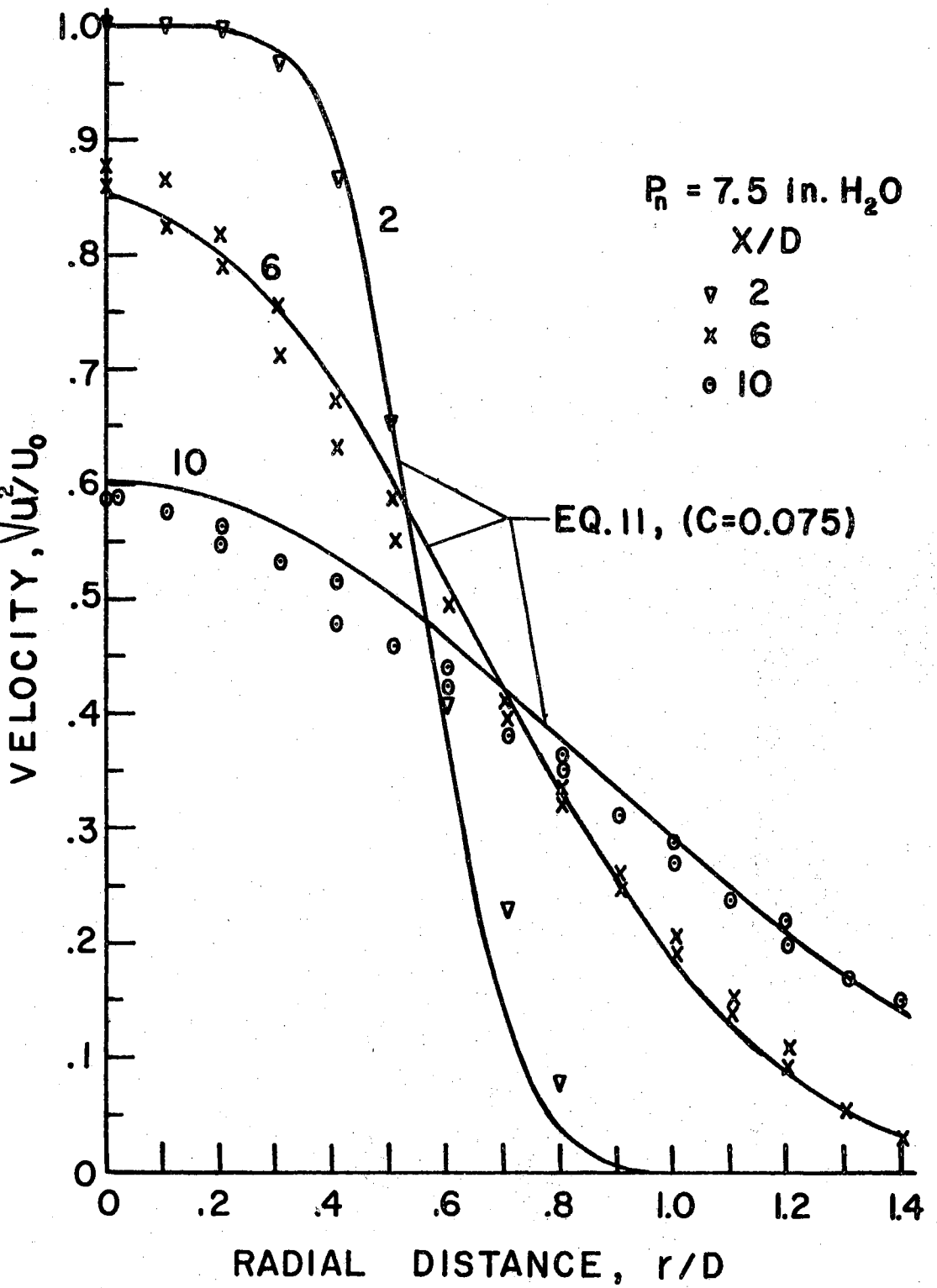

Figure 14. Free Jet Velocity Profiles

radial position. At 2 nozzle diameters downstream the agreement is within 1 per cent for r/D less than 0.5. However, in the high gradient region near the extremities of the jet, the data and Equation (11) differ by as much as 60 per cent. Part of this discrepancy may be the result of experimental errors. The measurements taken at 6 and 10 nozzle diameters are always within 20 per cent of the theoretical predictions and usually within 7 per cent. The disparity between experiment and theory may reduce for another value of C. The value of C (0.075) had been previously determined from centerline decay alone (Figure 13).

CHAPTER IV

CENTERLINE DECAY OF IMPINGING JETS

The introduction of a sizeable obstacle into a jet flow field alters the characteristics of the otherwise free jet. This chapter deals with the centerline total pressure decay of impinging jets.

Decay of Jet Impinging on a Large Flat Plate

LeClerc (13) and Schach (14) present inviscid analyses for the impingement of an axisymmetric jet on a flat plate normal to the axis. In the region from the nozzle exit to about 4 nozzle diameters downstream, the inviscid analyses satisfactorily predict the radial pressure distribution on the plate. Although these analyses give no indication of centerline distribution they provide information about the free streamlines. This information is useful in recognizing the extent of the plate influence on the impinging turbulent jet. Figure 15 shows the free streamline obtained by LeClerc (13). The distance from the plate, at which the free streamline deviates from its original position by some arbitrary amount (i.e., 0.01 D), is the hypothetical impingement distance, H. This impingement distance defines the approximate extent of plate influence on the free jet. Thus, in subsonic flow, the impinging jet behaves as a free jet until it approaches within the impingement distance of the flat plate.

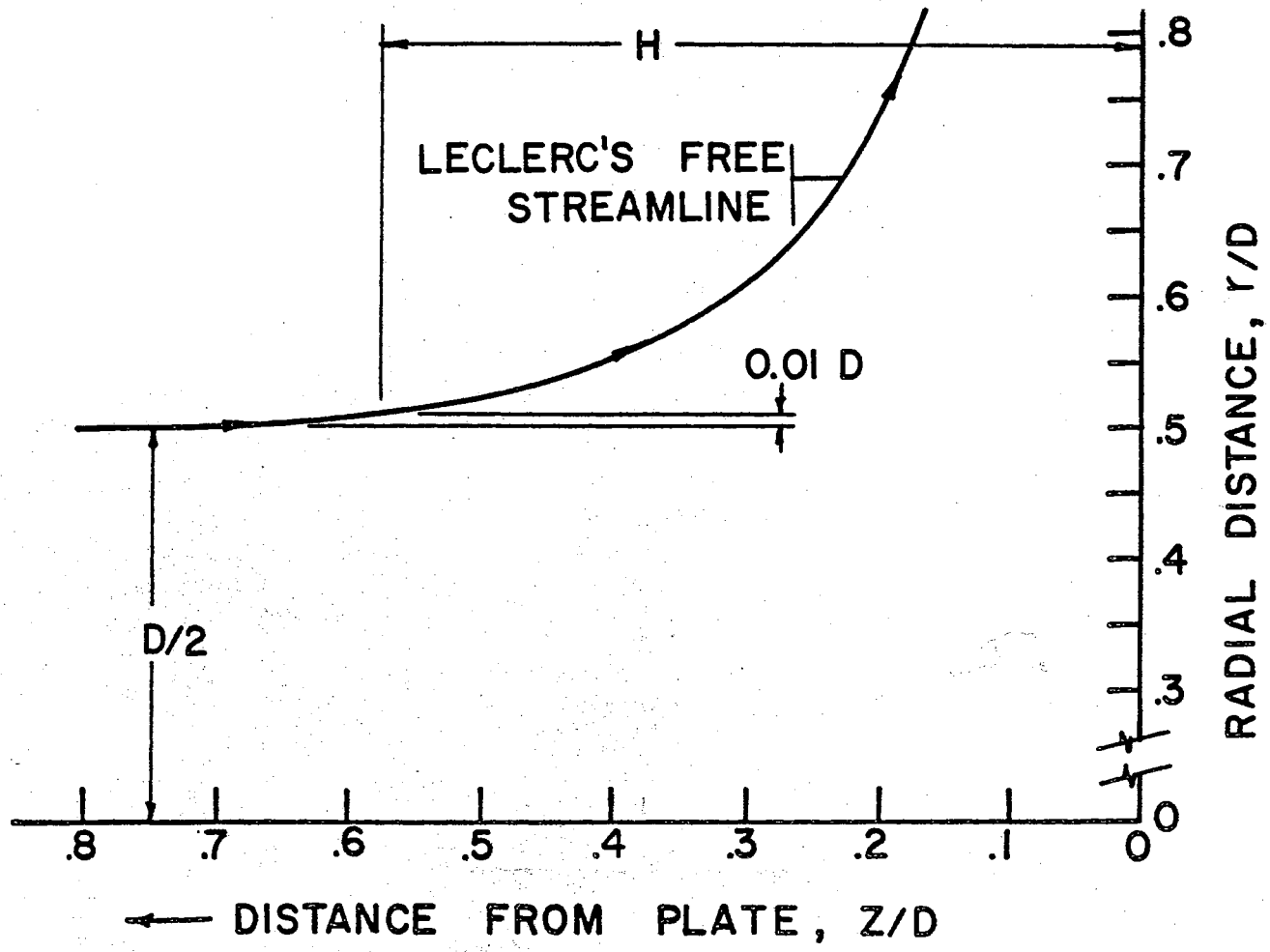

Figure 15. Free Streamline Position for Inviscid Jet Impinging on Flat Plate

The concept of an impingement distance is useful in visualizing the difference in the centerline pressure decay of free and impinging jets. As an example of the use of the impingement distance concept, Figure 16 shows a typical centerline decay curve for a free jet. A small total pressure probe located at X_p recovers the free jet total pressure. However, if a flat plate with a pressure tap in it replaces the probe, the free jet region extends only to $X_p - H$. At this location free jet entrainment terminates. If no losses occur in the region $(X_p - H) \leq X \leq X_p$, the centerline stagnation pressure measured on the plate at X_p equals the total pressure in the free jet at $X_p - H$. The centerline total pressure of the impinging jet, P_p, then becomes.

$$\frac{P_p}{P_n} = 1 - \exp\left[-\frac{D^2}{4C^2(X_p - H)^2}\right] \tag{20}$$

Since the precise impingement distance (H) and the amount of stagnation recovery are uncertain, it is more convenient to utilize a plate decay factor, C_p. Thus, Equation (20) changes to:

$$\frac{P_p}{P_n} = 1 - \exp\left[-\frac{D^2}{4C_p^2 X_p^2}\right] \tag{21}$$

where $C_p = C\,(1-H/X_p)$. The plate decay factor is always less than the free jet decay factor. When the distance downstream of the nozzle exit is between 4 and 10 nozzle diameters, C_p is between 80 and 90 per cent of C. As the distance increases beyond 10 nozzle diameters, the plate and free jet decay factors approach each other.

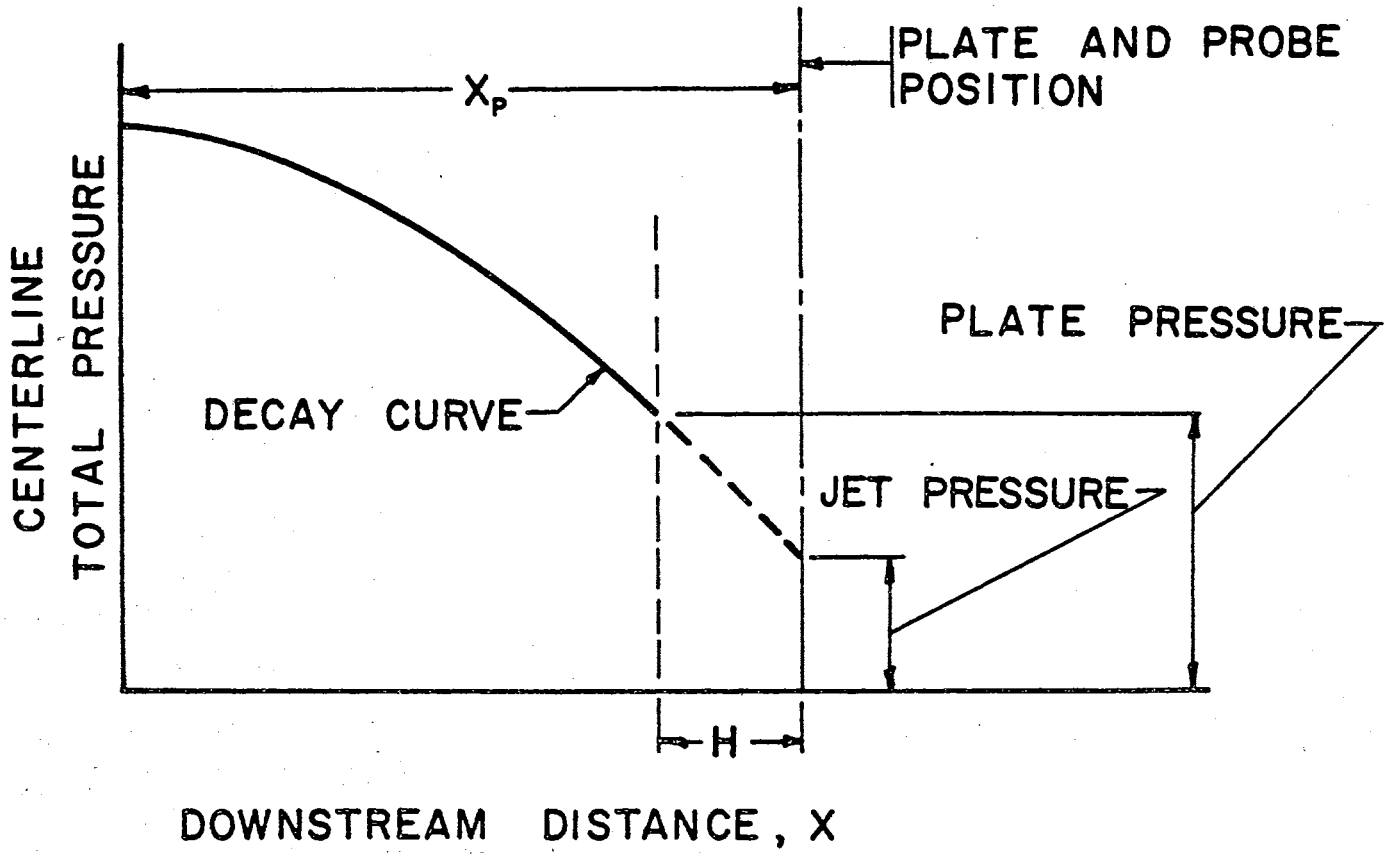

Figure 16. Schematic Representation of Total Pressure Recovered in Free and Impinging Jets

Experiments on Impinging Jets

Snedeker and Donaldson (15) perform an experimental investigation of jets impinging on flat and curved plates. However, their data are not presented in sufficient detail in the transition region to allow correlation with the work done here.

The present jet impingement experiments pertain to subsonic flow on flat plates and concentrate on the transition region ($4D \leq X \leq 10D$). The flat plates are at least 10 nozzle diameters square and each have a small pressure tap in the center (0.013 in. diameter tap for the 0.125 in. diameter nozzle and 0.020 in. diameter tap for the 0.500 in. diameter nozzle). The 0.125 in. diameter and 0.500 in. diameter emitter nozzles are the ones previously used in the free jet experiments.

Figures 17 and 18 show some typical centerline decay data for the 0.125 in. and 0.500 in. impinging jets and also show Equation (21) with the value of C_p calculated from the data using a least squares fit. In addition, Figures 17 and 18 present a comparison of the free jet results and the plate results. The plate decay factors are less than the free jet decay factors. For the 0.125 in. emitter, the ratio of plate to free jet decay factor (C_p/C) is 0.87 and for the 0.500 in. emitter the ratio is 0.89. In addition, the impingement data agrees well with the form assumed in Equation (21). For downstream distances of 9 nozzle diameters and less, the data is within 5 per cent of the analytical form. At 10 nozzle diameters the discrepancy increases to 8 per cent. Thus, the formulation derived for the free jet centerline decay approximates the impinging jet decay but requires a modified experimental constant.

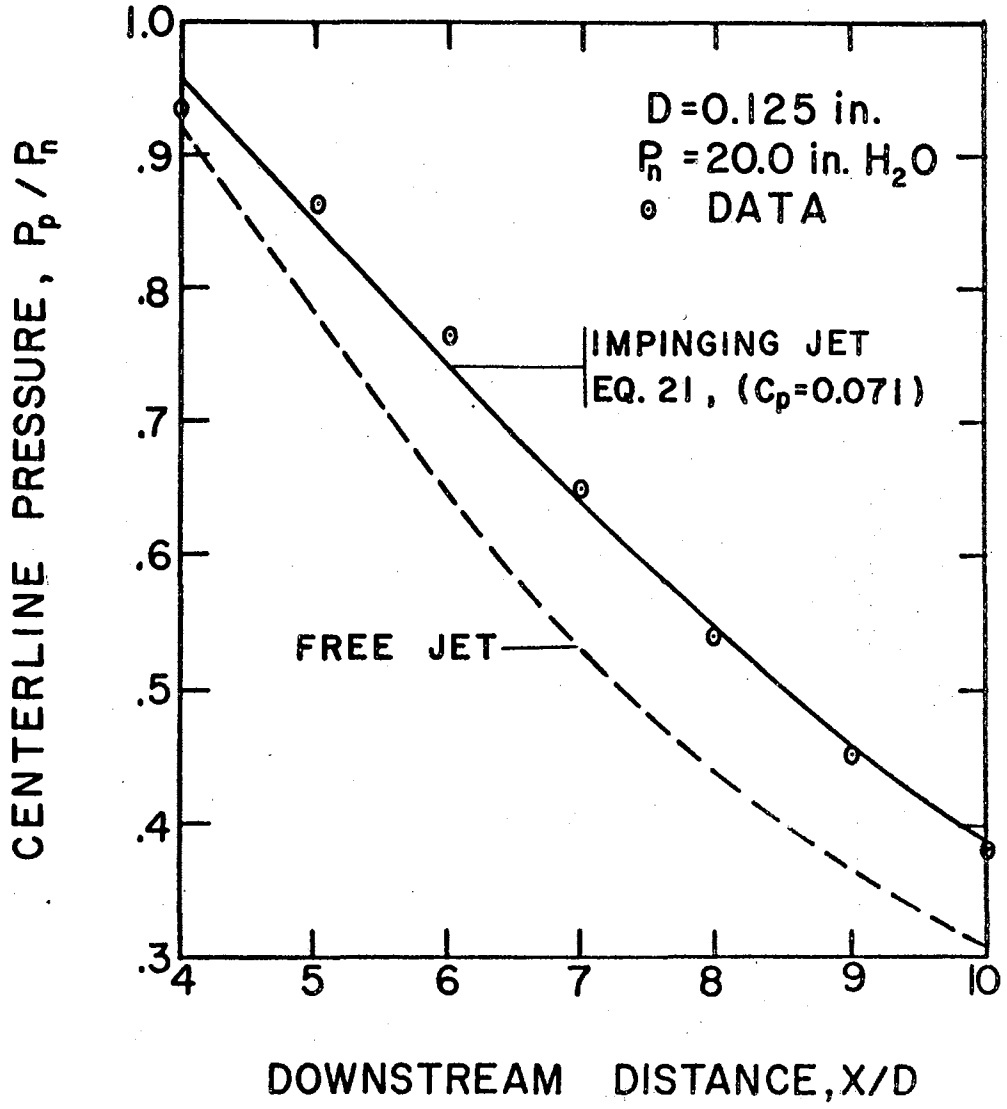

Figure 17. Centerline Total Pressure on Free and Impinging Jets (D = 0.125 in.)

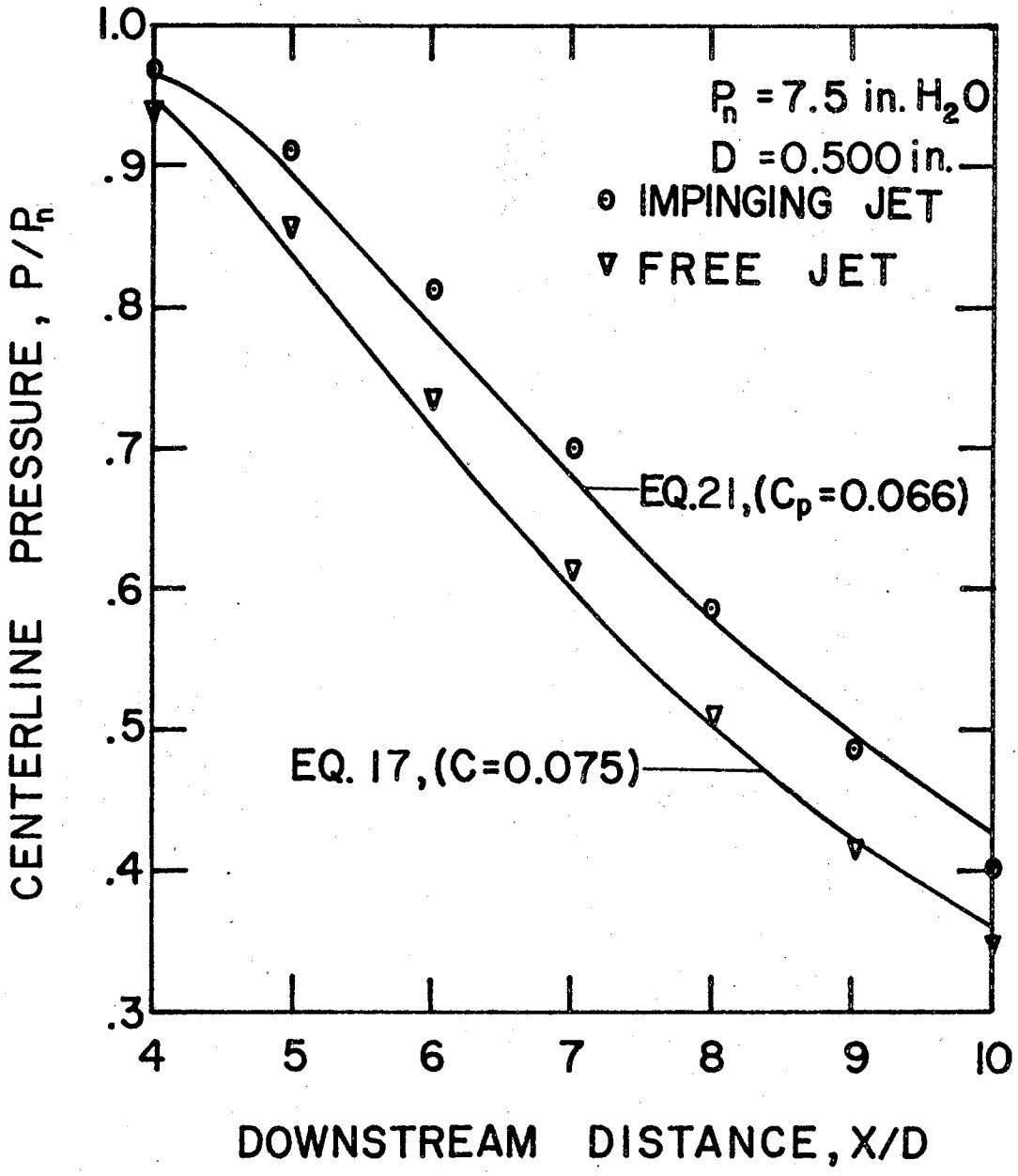

Figure 18. Centerline Total Pressure on Free and Impinging Jets (D = 0.500 in.)

Significance of Decay Curve Slope

In the development of an expression for the shape correction, the difference in centerline pressure between the free jet and the jet impinging on a flat plate is a significant factor. According to the concept of an impingement distance, the difference depends on the slope of the decay curve. The slope of the decay curve is obtained by differentiating Equation (21). The result is:

$$\frac{d(P/P_n)}{d(X/D)} = -\left[\frac{1}{2C_p^2(X_p/D)^3}\right] \exp\left[-\frac{D^2}{4C_p^2X_p^2}\right] \qquad (22)$$

In incremental form the left side of Equation (22) is $\Delta(P/P_n)/\Delta(x/D)$. The incremental distance, $\Delta(x/D)$, under consideration here is the impingement distance, H/D. If the impingement distance is equal to one, the incremental ratio reduces to $\Delta(P/P_n) \equiv (P-P_p)/P_n$. With this specification, Equation (22) gives an expression for a pressure difference that can be compared to data. Figure 19 shows Equation (22) and the difference between free and impinging jet centerline total pressure data. The data also include some measurements on a 1.94 in. diameter nozzle. These data combine some current flat plate measurements with the free jet data of Reid (16) on the same nozzle. Equation (22) and the data should agree only if the actual impingement distance (H/D) is equal to one as assumed. The data indicate that the impingement distance is less than one diameter. However, Figure 19 shows that the probe-plate difference does follow the general shape of the decay curve slope (Equation (22)).

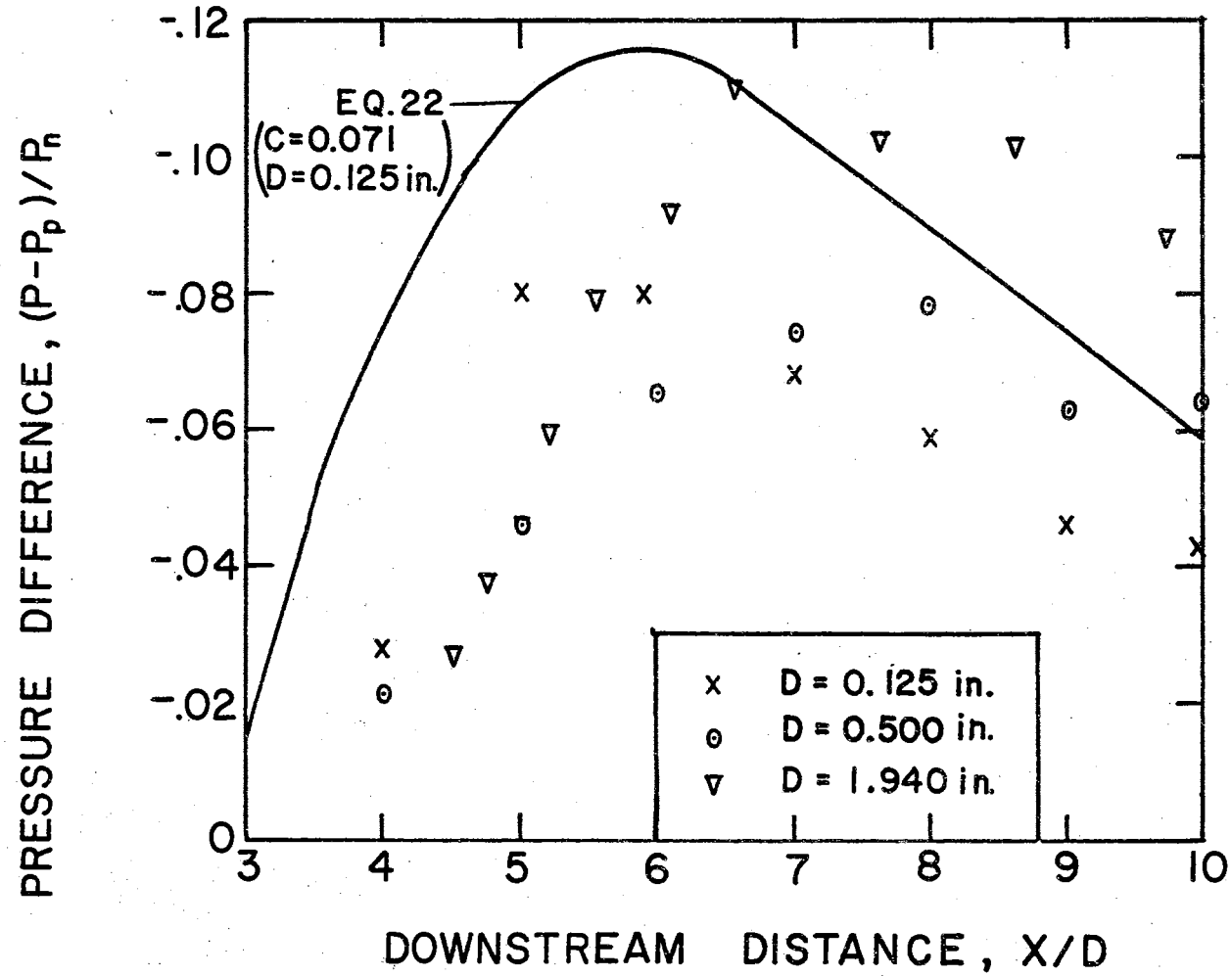

Figure 19. Difference in Centerline Pressure of Free and Impinging Jets

Hypothesis on the Effect of Plate Curvature

In the case of the impacting "jets" that occur in impact modulators, the dividing streamsurface is generally not flat. It is necessary, therefore, to consider the effects of plate curvature on the centerline decay. However, an extensive study of the influence of plate shape on the centerline decay is beyond the scope of this investigation. For this reason, the centerline decay of a jet impinging on a curved surface is hypothesized. The hypothesis is:

> The centerline pressure distribution in a jet impinging on a concave surface decays at a lesser rate than a jet impinging on a convex surface. The formulation for centerline decay given in Equations (16) and (17) represents the decay measured on a curved surface if an effective decay factor, C_e, is used.

The basis for this hypothesis is the interpolation and extrapolation of the data from the free jet and the jet impingement on a flat plate. Figure 20 shows some hypothetical centerline decays for curved plates. When the plate curvature is convex, the centerline decay is between the free jet and flat plate impingement decays. When the curvature is concave, the centerline pressures exceed those measured on a flat plate. The impingement distance probably increases with the concave surface and decreases with the convex surface.

Expression for Streamsurface Centerline Position

An expression for the streamsurface centerline position can now be obtained from Equation (16) and the centerline pressure balance shown in Figure 21. The nozzle chamber pressure is equivalent to the emitter pressure ($P_a = P_e$). At the balance point the centerline pressure equals

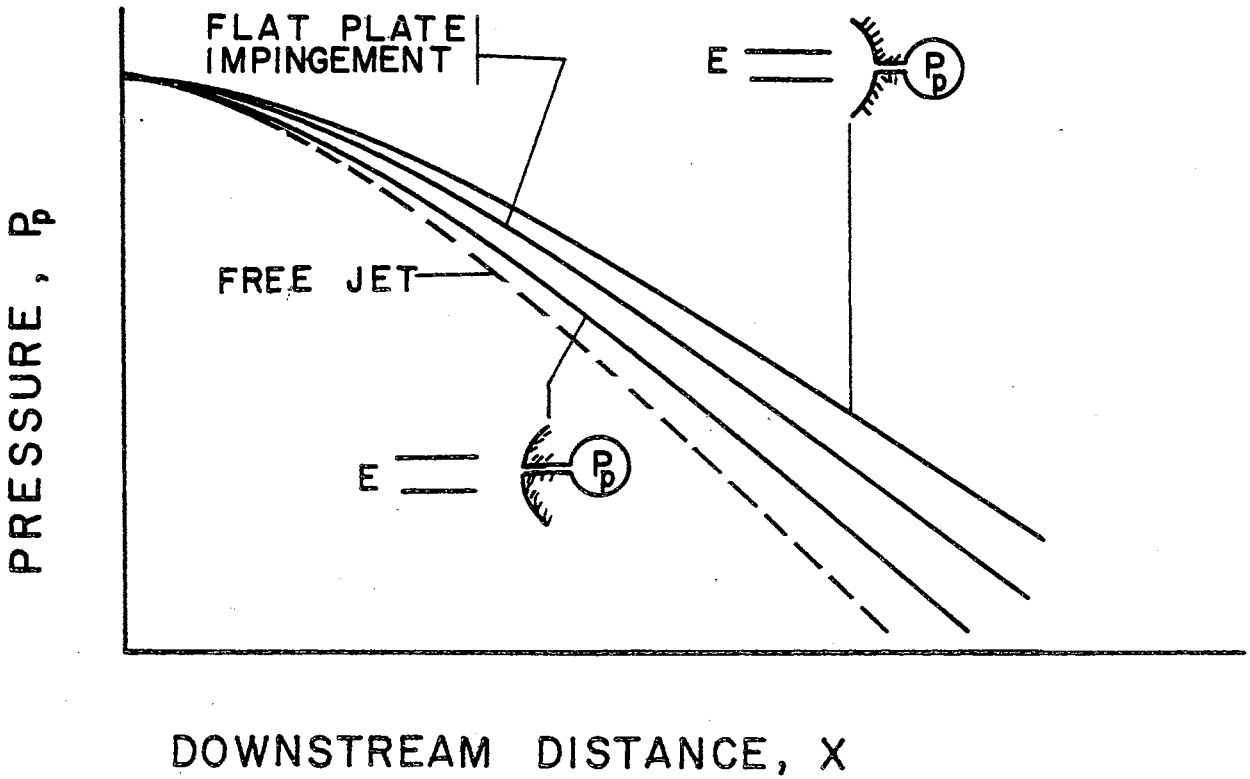

Figure 20. Hypothetical Representation of Pressure Distribution on Curved Surfaces

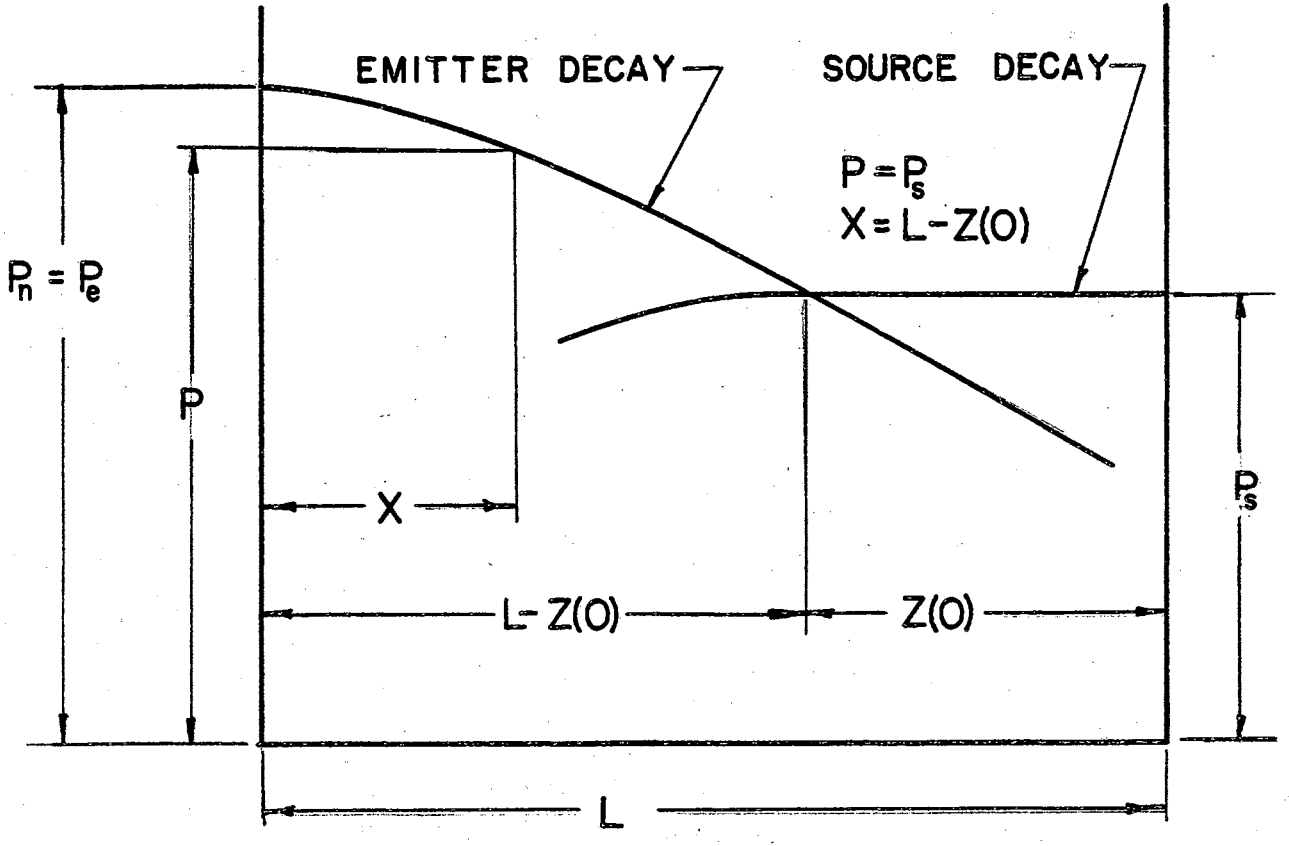

Figure 21. Pressure Balance

the source pressure ($P = P_s$) and the downstream distance is the difference between nozzle spacing and centerline streamsurface position. Thus, Equation (16) changes to:

$$\left[\frac{P_s}{P_e}\right]_a = 1 - \left(1 - \frac{P_{ca}}{P_e}\right)\exp\left[-\frac{D^2}{4C_e^2(L-Z(0))^2}\right] - \frac{P_{ca}}{P_e}\exp\left[-\frac{D_a^2}{4C_e^2(L-Z(0))^2}\right] \tag{23}$$

Equation (23) represents implicitly the functional relation given in Equation (2). When there is no annular control the streamsurface centerline position can be expressed explicitly as:

$$\frac{Z(0)}{D} = \frac{L}{D} - \sqrt{-\frac{1}{2C_e \ln(1 - P_s/P_e)}} \tag{24}$$

Expression for Shape Correction

Equation (6) presents the feedback correction in functional form. The expression derived here for that form, in effect, assumes that the feedback decay factor, C_f, is the product of the centerline decay curve slope (Equation (22)) and the difference, $Z(0) - Z(R)$. This difference is a measure of the streamsurface shape. When the streamsurface is flat ($Z(0) = Z(R)$) there is no correction. When the streamsurface is concave ($Z(R) > Z(0)$) the correction decay factor is negative. The assumed expression for the feedback decay factor is thus:

$$C_f = \frac{K_f[Z(0)/D - Z(R)/D]}{2C_p^2(L/D)^3}\exp\left[-\frac{1}{4C_p^2(L/D)^2}\right] \tag{25}$$

where K_f is the constant that determines the amount of feedback. This constant has not been verified experimentally. To determine the feedback decay factor would require a detailed study of the jet flow field and measurements of the jet impinging on a variety of convex and concave surfaces. This study treats K_f as a free constant and selects its value to produce the best agreement with experimental results. It is the only free constant used in the over-all model formulation. All other constants are determined experimentally.

Figure 22 shows Equation (25) with a specific plate decay factor and a typical value of the feedback constant, K_f. For a given nozzle spacing, the feedback decay factor is directly proportional to the difference, Z(O) - Z(R). When the nozzle spacing is small (<4D) or large (>10D), the feedback decay factor is small. The factor is most significant when the spacing is between 6 and 8 nozzle diameters. This corresponds to the region of maximum decay curve slope.

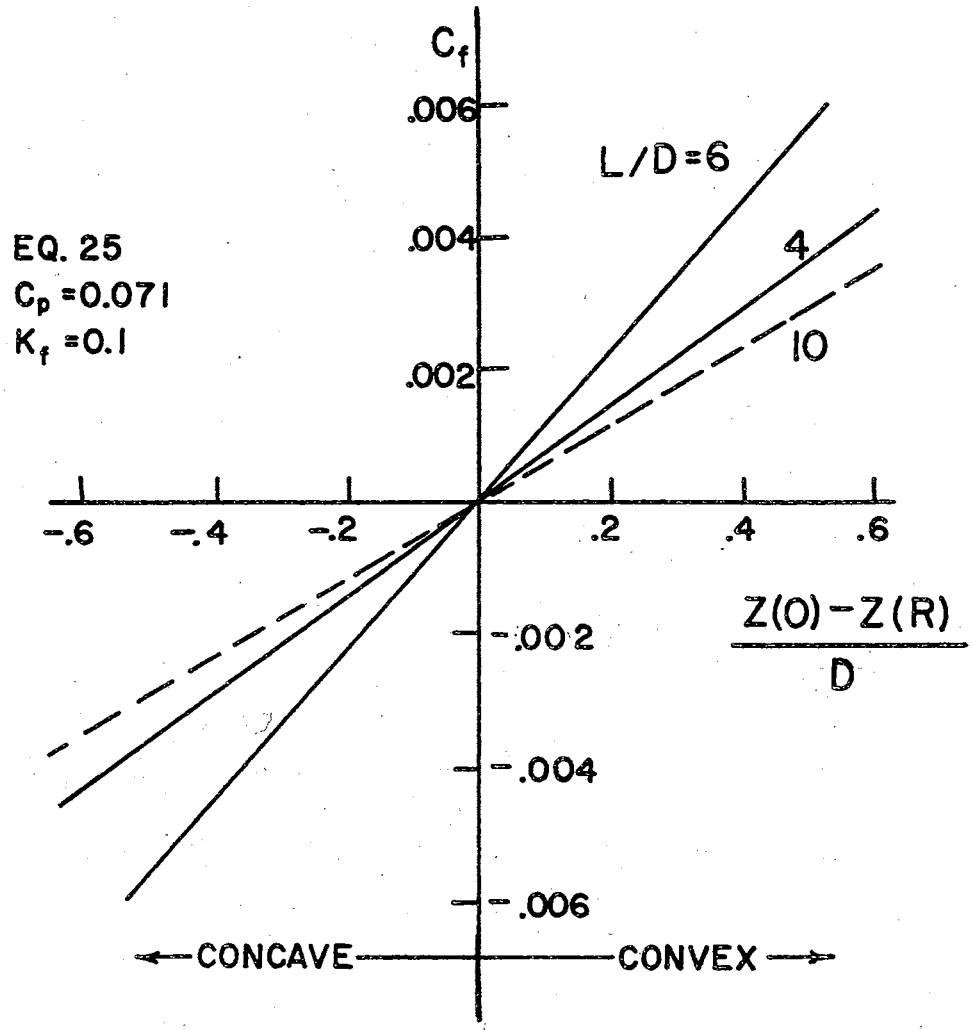

Figure 22. The Decay Correction Factor

CHAPTER V

FREE AND IMPINGING JETS WITH AUXILIARY FLOWS

To model impacting amplifiers requires a knowledge of the influence of relatively small annular and transverse auxiliary flows (auxiliary to primary force ratio less than 0.2) on the primary jet characteristics. Equation (1) shows that the plate decay factor is a function of emitter pressure, annular control pressure, transverse control pressure and geometry. However, this equation can be simplified because the controls are not applied simultaneously. For example, a transverse impact modulator, operates at a constant emitter pressure and without an annular control. Similarly, the emitter modulator has neither annular or transverse control. Thus, the functional form given in Equation (1) is separable into three distinct forms. Each form applies to a specific type of modulator. The forms are:

$$\left[C_p\right]_e = C_p\left[P_e,\ \text{geometry}\right] \qquad \text{Emitter Modulation} \qquad (26a)$$

$$\left[C_p\right]_a = C_p\left[P_e,\ P_{ca},\ \text{geometry}\right] \qquad \text{Annular Modulation} \qquad (26b)$$

$$\left[C_p\right]_t = C_p\left[P_e,\ P_{ct},\ \text{geometry}\right] \qquad \text{Transverse Modulation} \qquad (26c)$$

Effects of Emitter Pressure on Jet Decay

Figure 23 shows the effect of emitter pressure changes on the plate decay factor. For the particular nozzles used here (Figure 12)

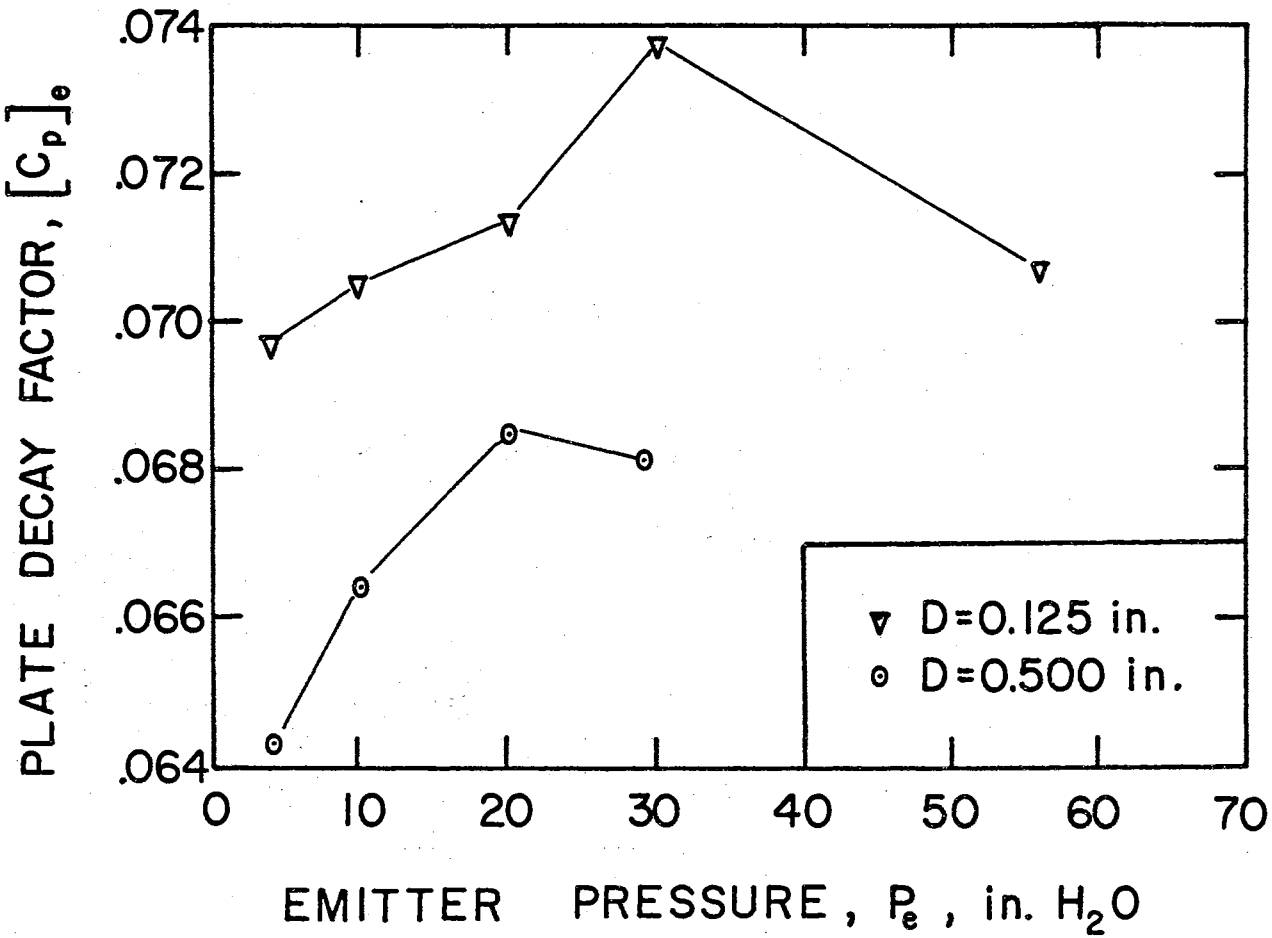

Figure 23. The Effect of Emitter Pressure on Plate Decay Factor

the decay factor increases until the emitter pressure reaches about 25 in. H_2O. At higher emitter pressures the plate decay factor decreases slightly. The predominant mechanism in emitter modulation, however, is not the change in plate decay factor but rather the change in emitter jet momentum. In going from the beginning of flow modulation to cutoff, the emitter pressure changes by only a small amount (about 1.0 in. H_2O). Thus, for practical purposes the plate decay factor for emitter modulation $[C_p]_e$ is essentially constant.

Effects of Annular Control Pressure on Jet Decay

Figure 24b shows the annular jet assembly used to determine the effects of annular control. It consists of an orifice plate, an auxiliary housing, a primary nozzle and a primary housing. The primary (or emitter) nozzle (D = 0.500 in. diameter) attaches rigidly to the primary housing and slides freely within the auxiliary housing. The distance between primary nozzle exit and orifice plate (setback, S) is continuously adjustable between 0 and 0.750 in. The orifice plate connects to the auxiliary housing. There are two interchangeable orifice plates (D_a = 0.550 in. diameter or 0.600 in. diameter).

Velocity profile measurements of the annular jet are made near the downstream face of the orifice plate (X/D = .125) with a linearized DISA constant temperature hot wire anemometer. The shaft of the hot wire probe support is 0.120 in. in diameter. The probe is also 0.120 in. in diameter. Two needle-like rods of less than 0.030 in. diameter support the wire which is 0.0002 in. in diameter and 0.060 in. in length. There is no evidence that the probe causes any blockage of jet flow.

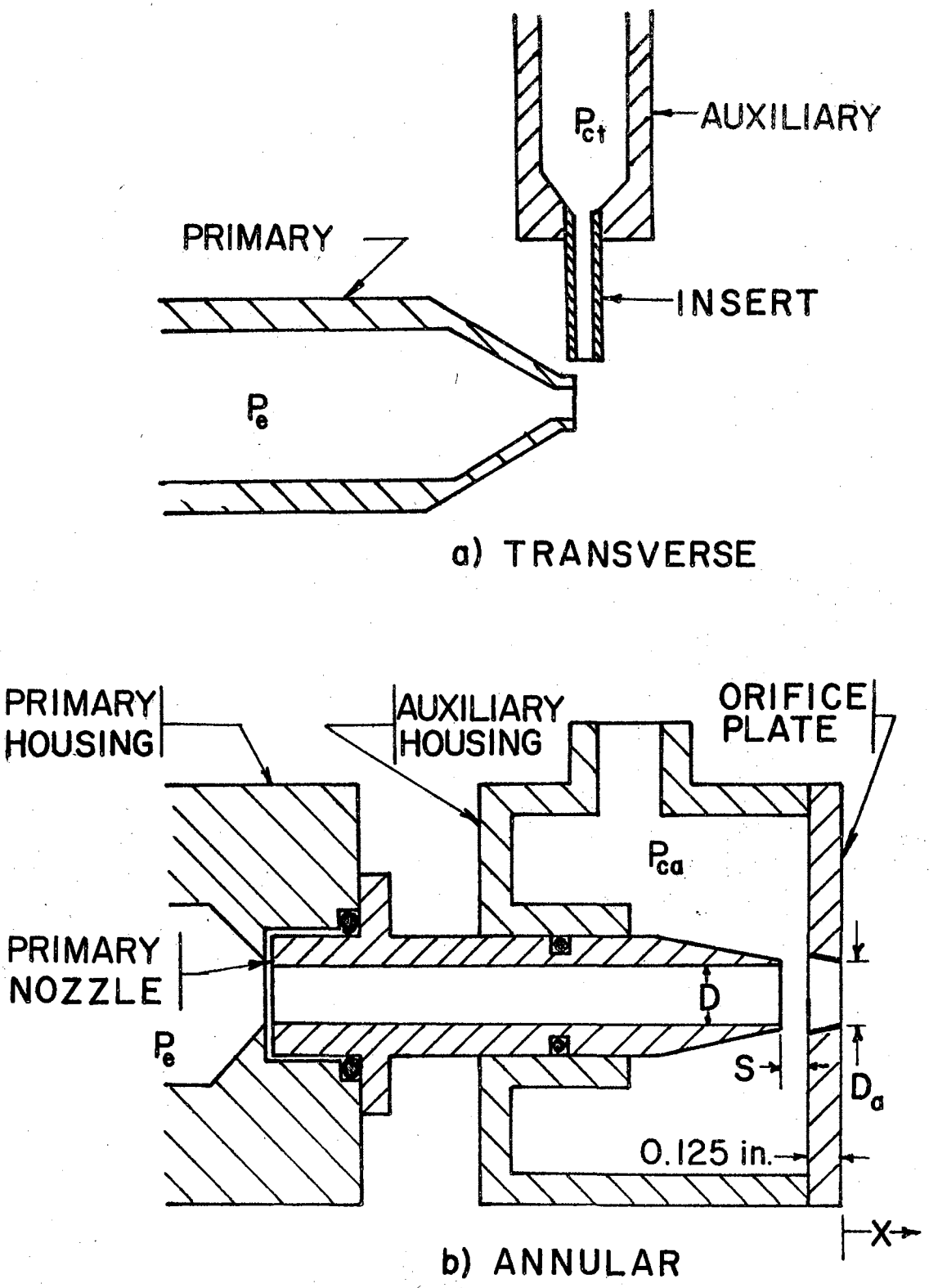

Figure 24. Experimental Arrangement for Auxiliary Flows

Appendix B presents the data in tabular form. For clarity, Figure 25 shows the test results with the discrete data points replaced by smooth curves through the data. The velocity profile without annular control pressure ($P_{ca} = 0$) has only one point of inflection. As the annular control pressure increases the velocity profiles exhibit two points of inflection. When $P_{ca} = 2$ in. H_2O, the points of inflection occur at r/D = .44 and r/D = .60. At $P_{ca} = 4$ in. H_2O, the inflection points move to r/D = .41 and .61.

Figure 26 shows some turbulence intensity profiles at the same downstream location (X/D = .125) as the velocity profiles. Each point of inflection in the velocity profiles corresponds to a peak in the turbulence intensity profiles. Thus, when the annular control is zero, there is only one turbulence intensity peak. For the cases with annular control pressure, there are two turbulence intensity peaks. When the annular control pressure is 2 in. H_2O ($P_{ca}/P_e = 0.286$), the peaks are about equal in height. At an annular control pressure of 4 in. H_2O ($P_{ca}/P_e = 0.572$), the outer peak is much higher. With further increase in the annular control pressure, the inner peak vanishes and the annular jet behaves as a single jet of diameter, D_a.

Figure 27 shows the turbulence intensity profiles at X/D = 2. At $P_{ca} = 2$ in. H_2O (where the two turbulence intensity peaks were about equal for X/D = .125), the resulting single peak is lower than the peaks of $P_{ca} = 0$ and $P_{ca} = 4$ in. H_2O. In general, the turbulence intensity downstream decreases whenever the outer peak at the nozzle exit is less than or about equal to the inner peak. This reduction in the turbulence intensity peak results in a decrease in plate decay factor.

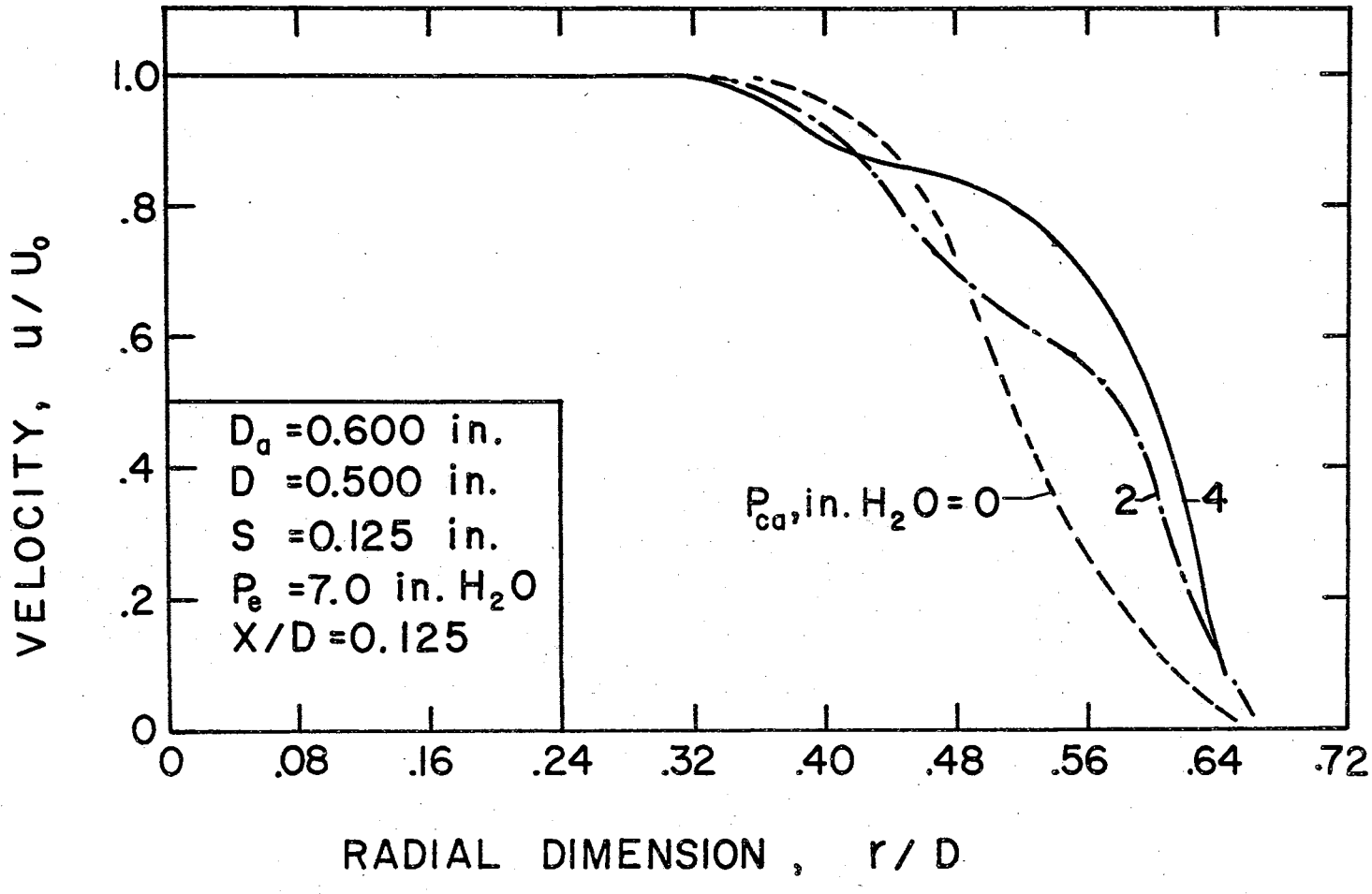

Figure 25. Velocity Profiles at Exit of Annular Nozzle

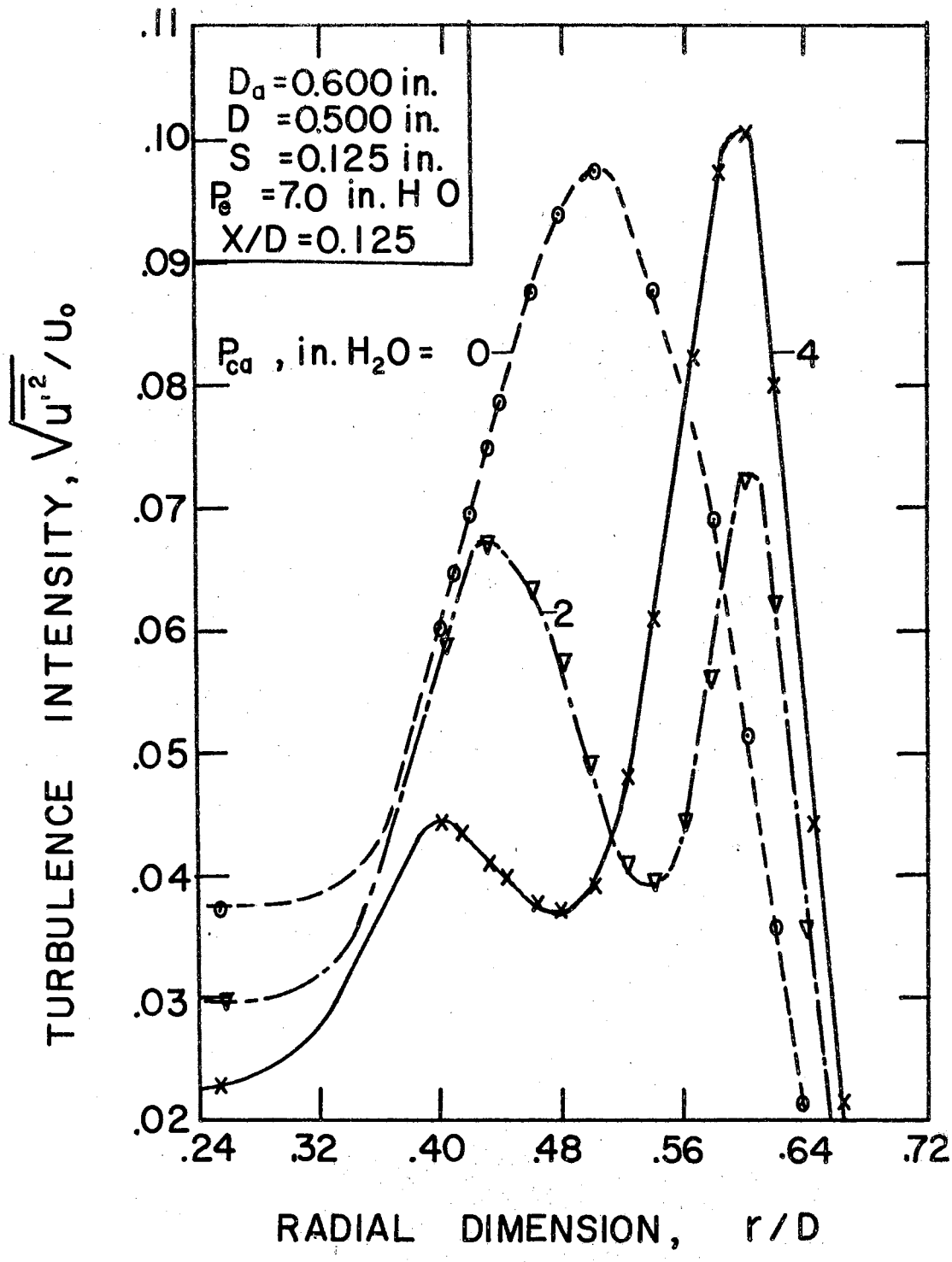

Figure 26. Turbulence Intensity Profiles of Annular Nozzle (X/D = 0.125)

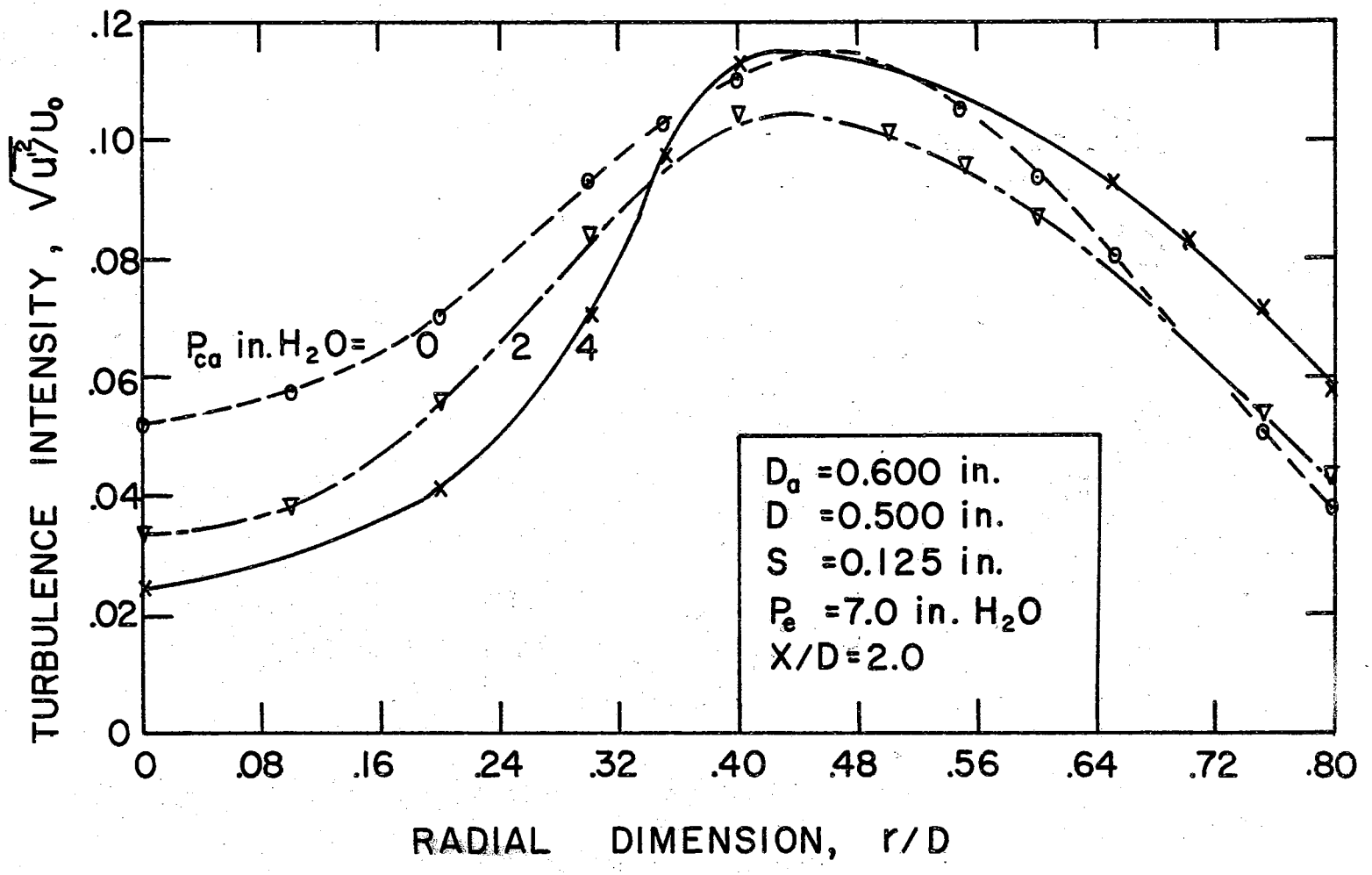

Figure 27. Turbulence Intensity Profiles of Annular Nozzle (X/D = 2.0)

Centerline decay measurements, similar to those already described in Chapter IV, are made with annular auxiliary flow superimposed on the primary jet flow. At the beginning of one of these tests, the primary nozzle pressure is selected. Then the annular control pressure is varied in increments. In all cases the application of annular flow alters the loading on the primary nozzle and requires a readjustment of primary nozzle pressure. Figure 28 shows some typical centerline total pressure distributions for the annular nozzle as measured on a flat plate. With no annular control pressure ($P_{c\,a}/P_e = 0$) the decay factor, calculated from a least squares fit to Equation (16), is 0.071. The decay factor reduces to 0.062 when the annular-to-primary total pressure ratio ($P_{c\,a}/P_e$) is 0.303. At this condition the annular flow is approximately one-third of the primary flow.

Figure 29 shows additional test results obtained with annular flow. This figure gives a graphical representation of the relation between the calculated plate decay factors and the force ratio, $P_{c\,a} A_{ca}/P_e A_e$. In general, the decay factor decreases until the force ratio is about 0.08. This force ratio corresponds roughly to the control pressure required to make the turbulence intensity peaks (at the nozzle exit) about equal. An increase in force ratio above 0.08 causes an increase in plate decay factor. In the low force ratio range the largest decay factor changes occur when $D_a = 0.550$ in. and $S = 0.125$ in. At higher force ratios, larger changes occur when the setback is 0.250 in. The effect of an increase in annular nozzle size is small in the low force range but a large difference in plate factor occurs in the high force ratio range. Deliberate lateral misalignments of the

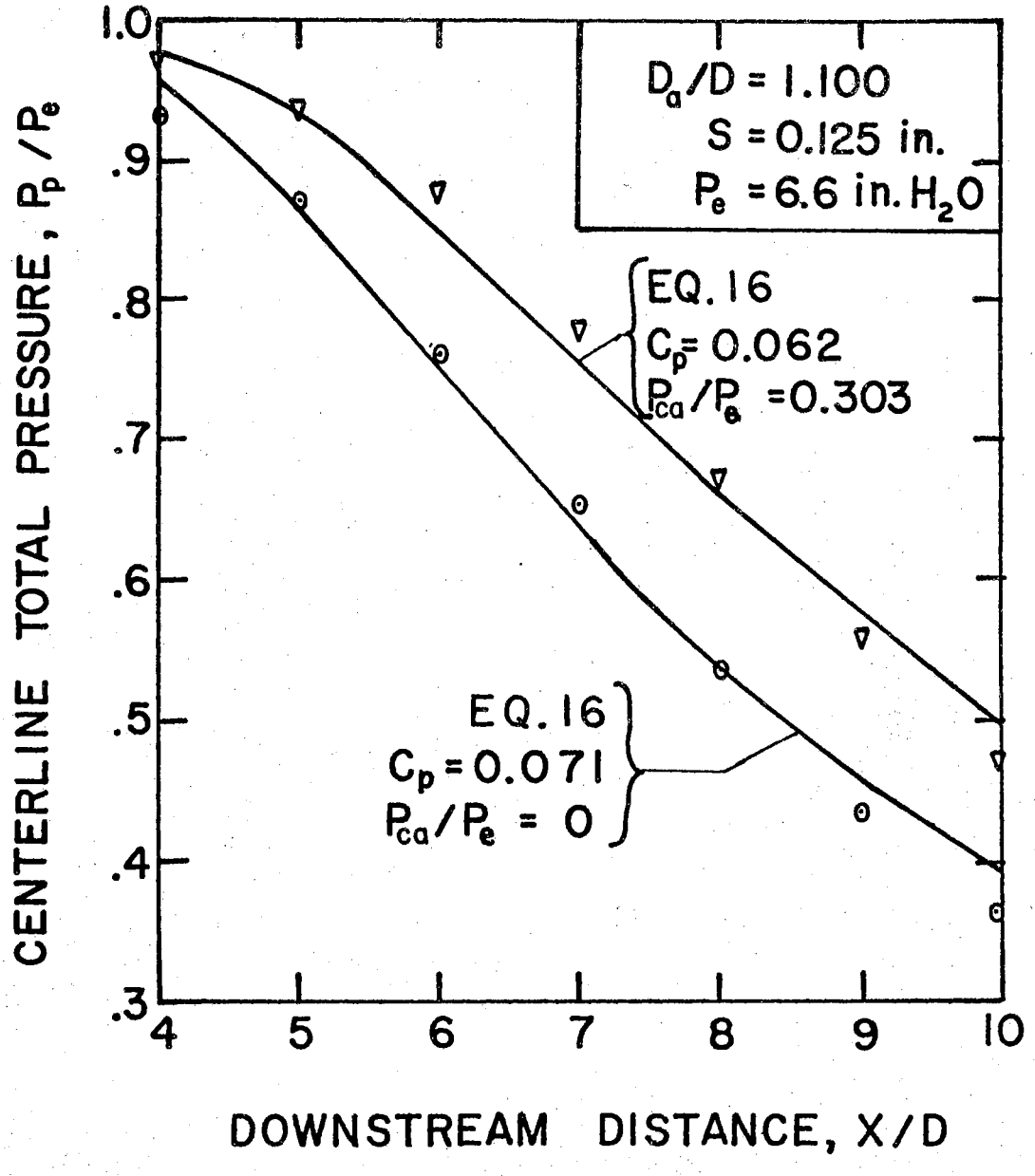

Figure 28. The Effect of Annular Control on Centerline Pressure Distribution

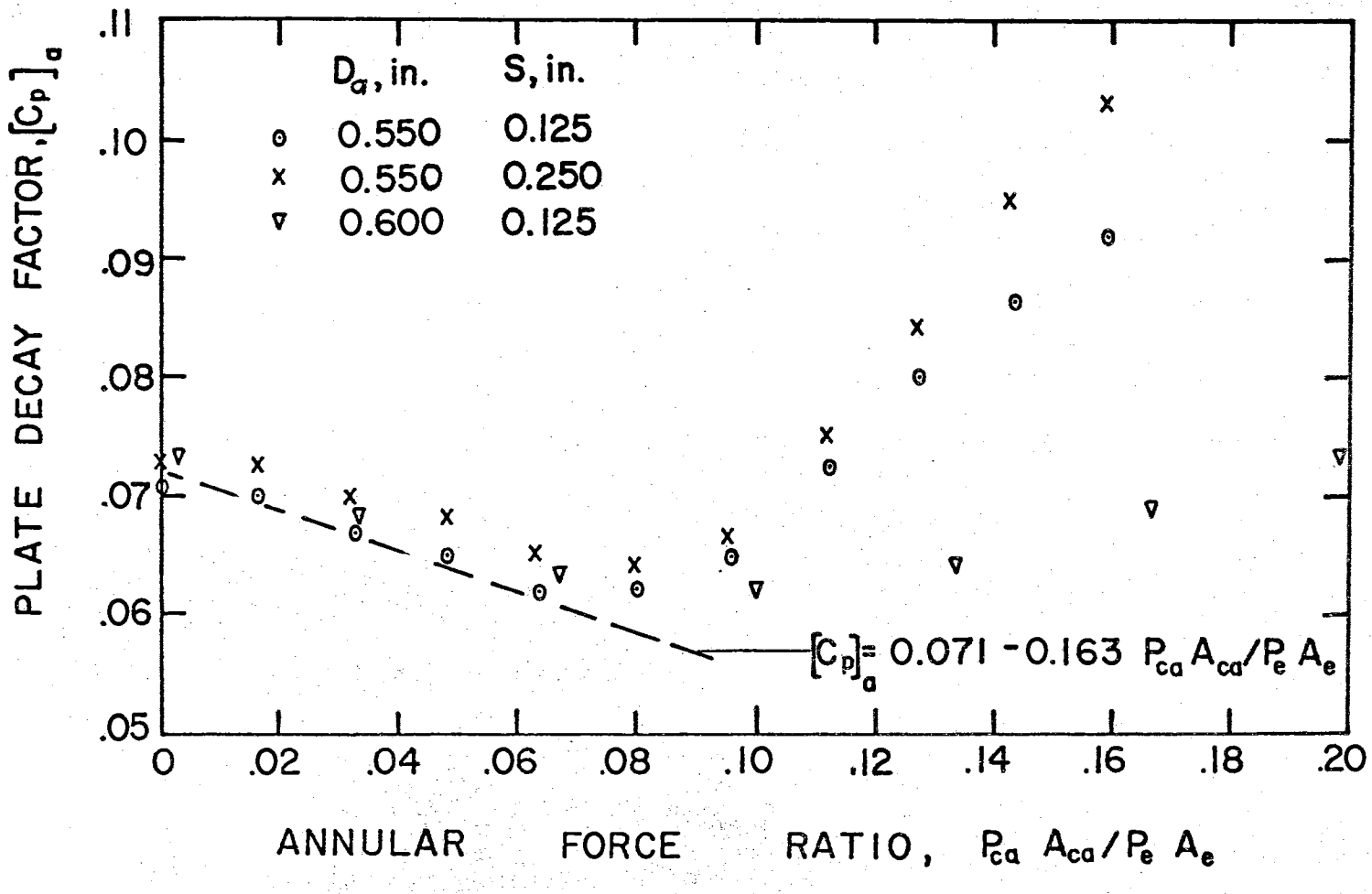

Figure 29. The Effect of Annular Momentum on Plate Decay Factor

orifice plate (as much as 0.1 D_a) did not affect the overall characteristics of the centerline decay.

Effects of Transverse Control Pressure on Jet Decay

The primary and auxiliary nozzles are perpendicular to each other in the transverse control experimental arrangement (Figure 24a). The primary nozzle is identical to that used in the experiments without auxiliary flow (Figure 12b). To supply the transverse flow, a control plennum is fabricated that accommodates either 0.250 in. or 0.500 in. diameter control nozzles. In all cases the primary and auxiliary nozzle centerlines are in the same horizontal plane.

Figure 30 shows the turbulence intensity measurements taken along the auxiliary nozzle axis and across the primary nozzle at X/D = .250. In this test the transverse control nozzle is 0.250 in. The horizontal scale on Figure 30 is broken and expanded to show the details of the turbulence intensity peaks. Three different control pressure levels (P_{ct} = 0, 1, and 2 in. H_2O) are represented. At all of these levels there is only one peak. However, the magnitude of the peak varies around the nozzle. The peak on the side nearer the application of control pressure signal increases in magnitude and moves towards the axis. The displacement is the result of penetration into the primary jet by the control jet. On the side opposite the control nozzle, the turbulence intensity peaks remain essentially unchanged in both magnitude and position with the application of a control signal.

Figure 31 shows the turbulence measurements made across the face of the transverse control nozzle close to its exit. The turbulence intensity parameter in Figure 31 is based on the centerline velocity of the

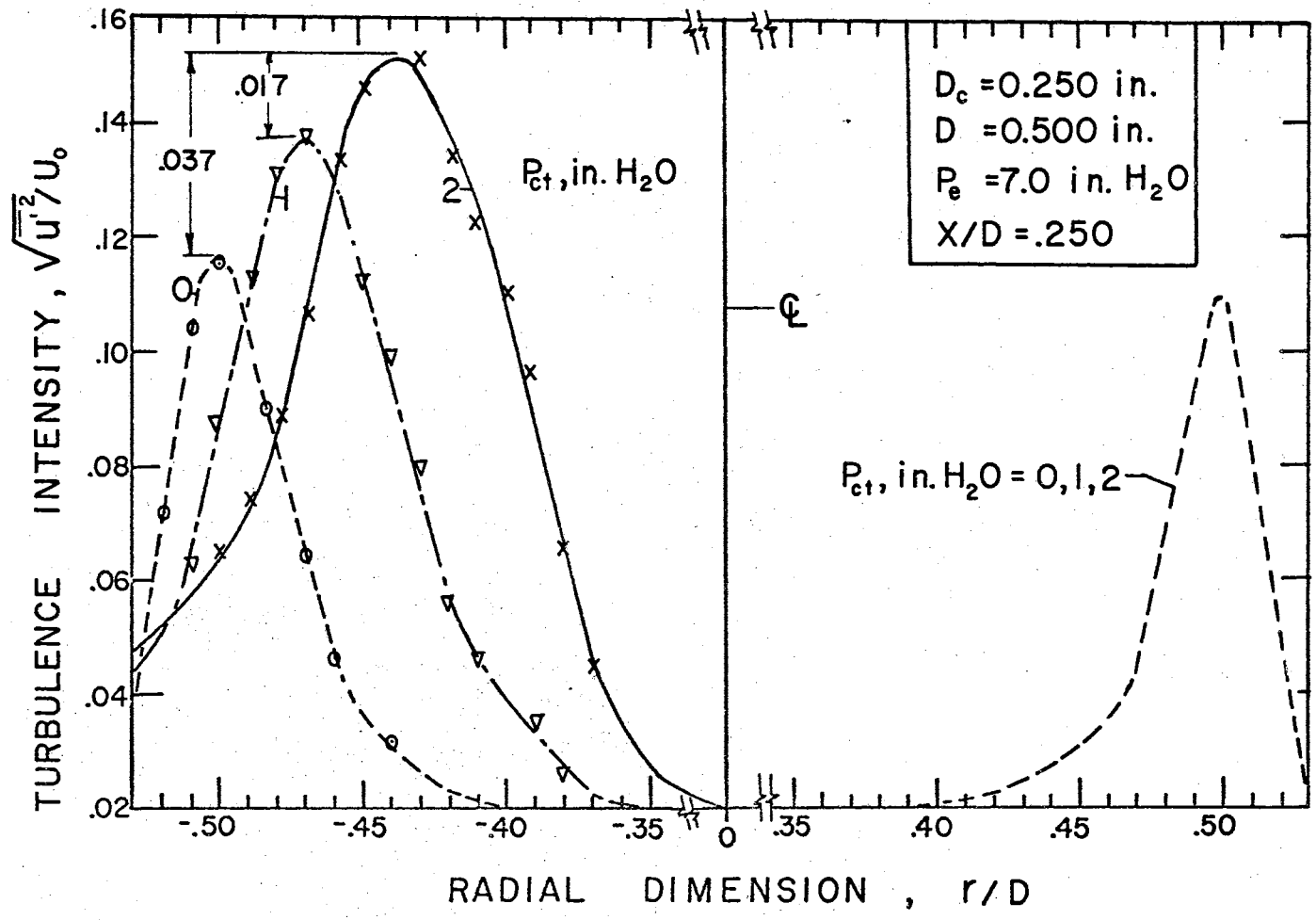

Figure 30. Turbulence Intensity Profiles of Nozzle with Transverse Flow (X/D = 0.250)

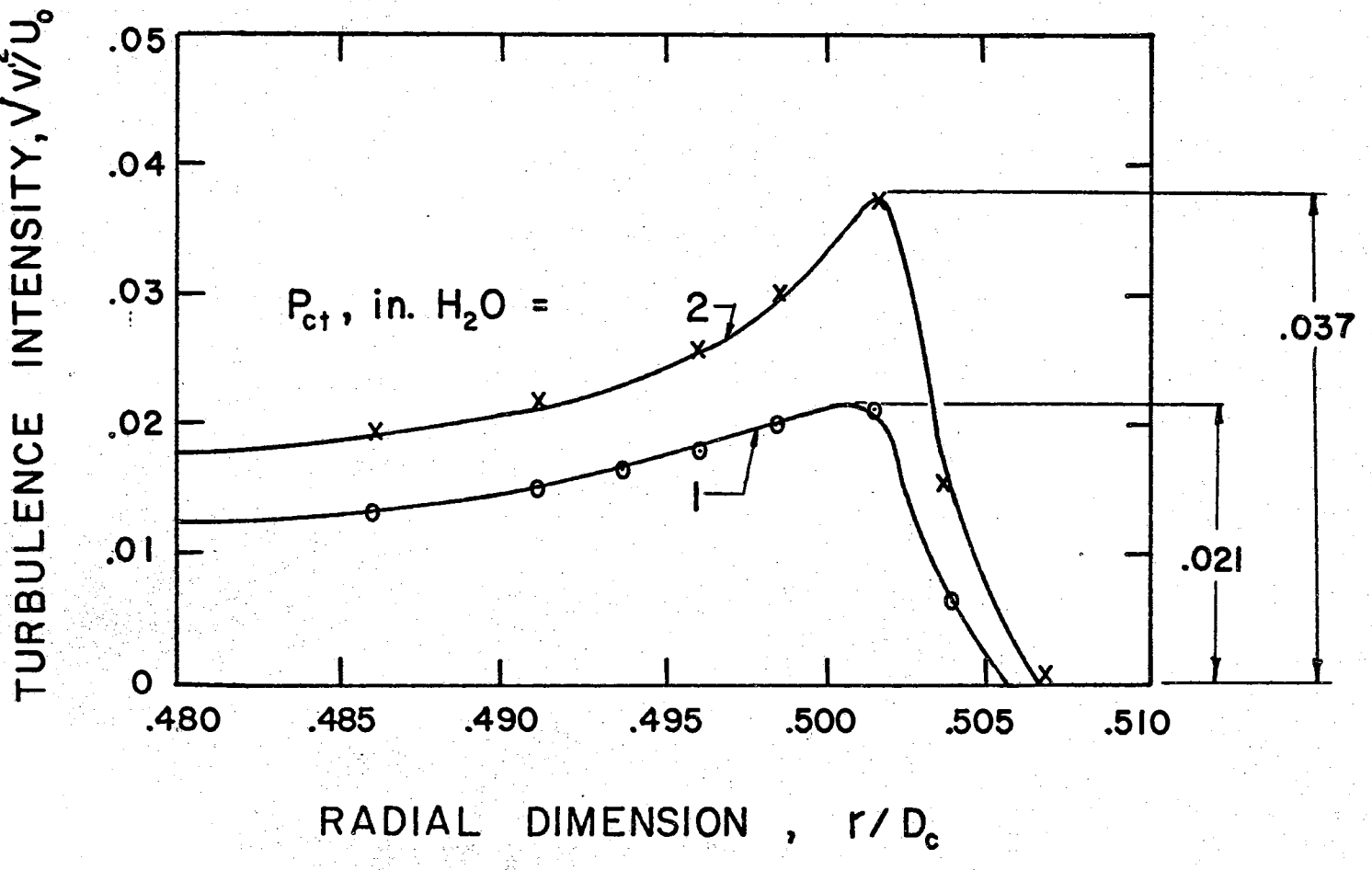

Figure 31. Turbulence Intensity Profiles at Exit of Transverse Nozzle

primary flow. The reason for this representation is that the turbulence fluctuations of the transverse control appear to augment those of the primary jet. For example, the peak turbulence intensity parameter, calculated for the transverse jet at P_{ct} = 2 in. H_2O, is 0.037. This amount is identical to the increase in turbulence intensity peak of the primary jet (Figure 30) for the same change in transverse control pressure. Similarly at P_{ct} = 1 in. H_2O, the control turbulence peak parameter is 0.021; whereas, the primary turbulence peaks differ by 0.020. More extensive measurements are needed to identify fully the effect of control jet turbulence intensity on the emitter jet turbulence intensity.

Figures 32 and 33 show some additional turbulence intensity measurements taken at X/D = 2 and X/D = 4. These figures show the gradual development of the turbulence intensity into the familiar symmetric pattern. The turbulence intensity peaks on each side of the centerline tend to equalize in magnitude and approach each other.

Figure 34 shows profiles measured with a total pressure probe six nozzle diameters from the primary nozzle exit. There is no correction for turbulence intensity in the total pressure data presented. Even with the increase in turbulence intensity caused by the control jet, the correction is small (less than 1 per cent). In this case, the transverse control nozzle has an 0.500 in. diameter. With no transverse flow (P_{ct}/P_e = 0) the horizontal and vertical profiles are the same. Upon the application of a control signal (P_{ct}/P_e = 0.035), the horizontal profile (Figure 34a) shows a decay of peak pressure, a small lateral displacement, and an apparent narrowing of the jet. A vertical profile taken at the horizontal position of maximum total pressure

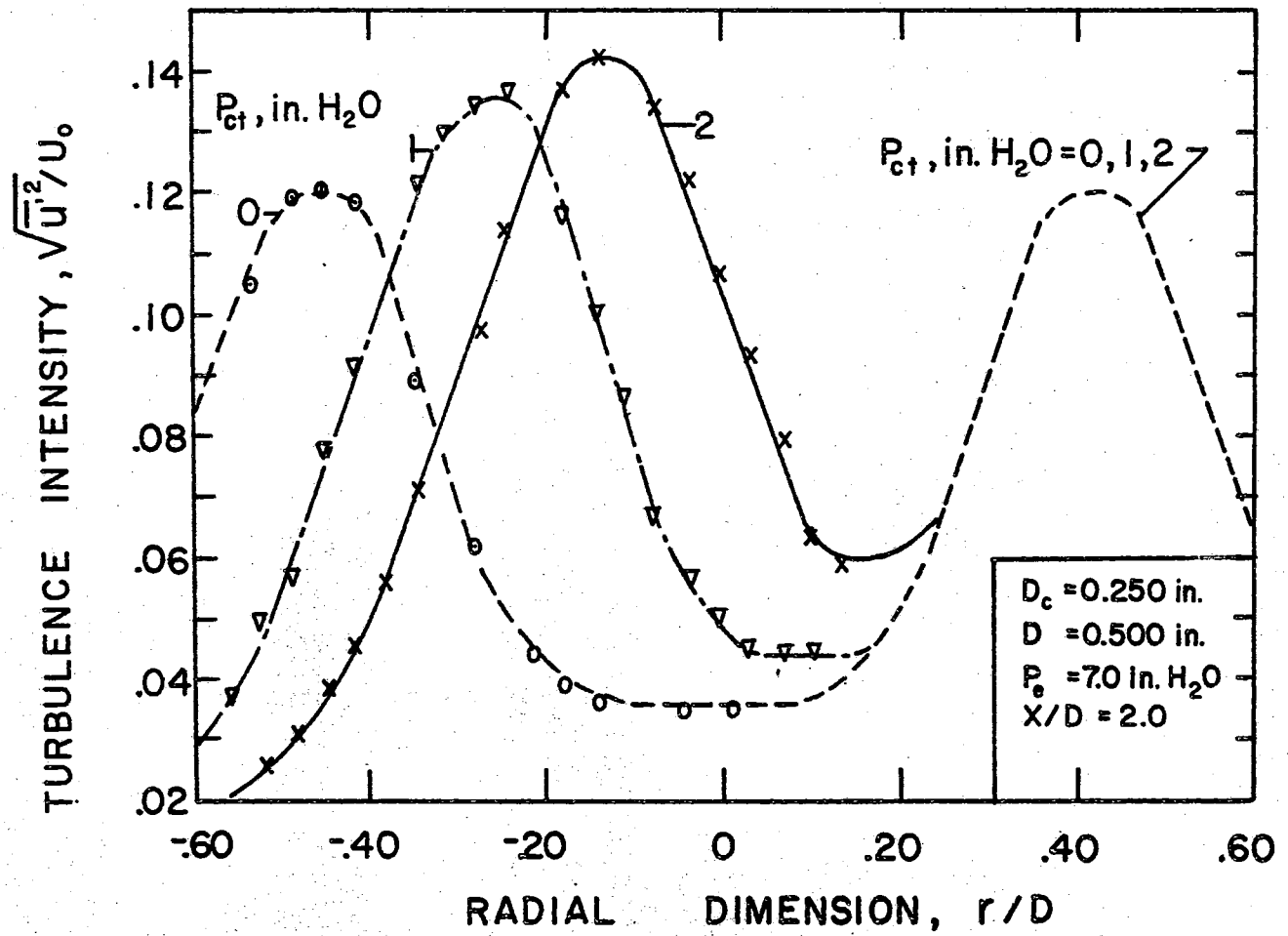

Figure 32. Turbulence Intensity Profiles of Nozzle with Transverse Flow (X/D = 2.0)

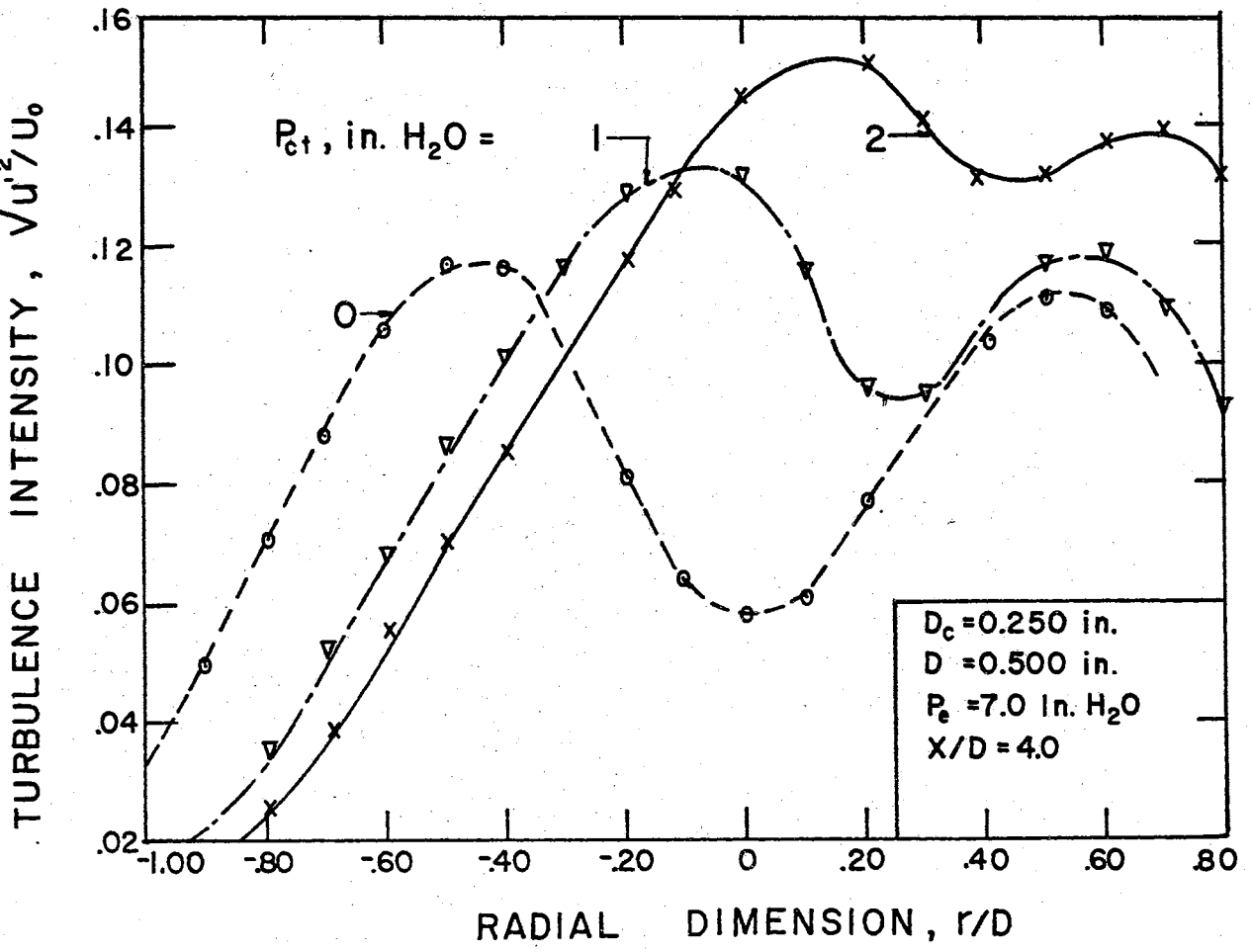

Figure 33. Turbulence Intensity Profiles of Nozzle with Transverse Flow (X/D = 4.0)

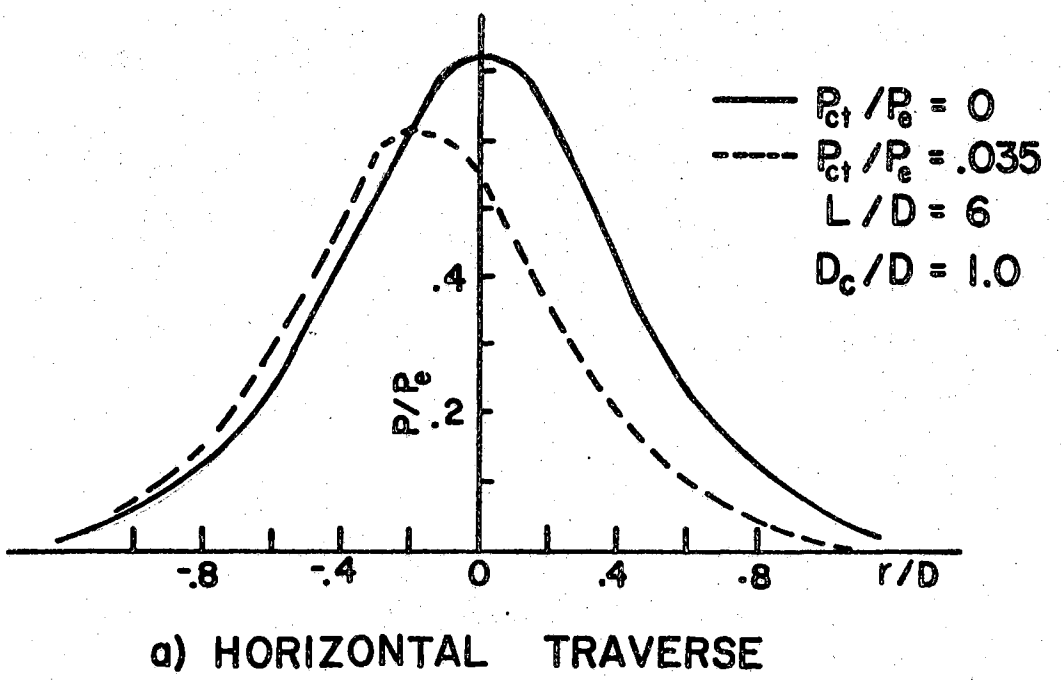

a) HORIZONTAL TRAVERSE

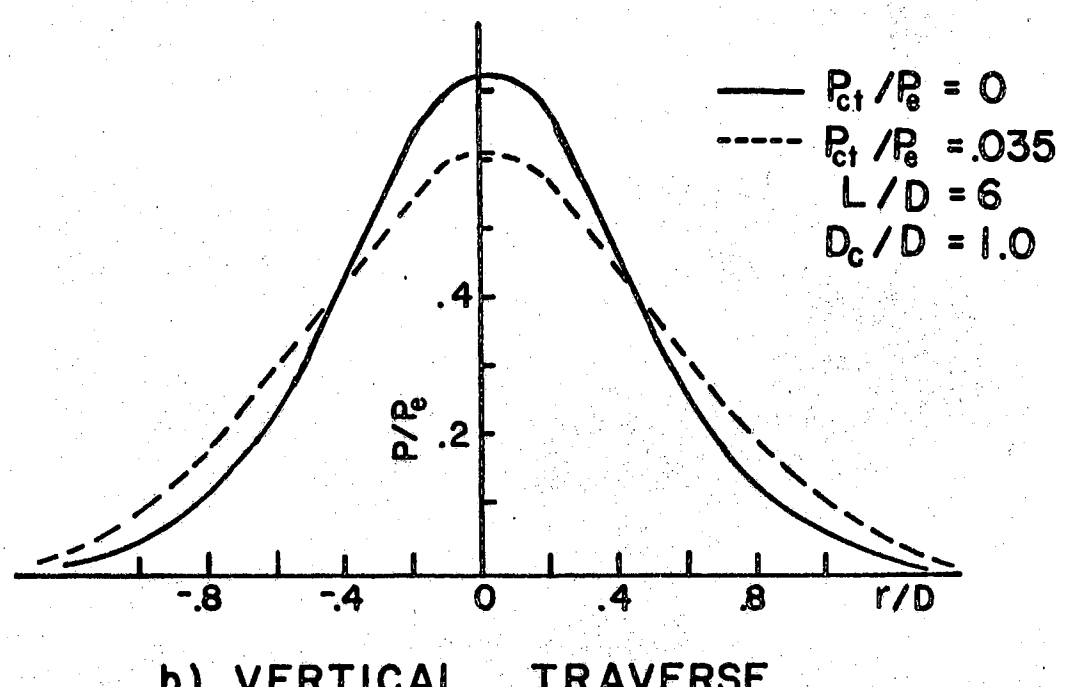

b) VERTICAL TRAVERSE

Figure 34. The Effect of Transverse Flow on Total Pressure Profiles

shows a widening (Figure 34b). Thus, transverse flow produces asymmetry in the jet flow, but the axial momentum of the jet is conserved. The results of the axisymmetric jet deflection measurements are different than those on two-dimensional jets. In the two-dimensional jet, the peak of the deflected jet maintains the same magnitude as the undeflected jet (Appendix A).

Figure 35 shows the corresponding turbulence intensity measurements. The predominant effect of transverse flow is to increase the turbulence intensity, and this in turn, increases the decay of the primary jet. Boyd and Barbin (17) have already shown that transverse flow above a certain threshold results in an earlier transition from laminar to turbulent jet flow. Another effect of transverse flow is to induce fully developed turbulence closer to the primary nozzle.

Figure 36 shows some typical "peak" total pressure decay curves. The total pressures are not centerline values because of the deflection of the jet. Nevertheless, the form derived for centerline decay (Equation(21)) fits the experimental data and also provides a convenient measure of the influence of transverse control.

Figures 37 and 38 show the relation between plate decay factor and transverse-to-primary force ratio for D = 0.500 in. and D = 0.125 in., respectively. For the 0.500 in. diameter emitter nozzle (Figure 37), the results indicate a larger increase in the plate decay factor with a 0.250 in. diameter control nozzle than with the 0.500 in. diameter control nozzle. The reason for the increased effect is that the smaller control jet contacts the primary jet in a more effective way. When the control nozzle and the emitter nozzle are the same size, some of the transverse control force passes above and below the emitter jet

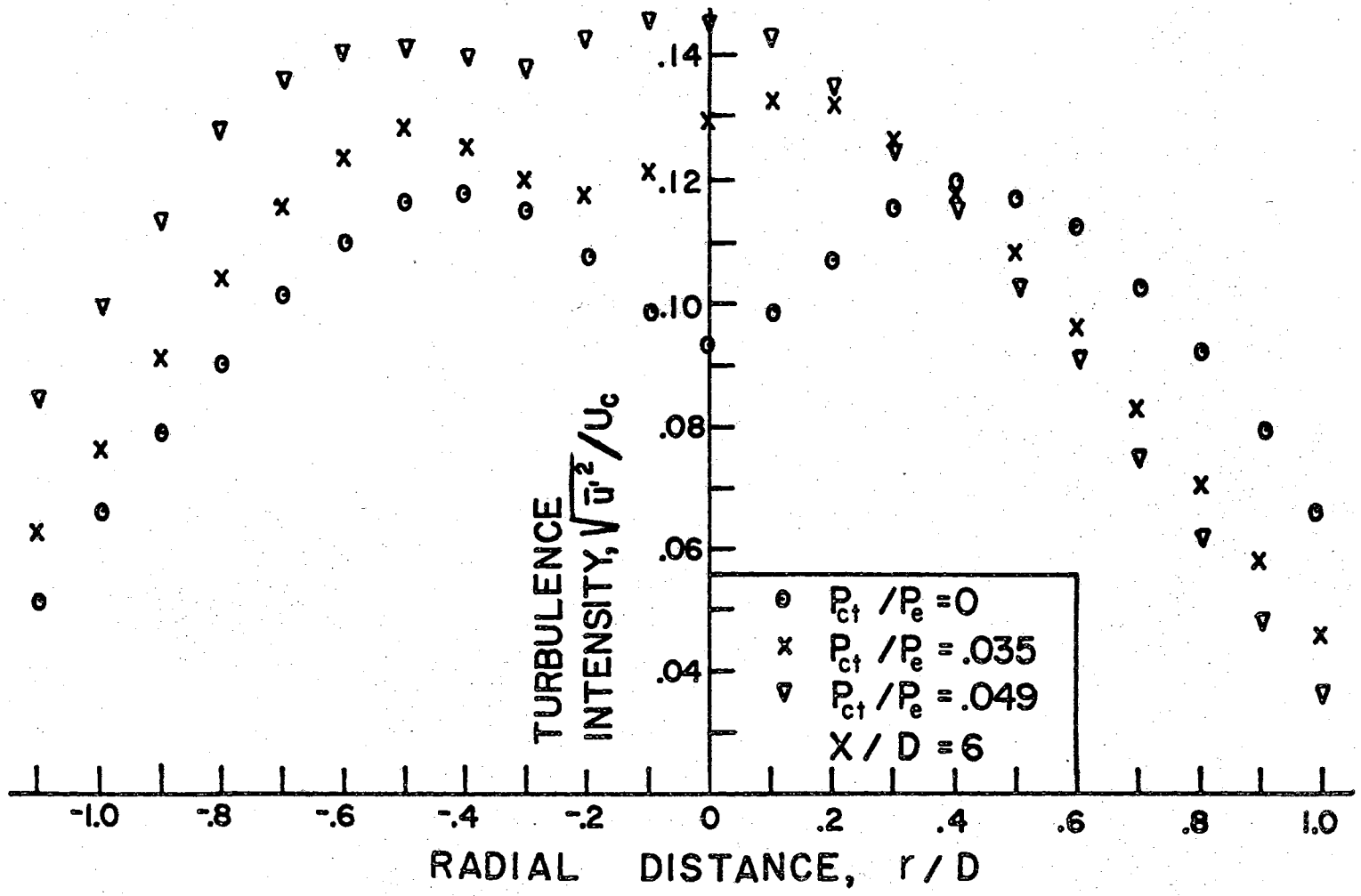

Figure 35. Turbulence Intensity Profiles of Nozzle with Transverse Flow (X/D = 6.0)

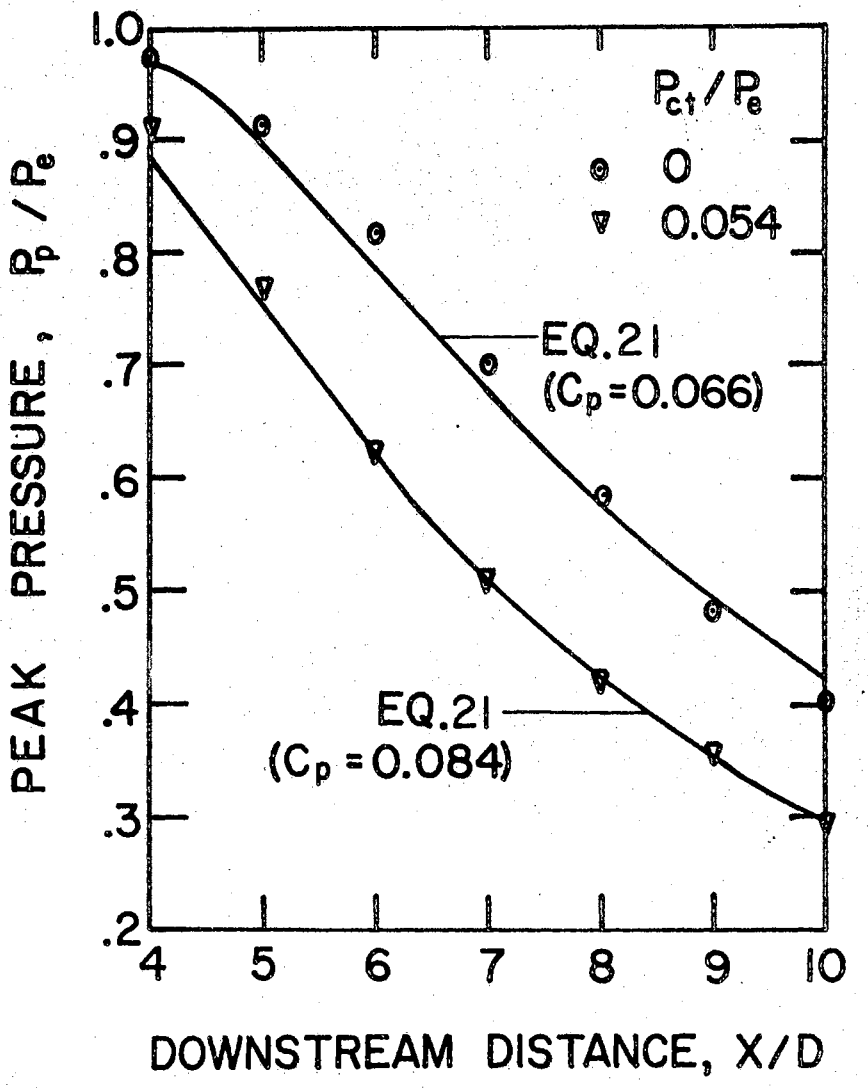

Figure 36. The Effect of Transverse Control on the Peak Pressure Distribution

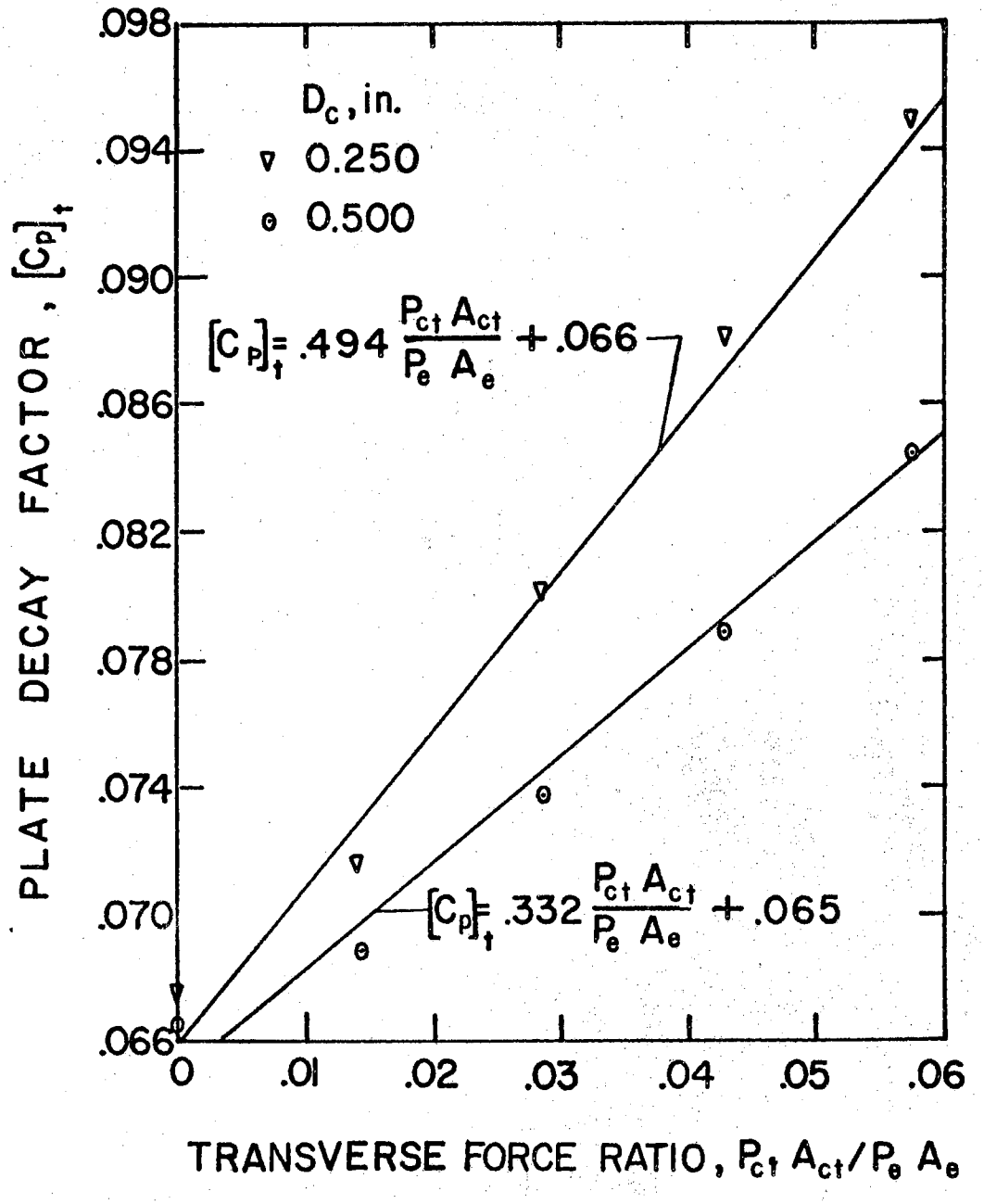

Figure 37. The Relation Between Transverse Momentum and Plate Decay Factor (D = 0.500 in.)

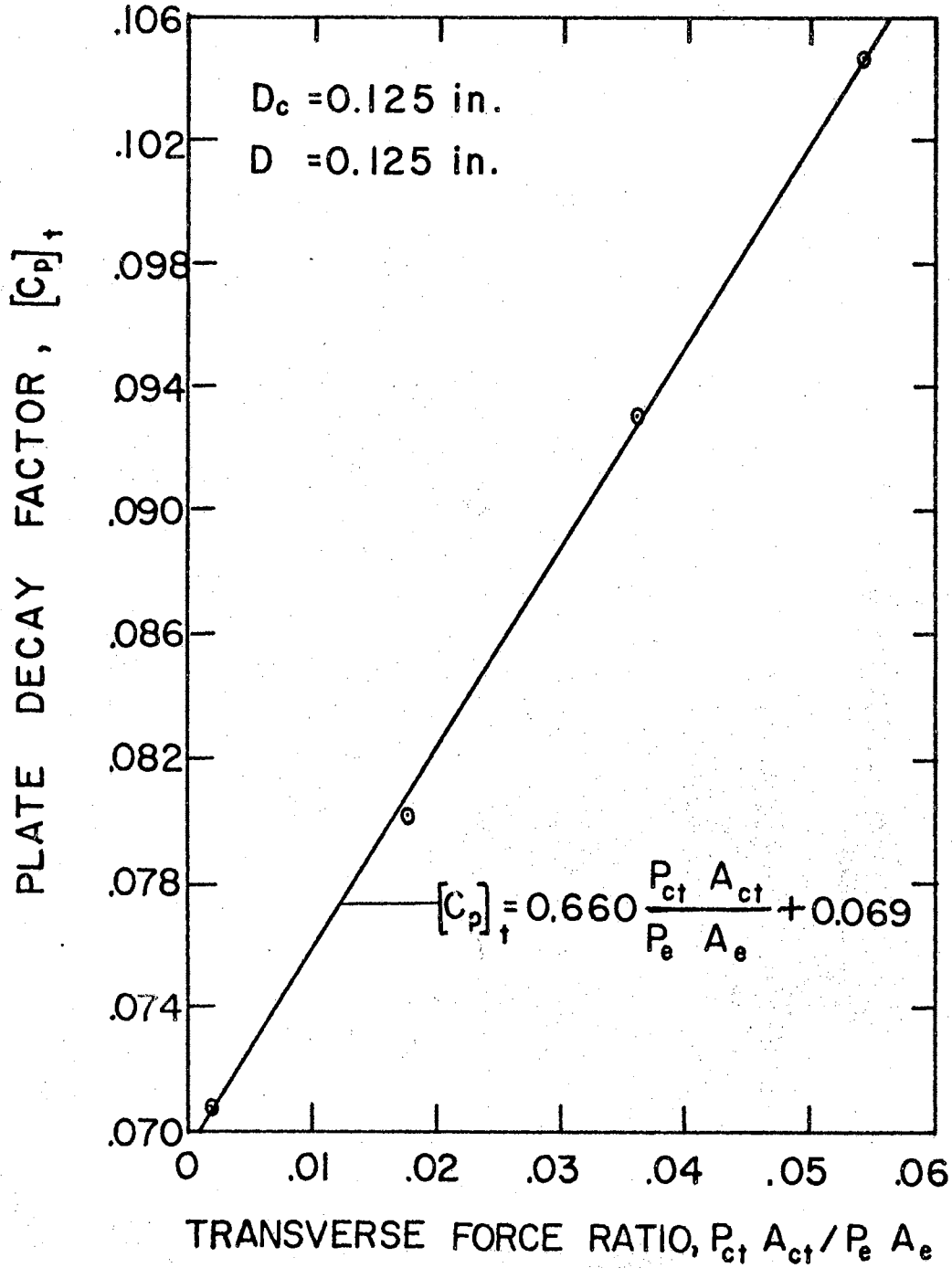

Figure 38. The Relation Between Transverse Momentum and Plate Decay Factor (D = 0.125 in.)

and is, therefore, wasted. At the same force ratio, the smaller control nozzle causes a 50 per cent larger change in the decay factor than the larger control nozzle. For the 0.125 in. emitter nozzle (Figure 38) an equal size transverse control nozzle is more effective in changing the decay factor than either of the control nozzles on the larger unit. The reason for this may be that the control inserts on the larger unit are long enough to build up a boundary layer at the control nozzle exit. If the control jet turbulence intensity always increases the primary jet turbulence intensity, then the longer control nozzle reduces the intensity of the control jet and, in turn, the primary jet. In general, then, the largest effects would seem to occur when the transverse control jet is small and turbulent.

Expressions for Emitter Jet Modulation and Impinging Jet Flow

From the foregoing, the expressions for the plate decay factor given in Equation (1) and modified in Equation (26) are:

1. Emitter Modulation

$$\left[C_p\right]_e = \text{Constant} \tag{27a}$$

The magnitude of the constant depends on the emitter pressure, the nozzle size, and the nozzle shape. This constant can be determined from centerline decay measurements on a flat plate and Equation (21).

2. Annular Modulation (Low range)

$$\left[C_p\right]_a = \left[C_p\right]_{ea} - K_a \frac{P_{ca}}{P_e} \left[\frac{D_a^2}{D^2} - 1\right] \tag{27b}$$

where K_a is the constant associated with annular control. The present measurements (Figure 29) give its value as 0.163 in the low force ratio range.

3. Transverse Modulation

$$\left[C_p\right]_t = \left[C_p\right]_{e\,t} + K_t \frac{P_{c\,t}}{P_e}\left(\frac{D_c^2}{D^2}\right) \qquad (27c)$$

where K_t is the constant associated with transverse control. According to the measurements (Figure 37) on the 0.500 in. diameter primary nozzle, K_t is 0.332 when $D_c/D = 1.0$ and is 0.494 when $D_c/D = 0.5$. In the case of the 0.125 in. diameter nozzle (Figure 38), K_t is 0.660.

Equations (27b) and (27c) present linear expressions for the relations between flat plate decay factor and force ratio. Figures 29, 37, and 38 indicate the fit of the linear forms to the data.

CHAPTER VI

STREAMSURFACE SHAPE AND SOURCE CHARACTERISTICS

The dividing streamsurface acts as a connection between the internal flow processes. Thus, the conceptual model requires some detailed information on streamsurface characteristics. Since an analytical treatment of the streamsurface is difficult, this investigation deals with the streamsurface experimentally.

Figure 39 shows a schematic drawing of the experimental apparatus used to determine the streamsurface shape and source flow modulation. The nozzles are 0.500 in. in diameter. Tests are conducted by fixing the source pressure and measuring Z(O), Z(R), and Q_s for different emitter pressures. The centerline distance (Z(O)) is measured by traversing a 0.031 in. O.D. static pressure probe along the nozzle axis and observing the position of the maximum pressure reading. The measurement of the curtain distance (Z(R)) follows a similar procedure except that the probe is a 0.031 in O.D. total pressure probe. For the curtain distance measurement the probe traverse is parallel to the jet axis but displaced by a distance equal to the radius of the source nozzle. In both cases, the assumption is that the location of the maximum pressure reading corresponds to the streamsurface position. Near cutoff and when the streamsurface moves inside the source nozzle, the centerline static pressure traverse produces pressure readings that are too flat to give a clear indication of the centerline position. In

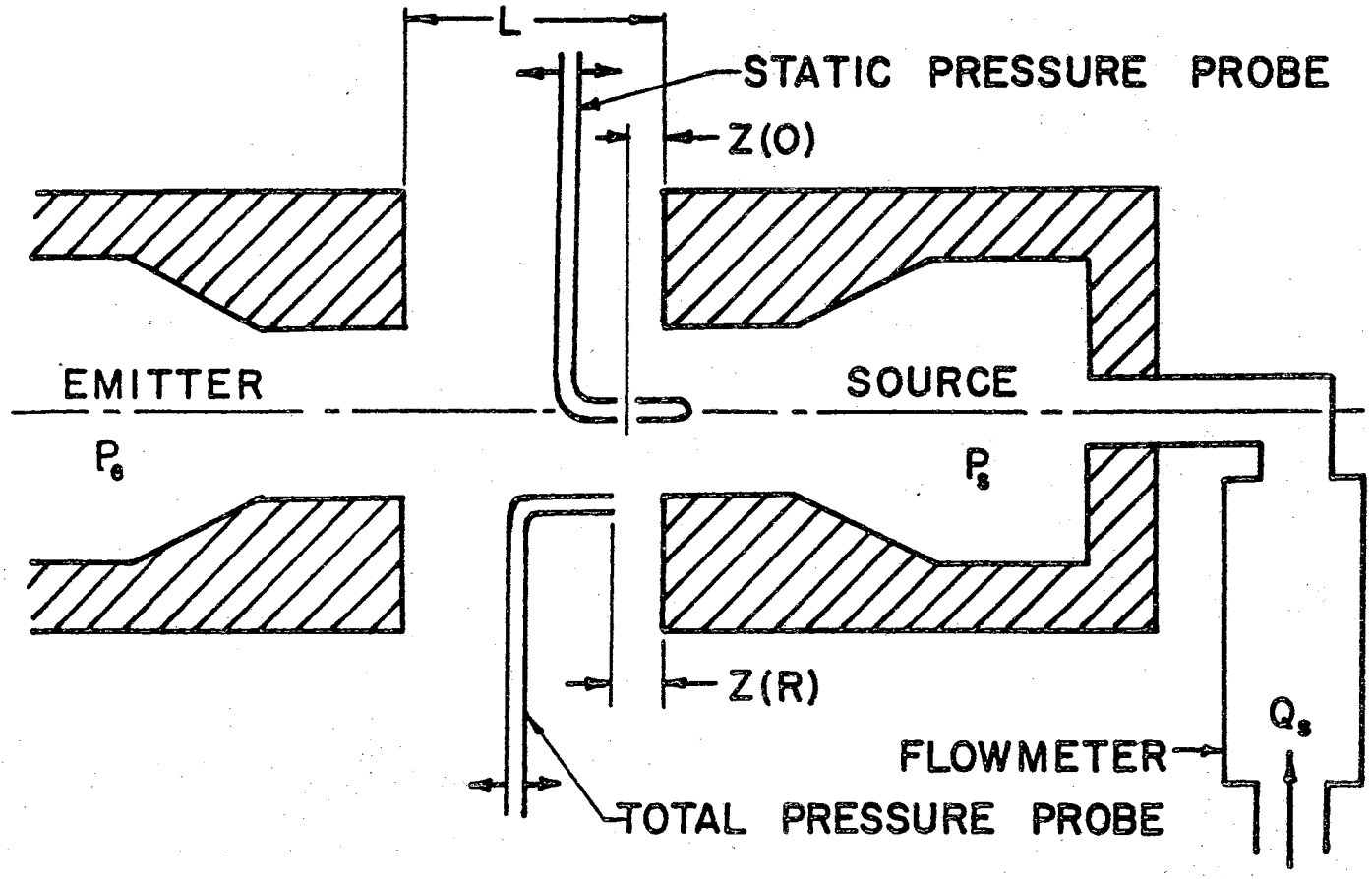

Figure 39. Experimental Apparatus for Measuring Streamsurface Position

this case Z(0) for cutoff is calculated from Equation (21) with the flat plate pressure ratio (P_p/P_n) equal to the cutoff pressure ratio (P_s/P_e) and $X_p = L - Z(0)$.

Results of Streamsurface Shape Experiments

Figure 40 shows the results (see Appendix B for data) of the centerline and curtain position measurements for tests at five different nozzle spacings from 5 to 9 nozzle diameters. In the operating range, the curtain distance is always small and varies between 0 and about 0.2 D. On the other hand, the centerline distance has values between -0.5 D and +0.6 D. The results show a slight dependency on nozzle spacing. At larger spacings, where the emitter jet has spread more, the curtain distances tend to be smaller.

Figure 41 shows the construction of some approximate dividing streamsurfaces from the centerline and curtain distance data of Figure 40. At cutoff (Z(R) = 0), the dividing streamsurface lies entirely within the source nozzle. The corresponding centerline distance is calculated at about Z(0) = -0.5 D. In this position the dividing streamsurface is concave. As the emitter pressure decreases and flow leaves the source nozzle, the dividing streamsurface flattens. The data indicates that the streamsurface is flat when Z(R) = Z(0) = 0.055 D. This occurs relatively close to the source nozzle exit. If the emitter pressure decreases further, the curvature of the streamsurface reverses. At the beginning of modulation (Z(R) = 0.200 D and Z(0) = 0.550 D), the streamsurface is convex. However, this investigation considers only a limited portion of the streamsurface ($r < D/2$). The entire streamsurface has a double curvature.

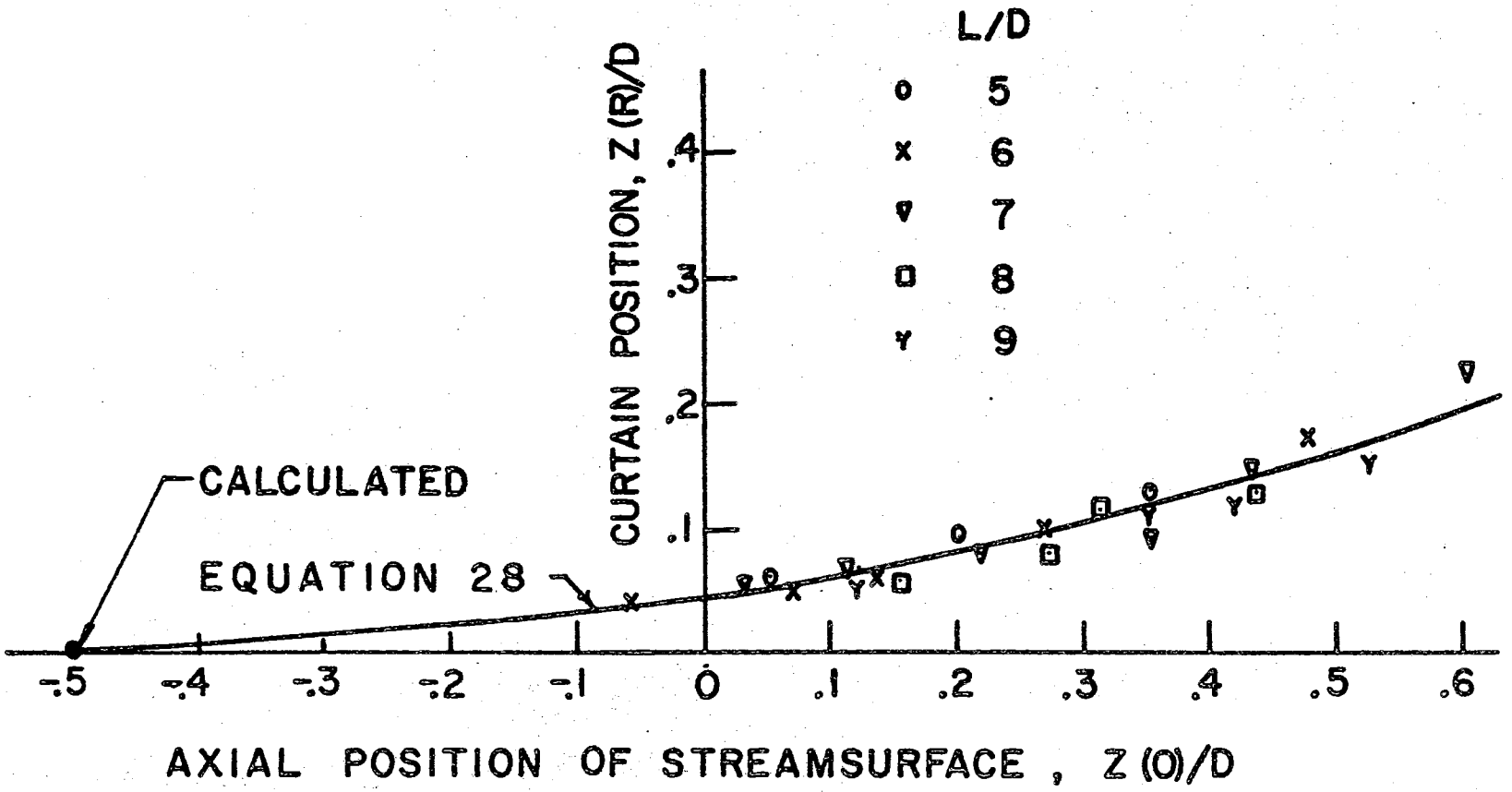

Figure 40. Relation Between Centerline and Curtain Positions of the Streamsurface

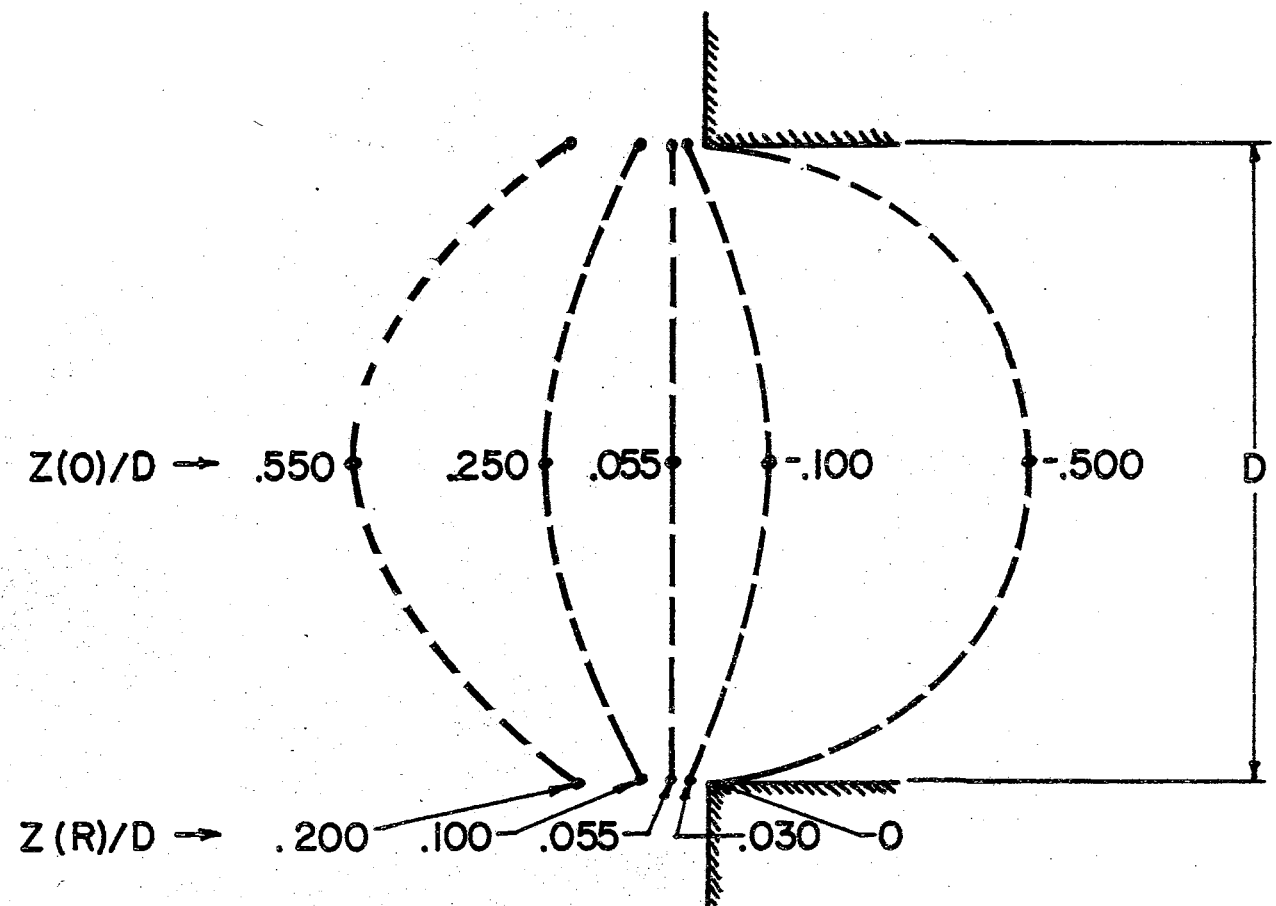

Figure 41. Streamsurface at Several Balance Positions

Expression for Streamsurface Shape

Figure 42 shows the data presented in Figure 40 on a log-log scale. To avoid negative values, a factor of 0.5 D is added to the centerline distance data. On the log-log representation, the experimental data fall approximately on a straight line that has a slope of 2. This suggests that a parabolic expression is appropriate for the streamsurface shape relation. The form of the relation becomes:

$$\frac{Z(R)}{D} = K_s \left[\frac{Z(0)}{D} + 0.5\right]^2 \qquad (28)$$

where K_s is a shape constant. The empirical expression developed in Equation (28) corresponds to the functional relationship formulated in Equation (3).

Calculations from the data, by the method of least squares, give a value of 0.16 for the shape constant. This is the value of K_s used in Chapter VIII to compare the model with the experimental characteristics.

Results of Source Flow Modulation Experiments

A total pressure probe traverse in the axial direction (but displaced from the axis) determines the curtain distance (Figure 39). Figure 43 shows the measured pressure distribution from some typical traverses (data in Appendix B) at a nozzle spacing of 6 diameters. The three traverses in Figure 43 represent the beginning of modulation range, the mid-range, and the cutoff range. Near the beginning of flow modulation ($Q_s/Q_m = 0.94$), the pressure at the nozzle exit is slightly less than atmospheric. The pressure builds up to a maximum at about

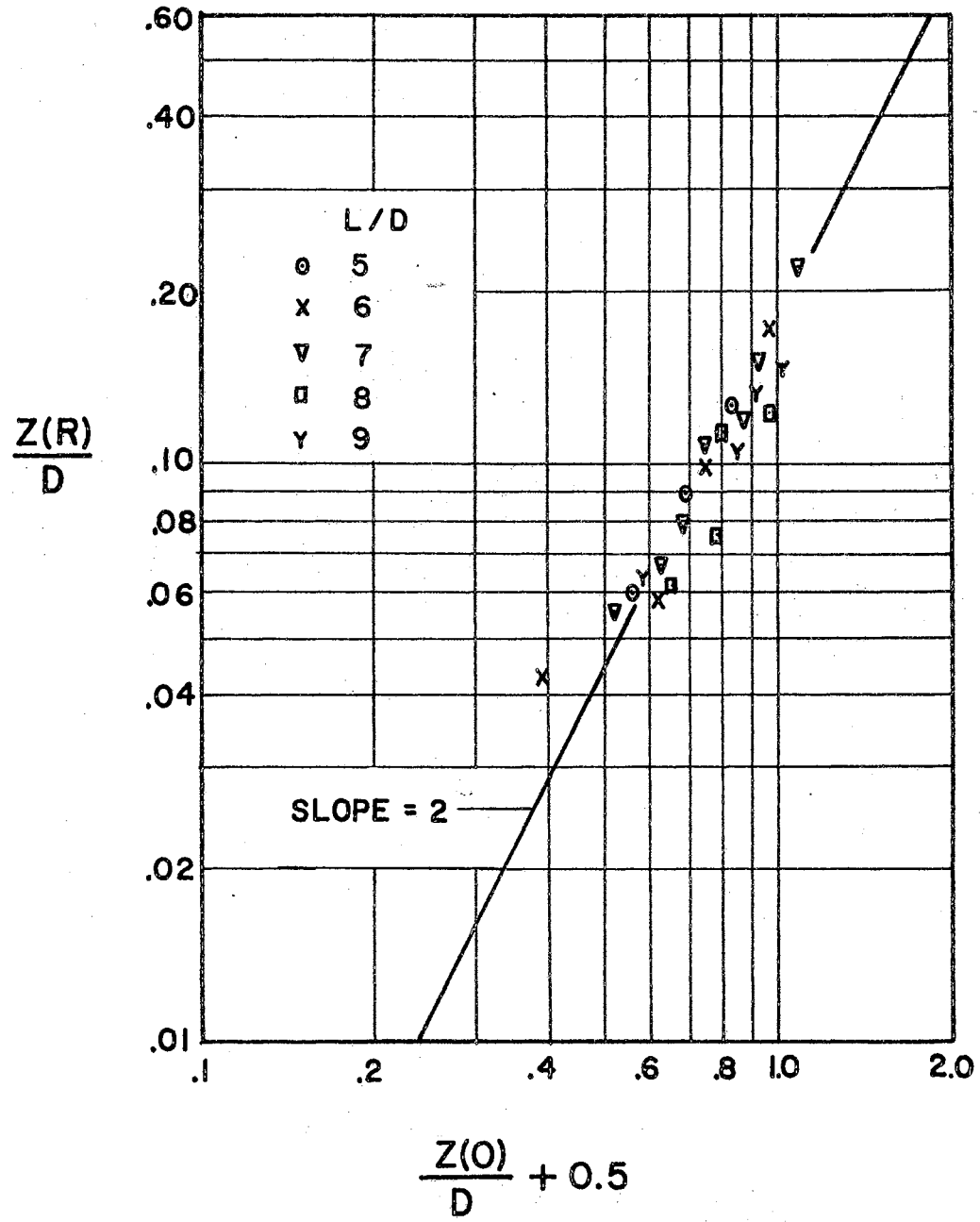

Figure 42. Streamsurface Positions on Log-Log Plot

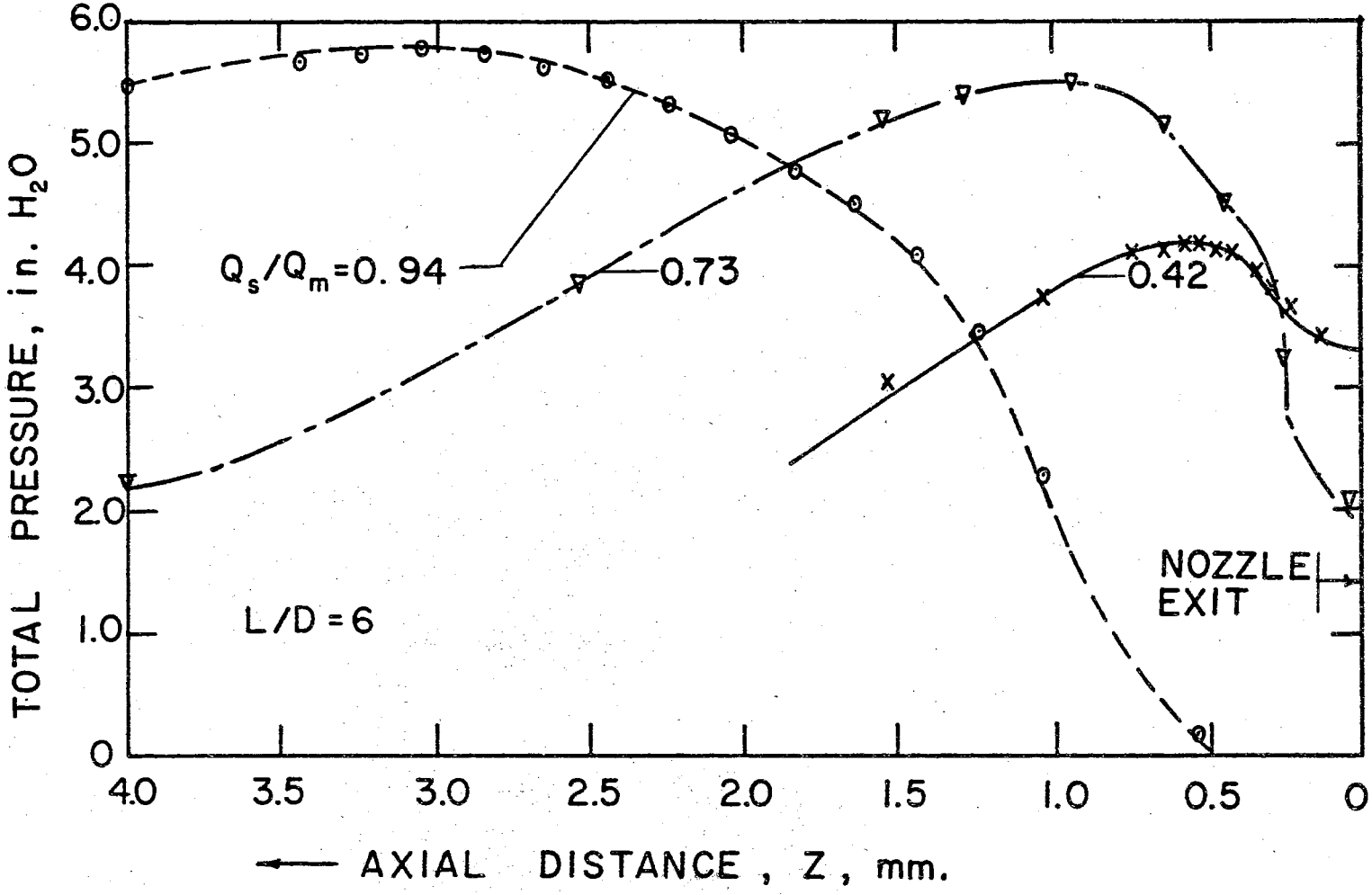

Figure 43. Total Pressure Distributions (r = R)

0.250 D (3.0 mm). For mid-range (Q_s/Q_m = 0.73) the probe reaches a maximum pressure at 0.080 D (1.0 mm.) from the source nozzle exit. Near cutoff (Q_s/Q_m = 0.42) the maximum occurs at 0.054 D (0.6 mm.). Although the pressure traverses are somewhat flat at the peak values, the positions of the maxima are clearly discernible.

Each traverse provides one data point of Q_s/Q_m vs. Z(R)/D. Figure 44 shows the relation between the distance at the maximum pressure value and the source flow during the traverse. Figure 44 also shows the flow modulation properties of a flat plate. In all the tests, the stream-surface obstruction allows more source flow than a flat plate at the same distance. The solid flat plate is not a good model for the dividing streamsurface because of the zero velocity condition at the surface of the plate.

Expression for Source Flow Modulation

The general shape of the data suggest an exponential relation between source flow (Q_s/Q_m) and curtain distance (Z(R)/D). To investigate this possibility, Figure 45 shows the data of Figure 44 on semi-log paper. The parameter, ($1-Q_s/Q_m$), is the ordinate instead of Q_s/Q_m because the data approaches $Q_s/Q_m = 1$. The semi-log graph (Figure 45) is almost linear for values of $1-Q_s/Q_m$ above 0.1. Since values less than 0.1 occur only in the region of amplifier saturation, the selection of an exponential form to represent the source flow relation is reasonable. The expression that corresponds to the functional relation of Equation (4) is:

$$Q_s/Q_m = 1 - \exp\left[-K_q Z(R)/D\right] \qquad (29)$$

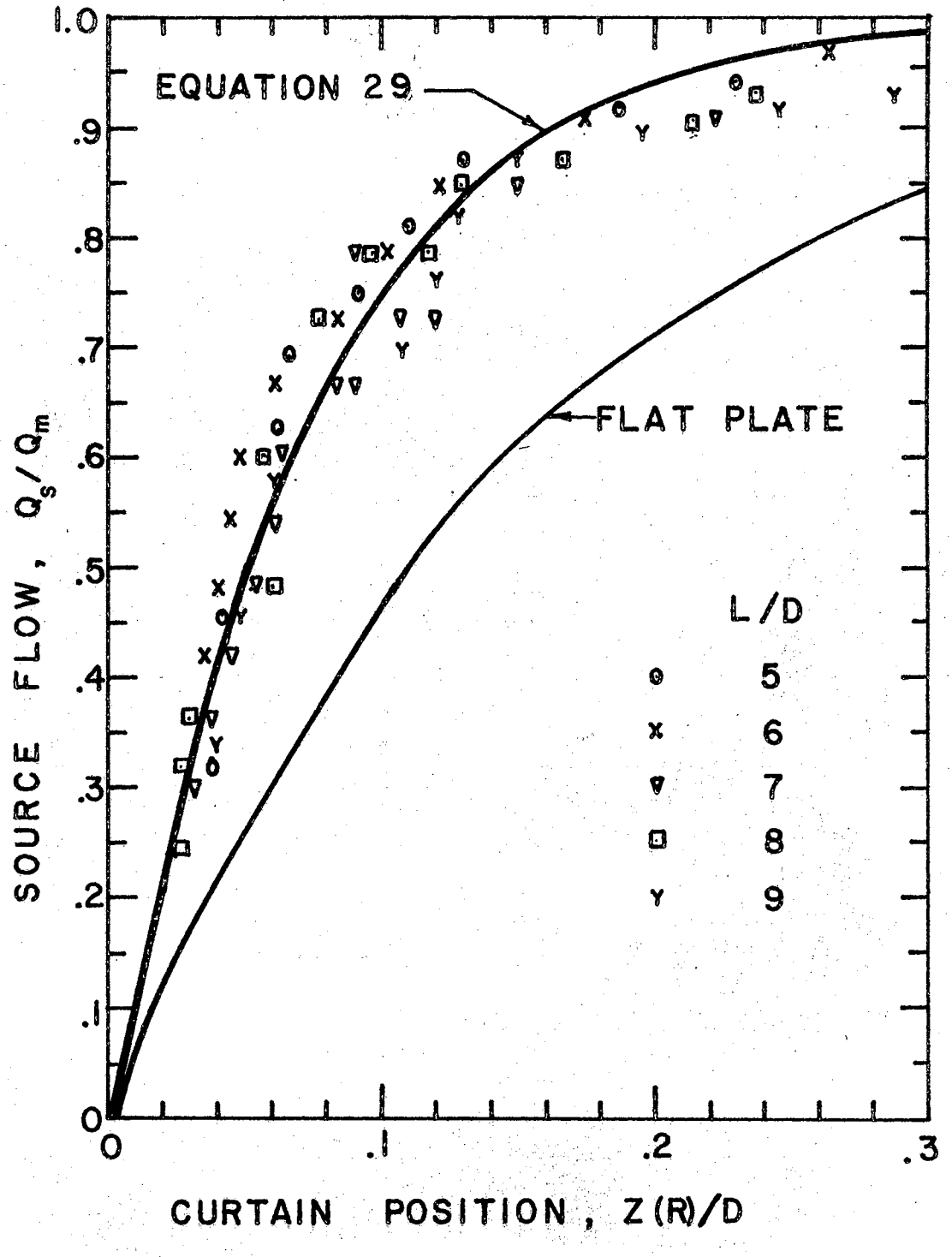

Figure 44. Source Flow Modulation as a Function of Curtain Distance

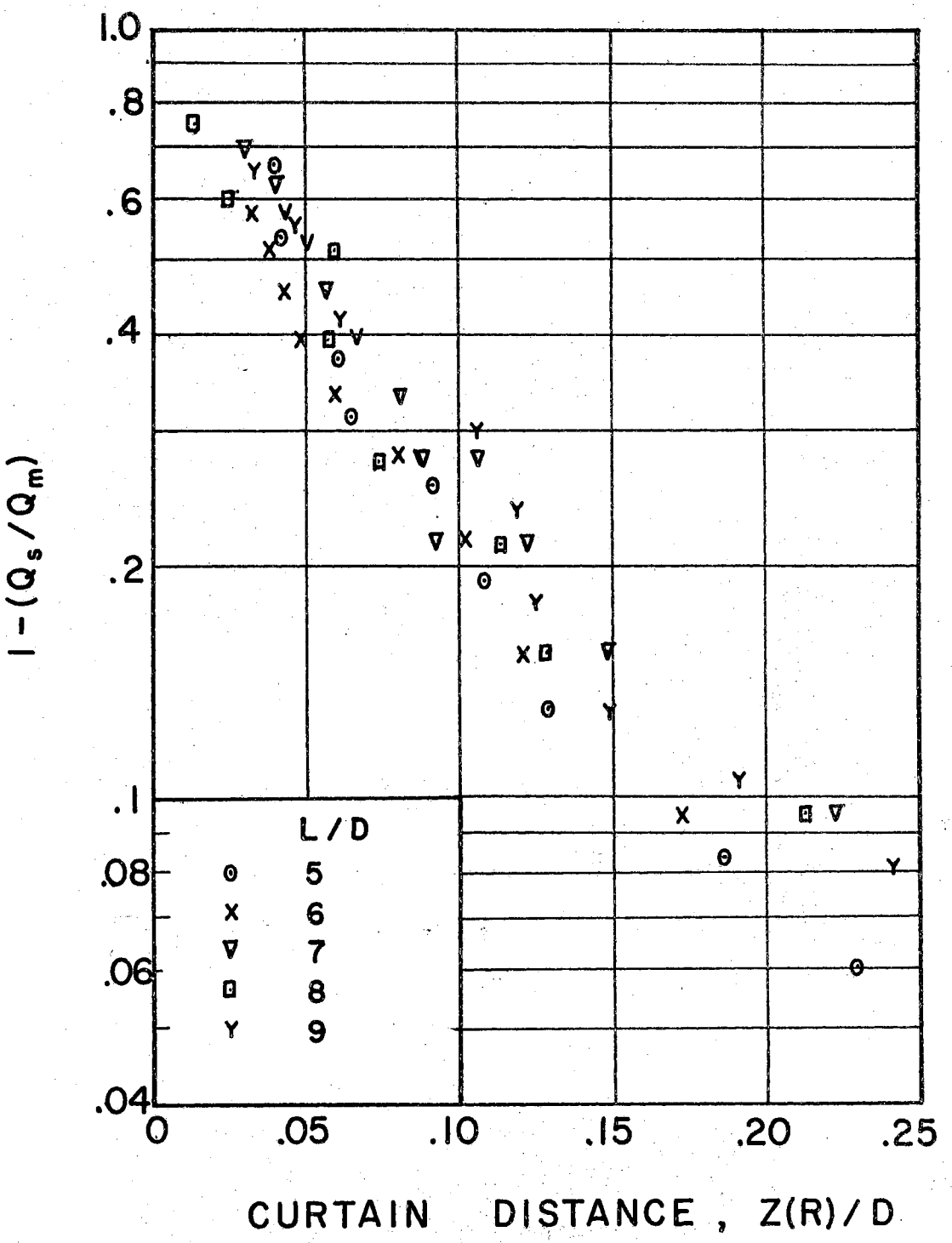

Figure 45. Source Flow Modulation on Semi-Log Plot

where K_q is a flow constant. A least squares fit of all the data yields a value of $K_q = 12.3$. However, the standard deviation from this value is large. When the data is restricted to values of $1 - Q_s/Q_m$ greater than 0.1, 95 per cent of the data fall within $K_q = 14.0 \pm 5.0$. A value of K_q equal to 14.0 is used to compare the model and the experimental characteristics (Chapter VIII). However, the effect of variations in K_q (and the other constants) on modulator pressure gain are examined in Chapter VII.

Energy Conversion

In an actual (commercially available) impact modulator an annular output chamber (Figure 46a) surrounds the source nozzle. The chamber acts as a circular static pressure tap at the exit of the source nozzle. When the flow from the source is cutoff, the output pressure is equal to the source pressure. In the mid-range of flow modulation, the source pressure at the nozzle exit is in the form of dynamic and static pressure. The directional orientation of the output chamber and the vector properties of the flow permit the chamber to sense only the static pressure portion. At the beginning of flow modulation, the source flow has a maximum value and the pressure in the output chamber is less than atmospheric pressure.

To describe the energy conversion accurately is complex for the actual output nozzle (Figure 46a). For the purposes of this investigation and for ease of fabrication, a simplified geometry is warranted. Figure 46b shows a convenient simplification and also a possible alternative to the actual geometry. The assumption of this geometry allows for static pressure measurements at the nozzle output. The assumption

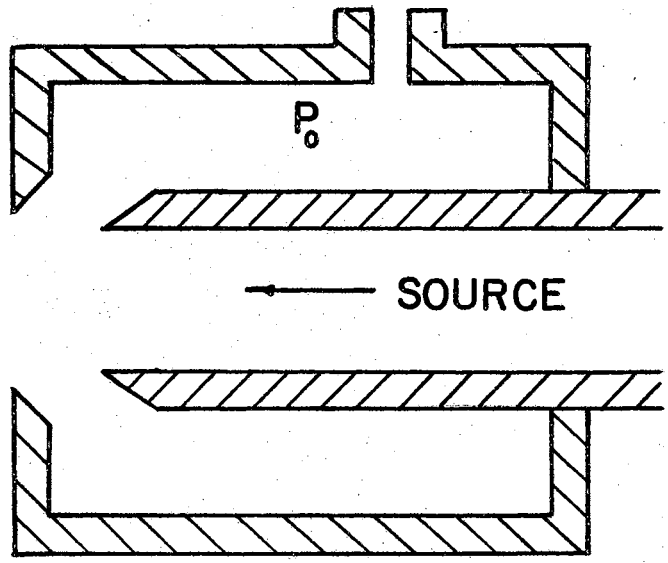

a) ACTUAL

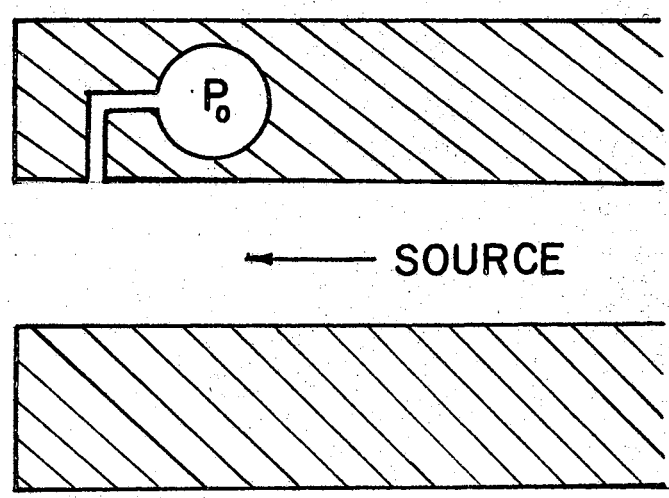

b) SIMULATED

Figure 46. Output Configurations

is most acceptable when the source flow is less than half of its maximum value.

Expression for Energy Conversion

With the simulated output chamber shape (Figure 46b) and the assumption of inviscid flow within the source nozzle, Bernoulli's equation is applicable and yields:

$$P_o/P_s = 1 - (Q_s/Q_m)^2 \qquad (30)$$

Equation (30) corresponds to the functional relation given in Equation (5). Figure 47 shows the relation between output pressure and source flow that is described in Equation (30). Figure 47 also shows the characteristics of an ideal converging-diverging nozzle with $A_{ca}/A = 1.2$. In this case the output pressure is the pressure at the nozzle throat. The ideal nozzle gives another approximation to the actual output chamber. The characteristics of the actual output chamber lie between the converging nozzle and the converging-diverging nozzle.

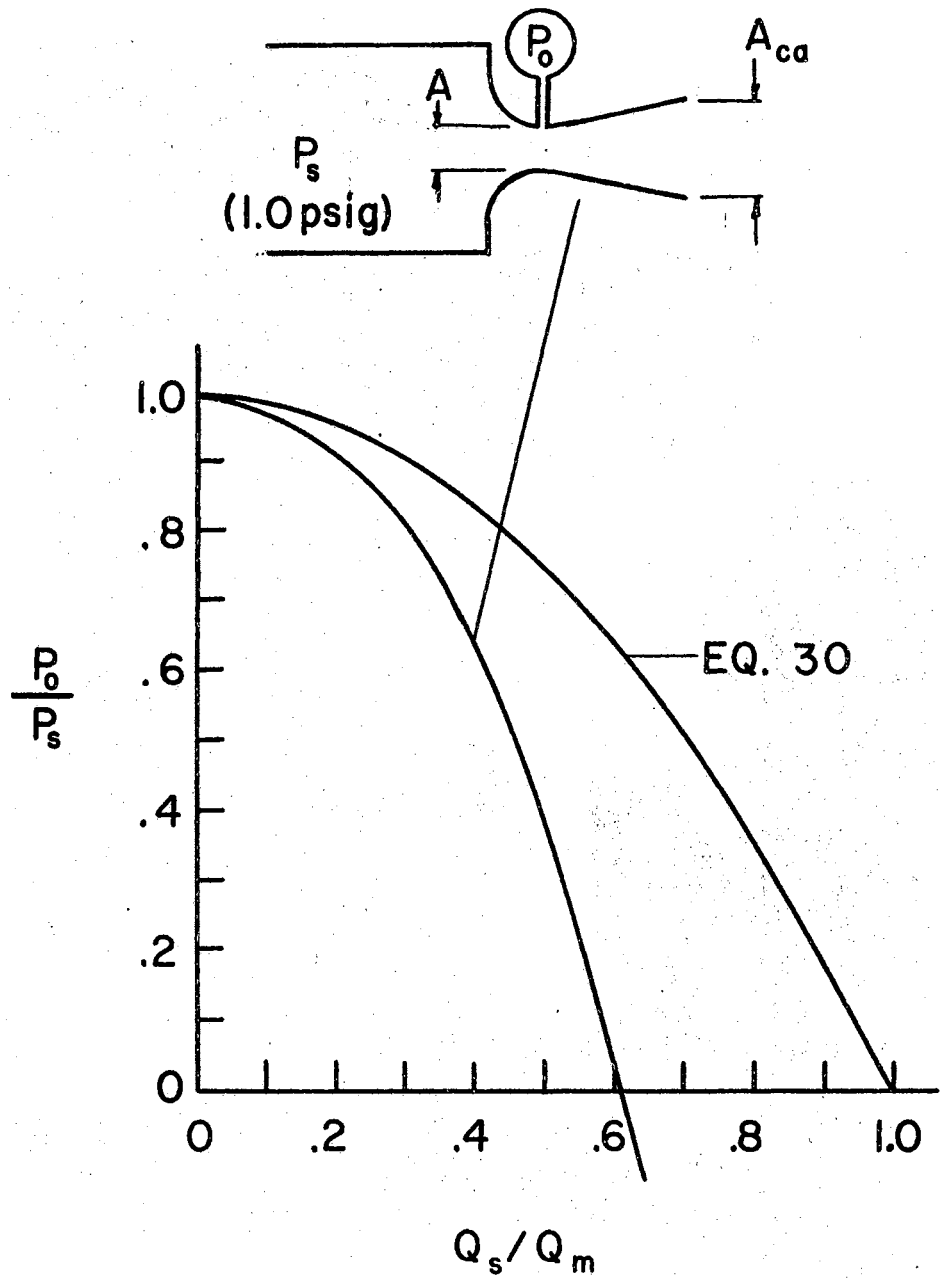

Figure 47. Schematic of the Relation Between Output Pressure and Source Flow

CHAPTER VII

PRESSURE GAINS CALCULATED FROM MODEL

The incremental pressure gain of a fluidic amplifier, G_p, is defined as:

$$G_p \equiv \frac{dP_o}{dP_c} \tag{31}$$

where P_c is the control pressure. This is P_e, P_{ca}, or P_{ct} for emitter, annular or transverse modulation, respectively. Manipulation of the functional relations (Equations (1) - (6)) for the model leads to the formulation of the blocked load pressure gain for each type of impact modulator. When the modulator operates at a constant source pressure and with a fixed geometry, the general expression for the incremental pressure gain is:

$$G_p = \frac{A' \left[\frac{\partial Z(o)}{\partial P_c} + \frac{\partial Z(o)}{\partial C_e} \left[\left(1 + \frac{\partial C_f}{\partial C_p} \right) \left(\frac{dC_p}{dP_c} \right) \right] \right]}{B} \tag{32}$$

where

$$A' = \left(\frac{dP_o}{dQ_s} \right) \left(\frac{dQ_s}{dZ(R)} \right) \left(\frac{dZ(R)}{dZ(o)} \right)$$

and

$$B = \left[1 - \left(1 - \frac{dZ(R)}{dZ(o)} \right) \left(\frac{\partial Z(o)}{\partial C_e} \right) \left(\frac{\partial C_f}{\partial (Z(o) - Z(R))} \right) \right]$$

There are eight derivatives and partial derivatives in Equation (32). These derivatives are expressible in terms of the modulator parameters through the application of the empirical expressions given in Equations (23), (25), and (27) - (30). The equations below, (Equations (33) through (40)) present the derivatives in terms of the system parameters.

1. From Equation (23)

$$\left[\frac{\partial Z(0)/D}{\partial P_{ca}/P_e}\right]_a = \frac{\exp\left[-\frac{D_a^2/D^2}{E'}\right] - \exp\left[-\frac{1}{E'}\right]}{\left(1 - \frac{P_{ca}}{P_e}\right)\exp\left[-\frac{1}{E'}\right] + \exp\left[-\frac{D_a^2/D^2}{E'}\right]} \quad \text{(annular)} \tag{33a}$$

$$\left[\frac{\partial Z(0)/D}{\partial P_e/P_s}\right]_e = -2E'\left(\frac{L}{D} - \frac{Z(0)}{D}\right)\sinh^2\frac{1}{2E'} \quad \text{(emitter)} \tag{33b}$$

$$\left[\frac{\partial Z(0)/D}{\partial P_{ct}/P_e}\right] = 0 \quad \text{(transverse)} \tag{33c}$$

where

$$E' = 4C_e^2\left(\frac{L}{D} - \frac{Z(0)}{D}\right)^2$$

and

$$\frac{\partial Z(0)/D}{\partial C_e} = \frac{\left(1 - \frac{P_{ca}}{P_e}\right)J\exp\left[-\frac{1}{E'}\right] + \frac{P_{ca}}{P_e}J\exp\left[-\frac{D_a^2/D^2}{E'}\right]}{\left(1 - \frac{P_{ca}}{P_e}\right)\exp\left[-\frac{1}{E'}\right] + \frac{P_{ca}}{P_e}\frac{D_a^2}{D^2}\exp\left[-\frac{D_a^2/D^2}{E'}\right]} \quad \text{(annular)} \tag{34a}$$

$$\frac{\partial Z(0)/D}{\partial C_e} = J \quad \text{(emitter and transverse)} \tag{34b}$$

where

$$J = \frac{\frac{L}{D} - \frac{Z(O)}{D}}{C_e}$$

2. From Equation (25)

$$\frac{\partial C_f}{\partial(Z(O) - Z(R))} = \frac{K_f\left[\frac{Z(O)}{D} - \frac{Z(R)}{D}\right]}{C_p^3\ (L/D)^3}\left[\frac{1}{4C_p^2(L/D)^2} - 1\right] \exp -\left[\frac{1}{4C_p^2(L/D)^2}\right] \tag{35}$$

and

$$\frac{\partial C_f}{\partial(Z(O) - Z(R))} = \frac{K_f\ \exp\left[-\frac{1}{4C_p^2(L/D)^2}\right]}{2\ C_p^2(L/D)^3} \tag{36}$$

3. From Equation (27)

$$\frac{dC_p}{dP_e} = 0 \quad \text{(emitter)} \tag{37a}$$

$$\frac{dC_p}{dP_{ca}} = -\ K_a\left[\frac{D_a^2}{D^2} - 1\right] \quad \text{(annular)} \tag{37b}$$

$$\frac{dC_p}{dP_{ct}} = K_t\ \frac{D_c^2}{D^2} \quad \text{(transverse)} \tag{37c}$$

4. From Equation (28)

$$\frac{dZ(R)/D}{dZ(O)/D} = 2\ K_s\left[\frac{Z(O)}{D} + 0.5\right] \tag{38}$$

5. From Equation (29)

$$\frac{d(Q_s/Q_m)}{dZ(R)/D} = K_q \exp\left[- K_q Z(R)/D\right] \tag{39}$$

6. From Equation (30)

$$\frac{dP_O/P_s}{dQ_s/Q_m} = - 2\, Q_s/Q_m \tag{40}$$

Emitter Modulator Pressure Gain

In the case of emitter modulation, the annular and transverse control pressures are zero. The control pressure is the emitter pressure. Thus, from Equation (32) the emitter modulator pressure gain is:

$$G_{pe} = \frac{A' \left[\frac{\partial Z(O)}{\partial P_e} + \frac{\partial Z(O)}{\partial C_e}\left(1 + \frac{\partial C_f}{\partial C_p}\right)\left(\frac{dC_p}{dP_e}\right)\right]}{B} \tag{41}$$

The emitter modulator pressure gain given by Equation (41) is calculable for specific values of the parameters by means of the expressions derived for the derivatives in Equations (33) - (40). Figures 48 and 49 show some typical results. Figure 48 shows the relation (without feedback) between mid-range ($P_O/P_s = 0.5$) pressure gain and nozzle spacing for various values of the plate decay factor. Figure 49 shows the same relation with feedback. The constant K_f is chosen as 0.08 because this value provides the best fit to the experimental data presented in Chapter VIII. In both cases the gain increases as the nozzle spacing decreases. This is a result of the contribution of the term $\partial(Z(O)/D)/\ \partial(P_e/P_s)$ given by Equation (33b). Feedback acts to

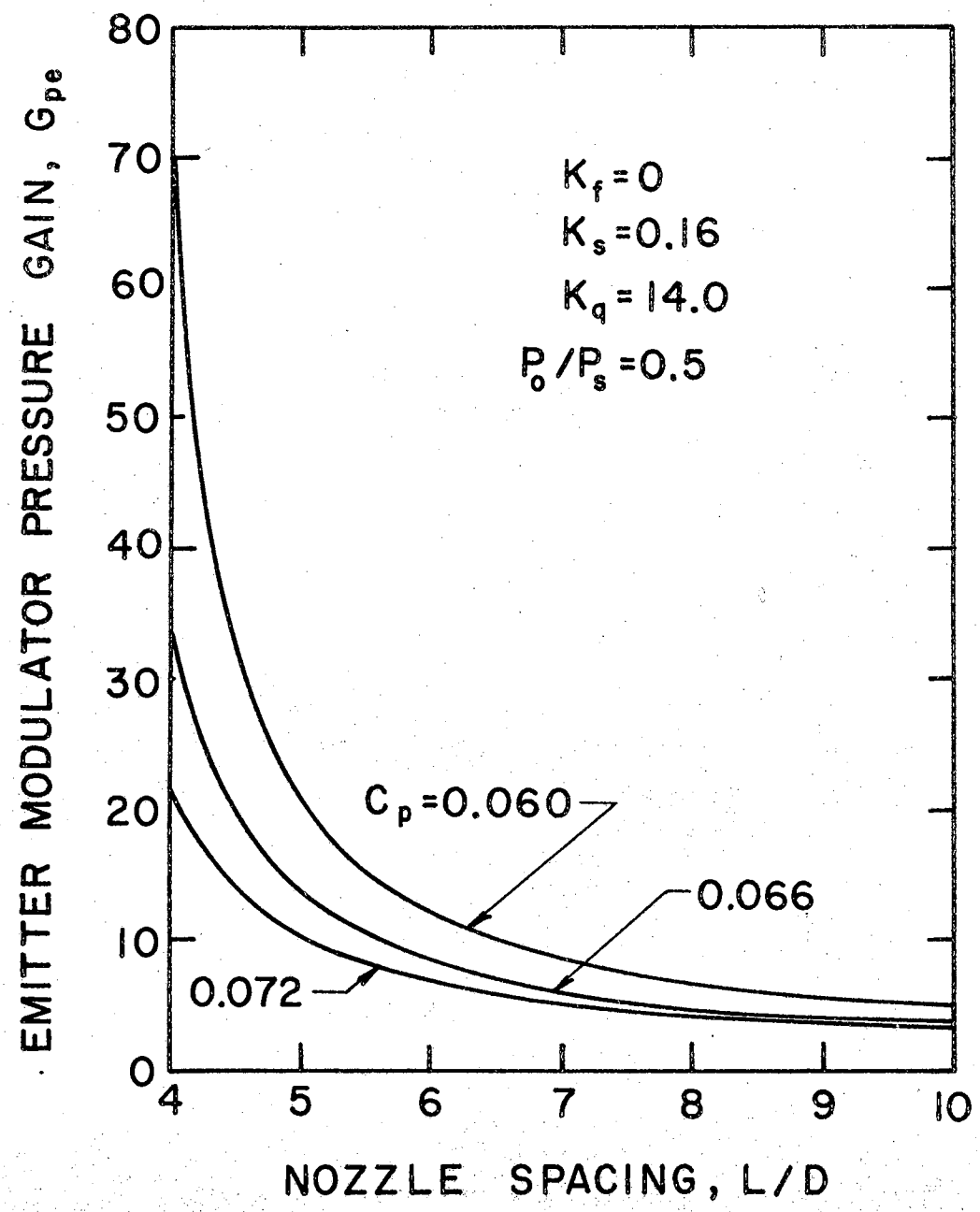

Figure 48. Emitter Modulator Pressure Gain Without Feedback (Model)

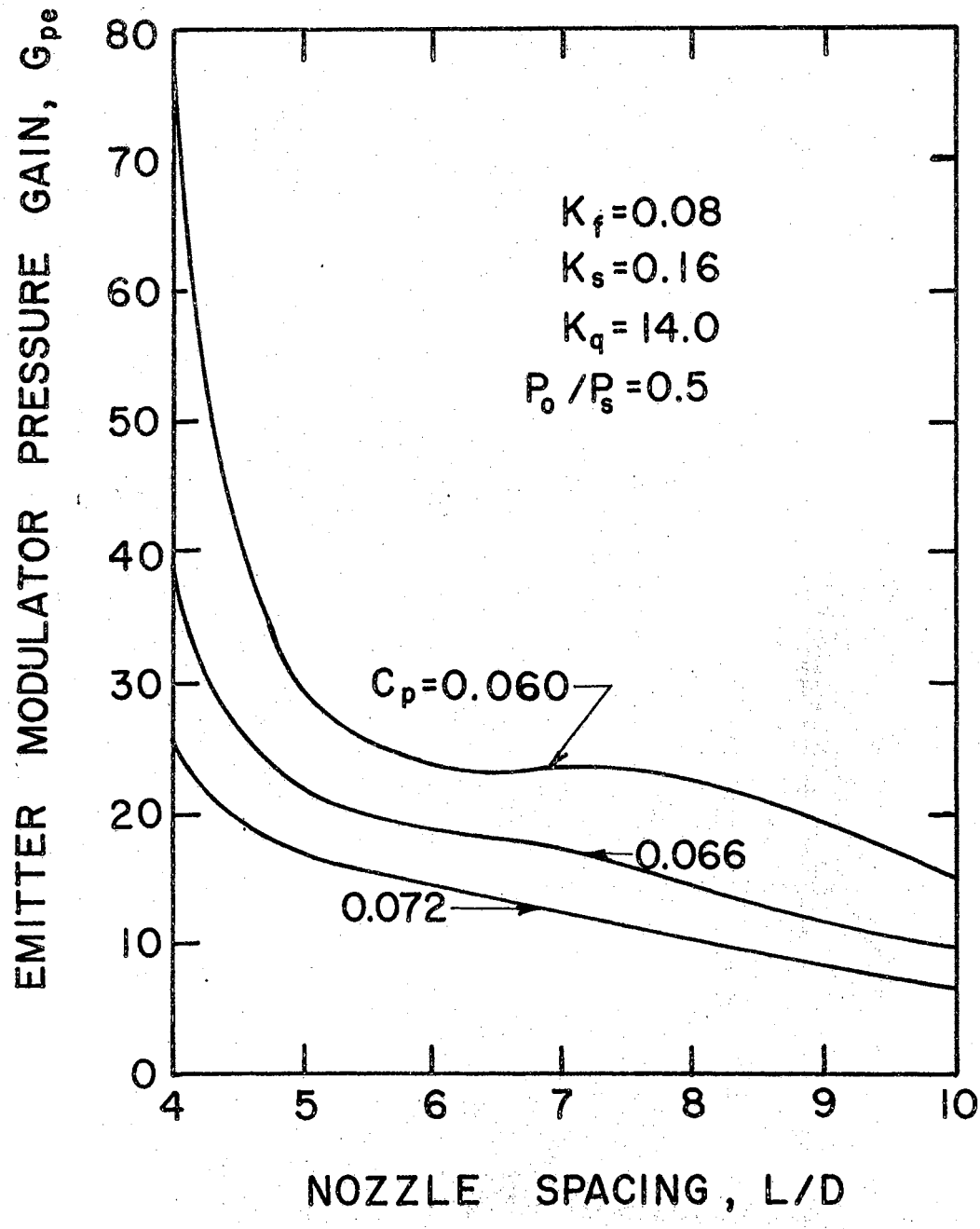

Figure 49. Emitter Modulator Pressure Gain With Feedback (Model)

increase the pressure gain, particularly at nozzle spacings between 6 and 8 diameters. The plate decay factor exerts a considerable influence on the pressure gain. The gain increases as the plate decay factor decreases. A later section considers the sensitivity of the plate decay factor in greater detail.

Annular Modulator Pressure Gain

In annular modulation the emitter pressure is constant and there is no transverse control pressure. The annular modulator pressure gain derives from Equation (32) and is:

$$G_{pa} = \frac{A' \left[\frac{\partial Z(0)}{\partial P_{ca}} + \frac{\partial Z(0)}{\partial C_e} \left(1 + \frac{\partial C_f}{\partial C_p} \right) \left(\frac{dC_p}{dP_{ca}} \right) \right]}{B} \qquad (42)$$

The annular modulator pressure gain is calculated from the combination of Equation (42) and Equations (33) - (40). Figure 50 shows the relation between pressure gain and nozzle spacing for various values of annular to emitter nozzle size without feedback. Figure 51 shows the same relation with feedback. A nominal value of the plate decay factor, $C_p = 0.072$, is used. For the case without feedback, the gain is almost independent of nozzle spacing. There is a very slight peak that occurs at a spacing of about 6 nozzle diameters. The reason for the relative flatness is that the additive terms in the numerator of Equation (42) are of opposite sign at the lower spacings. The application of feedback causes pronounced peaks in pressure gain at about 7 nozzle diameters. As in the emitter modulator, the feedback effects are greatest for nozzle spacings between 6 and 8 nozzle diameters. The effect of

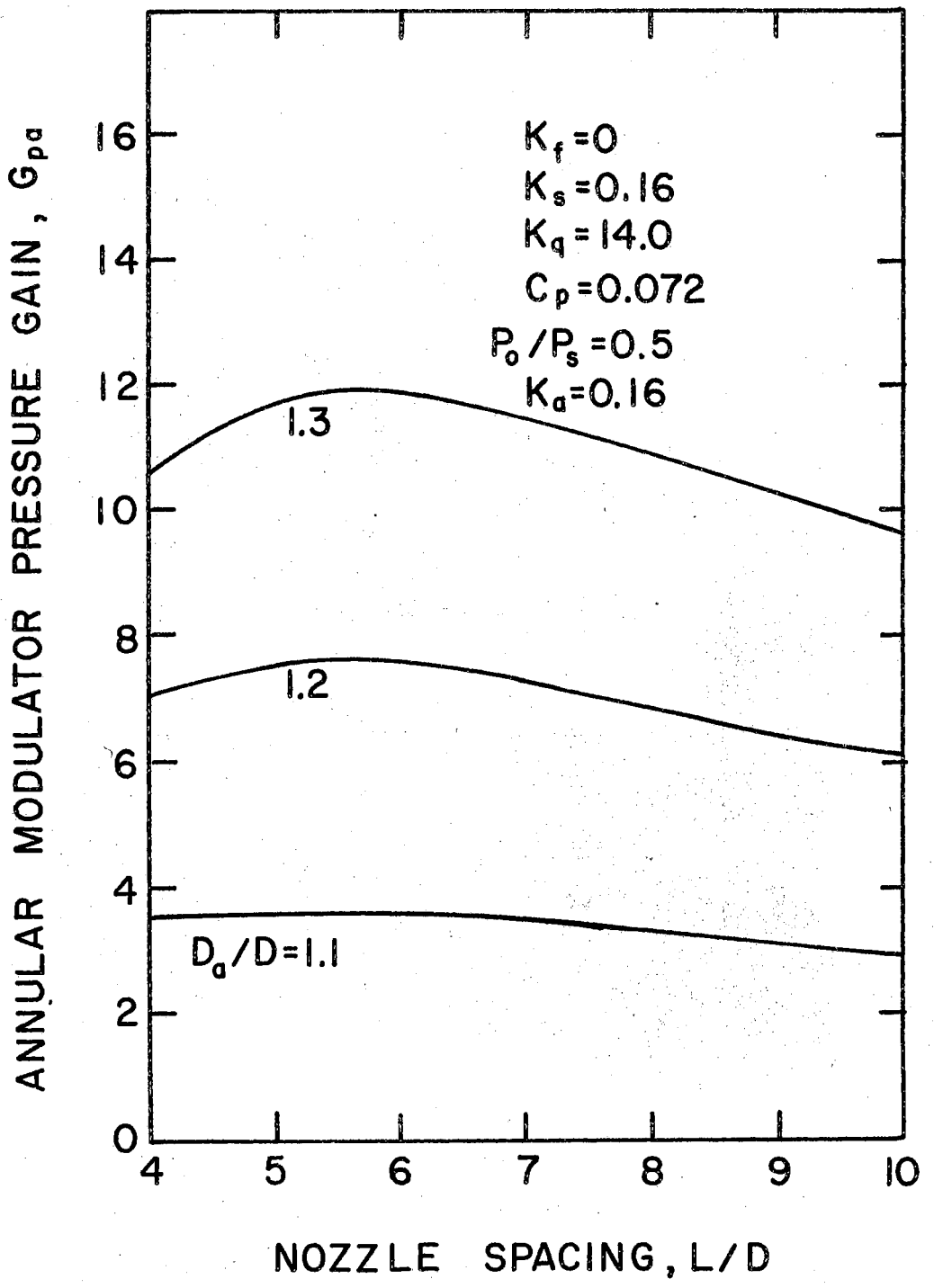

Figure 50. Annular Modulator Pressure Gain Without Feedback (Model)

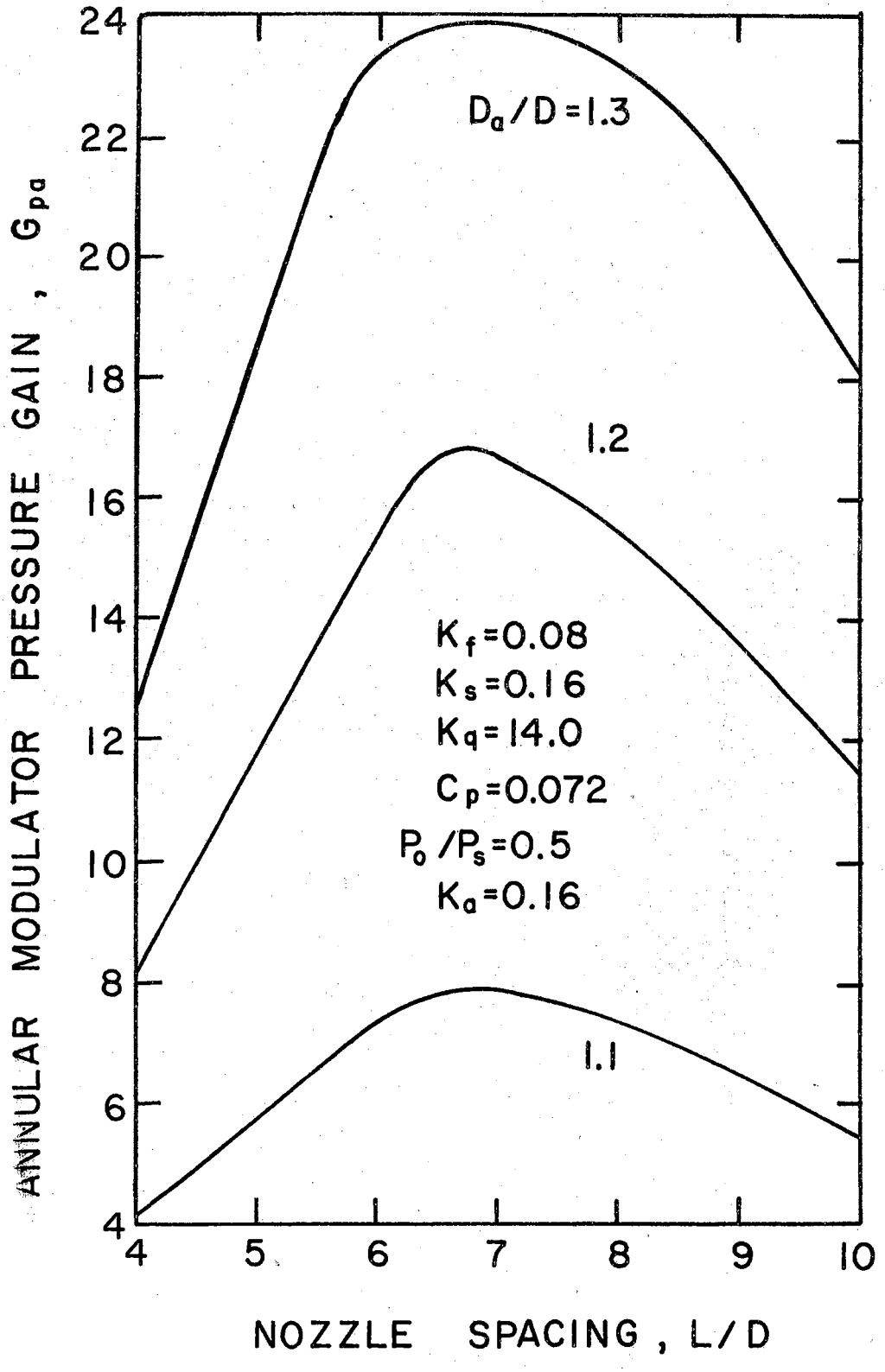

Figure 51. Annular Modulator Pressure Gain With Feedback (Model)

increasing the size of the annular nozzle, with or without feedback, is to increase the pressure gain.

Transverse Modulator Pressure Gain

In transverse modulation there is no annular control pressure, and the emitter pressure remains constant. The value of the emitter pressure is fixed so that modulation begins somewhere between the cutoff and beginning positions of emitter modulation. The adaptation of Equation (32) to transverse modulation results in:

$$G_{pt} = \frac{A'\left[\frac{dZ(0)}{dC_e}\left(1 + \frac{\partial C_f}{\partial C_p}\right)\left(\frac{dC_p}{dP_{ct}}\right)\right]}{B} \qquad (43)$$

The transverse modulator pressure gain is obtained in terms of the various parameters from Equations (33) to (40) and Equation (43). Figures 52 and 53 show some typical values of mid-range transverse pressure gain as a function of nozzle spacing and transverse control size. The transverse pressure gain is negative because A' is negative and dC_p/dP_{ct} is positive. The effect of feedback is to increase the peak value in the vicinity of the maximum (about L = 7.0 D). As in annular modulation, the gain increases as the control nozzle size increases. However, if an equal size modulator acts as a load on the modulator under consideration, the pressure gain of units with $D_c/D = 0.5$ is larger than those with $D_c/D = 1.0$.

In the consideration of pressure gain for the various types of modulation, only the mid-range values ($P_o/P_s = 0.5$) have been presented. However, the gain of the modulators is not constant throughout the operating range. Figure 54 shows the effect of output pressure on

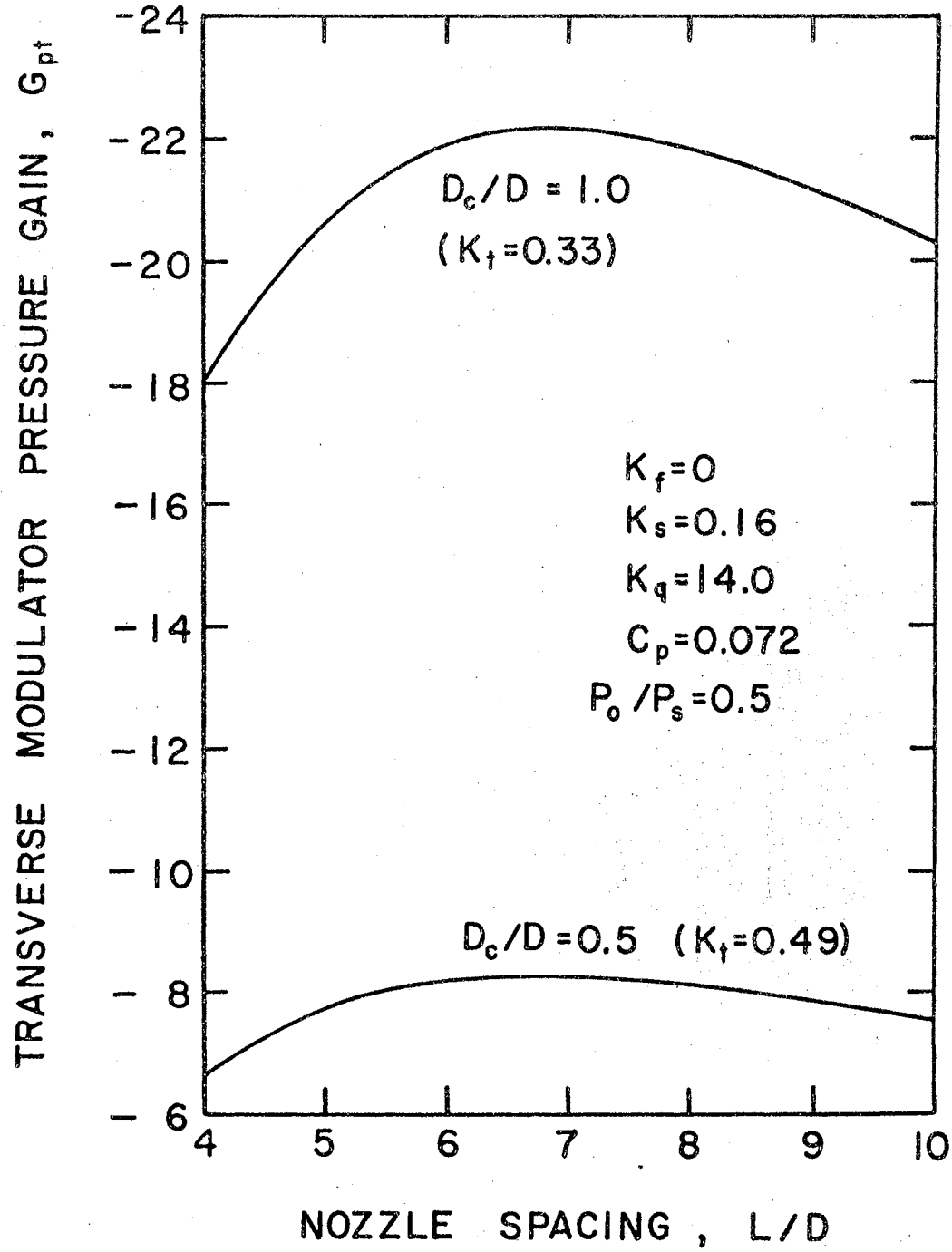

Figure 52. Transverse Modulator Pressure Gain Without Feedback (Model)

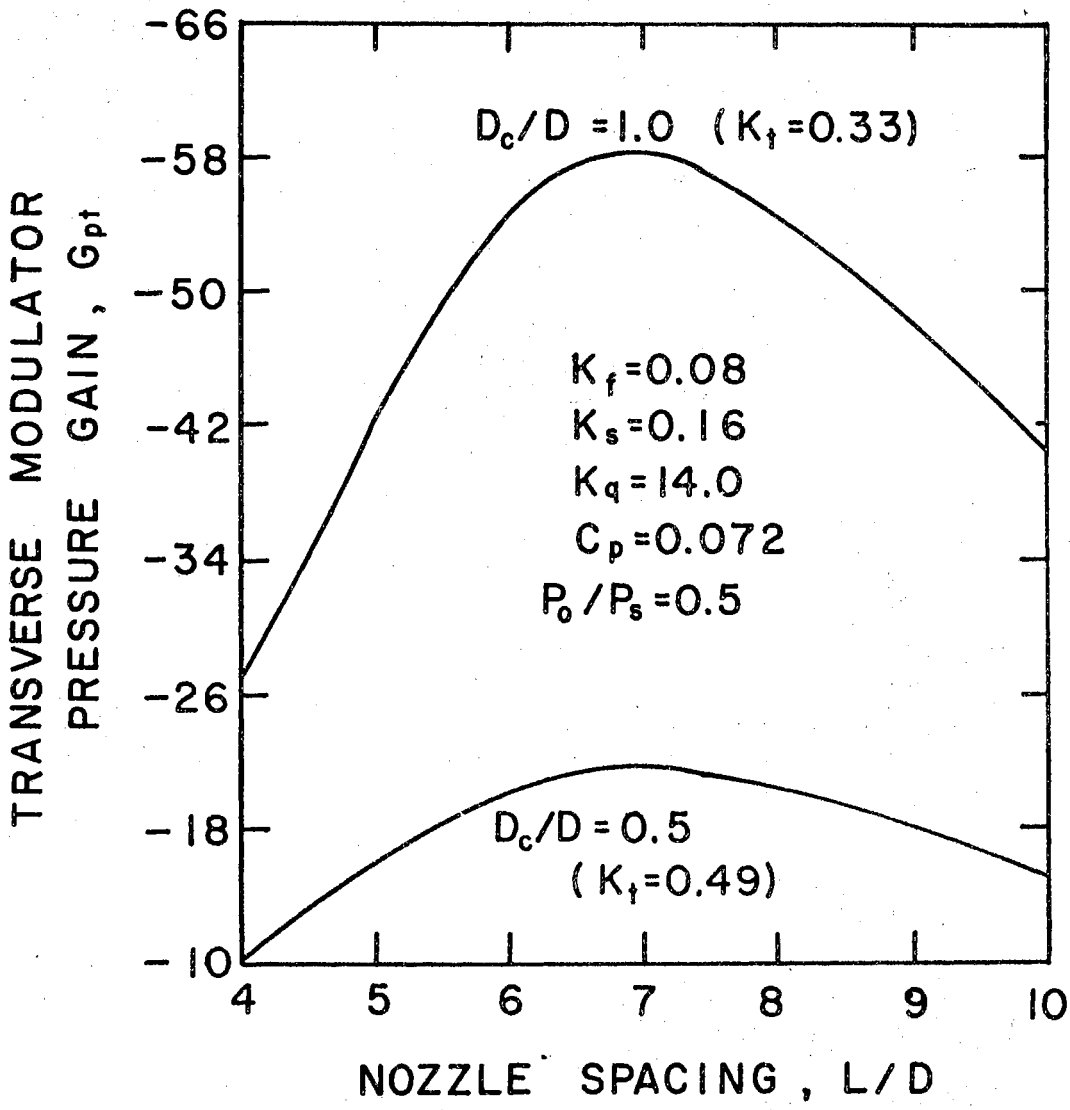

Figure 53. Transverse Modulator Pressure Gain With Feedback (Model)

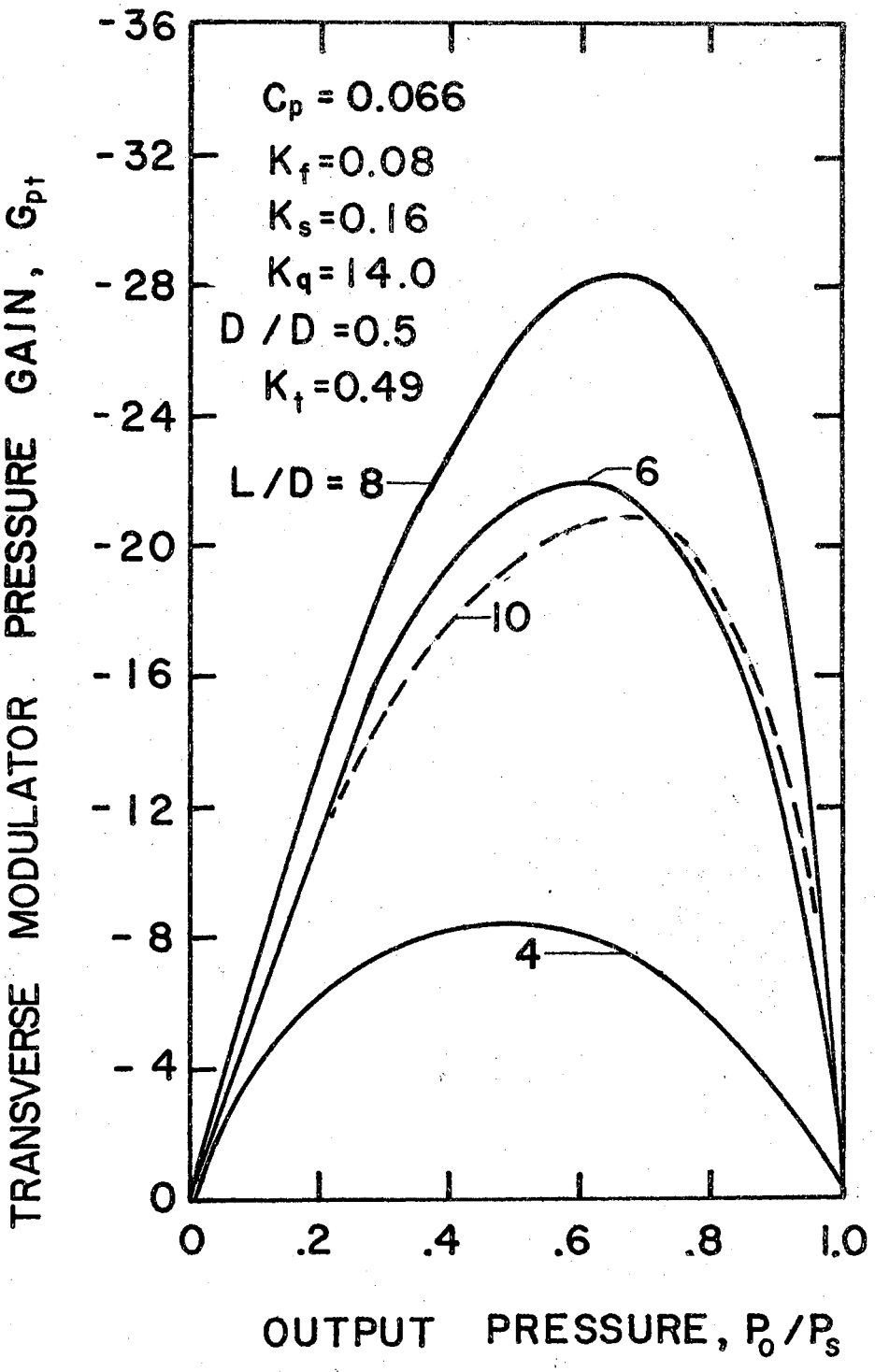

Figure 54. The Effect of Output Pressure on the Transverse Modulator Pressure Gain (Model)

the transverse modulator pressure gain. The gain is zero at the extreme values of the output pressure ratio (P_o/P_s = 0.0, 1.0). The zero gain value at P_o/P_s = 0 is the result of a zero value of the term $d(Q_s/Q_m)/ d(Z(R)/D)$ (Equation (39)). At cutoff (P_o/P_s = 1.0) the gain is zero because the term $d(P_o/P_s)/ d(Q_s/Q_m)$ (Equation (40)) is zero. In the region of P_o/P_s from 0.2 to 0.8, the gain values are uniform enough so that input-output characteristics have the appearance of linearity. The maximum value of gain occurs slightly above midrange. The position of the maximum is a function of the nozzle spacing. When the spacing increases, the maximum gain value moves towards cutoff (P_o/P_s = 1.0).

Sensitivity of Parameters

The pressure gain of the conceptual model depends upon the following eight parameters:

1. Nozzle spacing, L/D
2. Control size, D_a/D or D_c/D
3. Output pressure, P_o/P_s
4. Flow constant, K_q (Equation (29), page 85)
5. Feedback constant, K_f (Equation (25), page 49)
6. Shape constant, K_s (Equation (28), page 82)
7. Plate decay factor, C_p (Equation (21), page 39)
8. Modulation constant, K_a or K_t (Equation (27), page 75)

The previous section showed the effect of the first three parameters. The emphasis here is on the last five parameters.

To determine the sensitivity of a parameter, the parameter is varied about its expected value while the other parameters are fixed. The sensitivity of a particular parameter is defined as the ratio of

the percentage change in pressure gain to the percentage change in the parameter. That is:

$$S_{G_x}^{G_p} \equiv \frac{\Delta G_p / G_p}{\Delta K_x / K_x} \tag{44}$$

where K_x, represents the parameter. Figures 55, 56, 57, and 58 show the relation between pressure gains and the parameters, K_q, K_f, K_s and C_p. The solid dots on each figure indicate the nominal value of the parameter when it is not the independent variable. Equation (44) and Figures 55, 56, 57, and 58 are used to calculate the sensitivities shown in Table I.

TABLE I

PARAMETER SENSITIVITY

Parameter	Emitter	Modulator	
		Annular	Transverse
Flow constant, K_q	0.82	0.79	0.96
Feedback constant, K_f	1.31	1.20	1.41
Shape constant, K_s	0.47	0.43	0.58
Plate decay factor, C_p	2.86	2.19	2.47
Modulation constant, K_a or K_t	--	0.80	1.00

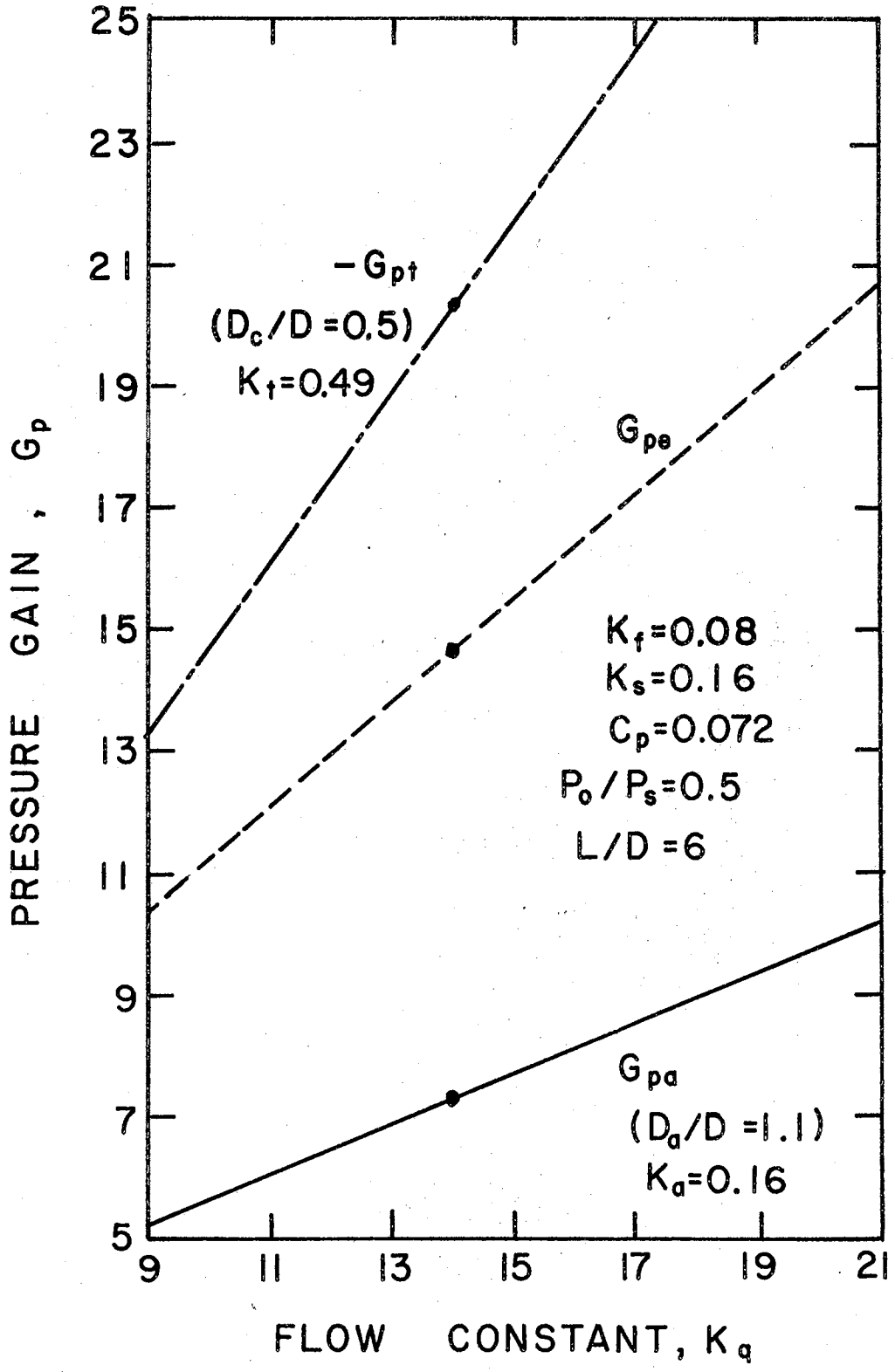

Figure 55. The Effect of Flow Constant on Pressure Gain (Model)

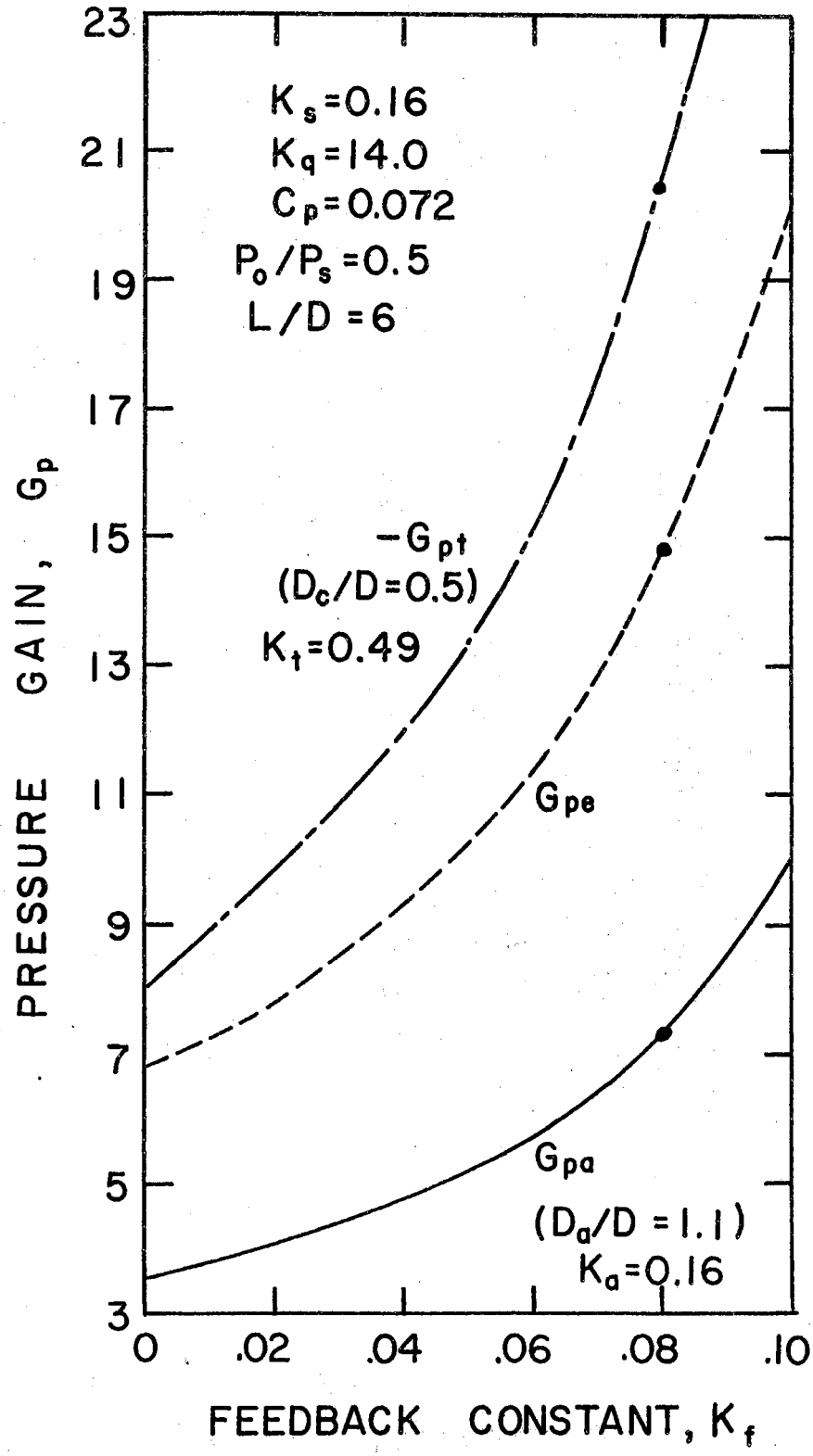

Figure 56. The Effect of Feedback Constant on Pressure Gain (Model)

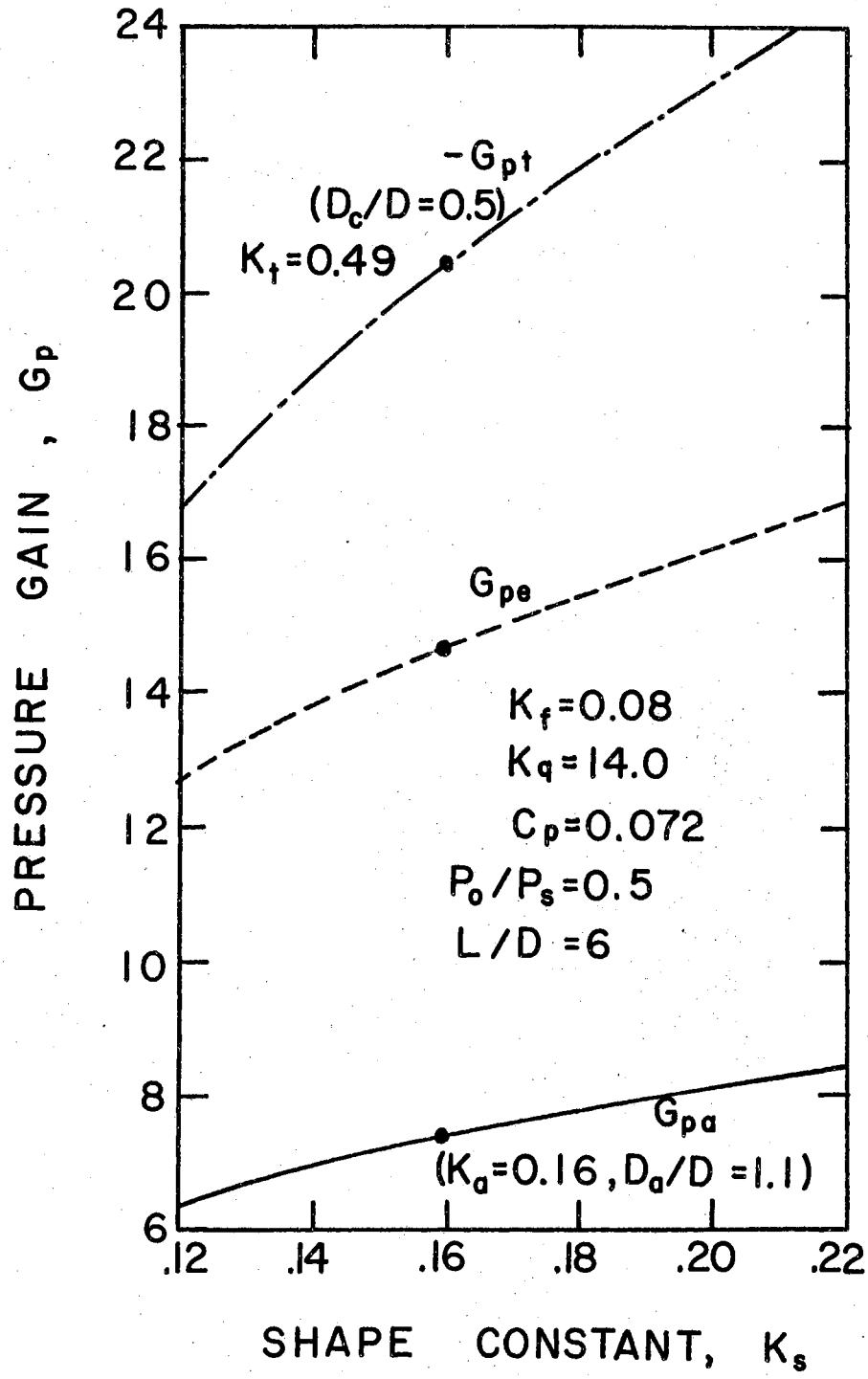

Figure 57. The Effect of Shape Constant on Pressure Gain (Model)

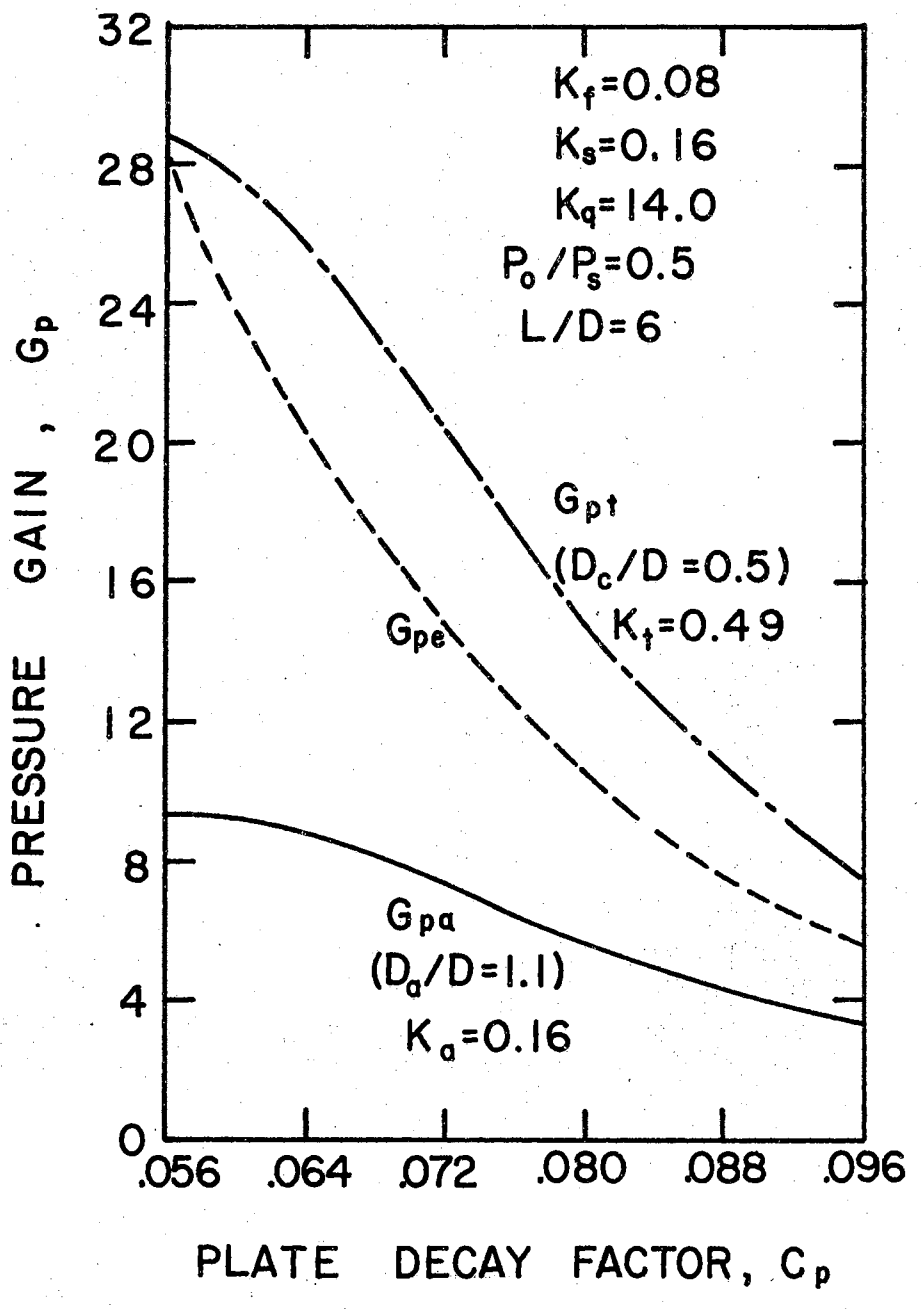

Figure 58. The Effect of Plate Decay Factor on Pressure Gain (Model)

Table I shows that the plate decay factor is the most sensitive parameter. It has about twice the sensitivity of the next most sensitive parameter, the feedback constant. The least sensitive parameter is the shape constant. This is fortunate since the shape constant is difficult to measure. In general, the sensitivity of the parameters is greatest for transverse modulation and smallest for annular modulation. The modulation constant, K_a or K_t, has about the same sensitivity as the flow constant, K_q.

The relation between the five parameters and the pressure gain is always single valued. This is in contrast to the effects of the nozzle spacing and output range parameters which tend to produce peaks in the value of pressure gain.

CHAPTER VIII

CHARACTERISTICS OF IMPACT MODULATORS

The input-output characteristics of impact modulators are calculated from Equations (23), (25), and (27) through (30). In the case of annular and transverse modulation the calculation requires an iterative procedure to account for the changes in the plate decay factor that occur during modulation. To determine the adequacy of the conceptual model, the calculated characteristics are compared with the characteristics measured on experimental modulators. The comparison is between the input-output characteristics rather than the pressure gains because the experimental results apply directly, without differentiation of the data. In addition, the gain variations with output pressure, the linearity, and the saturation characteristics of the modulator are more clearly evident from plots of the input-output characteristics.

For convenience the nominal values of plate decay factor used to determine the experimental characteristics are repeated below:

$$[C_p]_a = 0.066 \qquad (0.500 \text{ in. diameter})$$

$$[C_p]_a = 0.073 \qquad (0.125 \text{ in. diameter})$$

$$[C_p]_{aa} = 0.071$$

$$[C_p]_{at} = 0.066 \ .$$

Slight variations from these values result from the effect of emitter pressure on the plate decay factor (see Figure 23).

Direct Emitter Modulator Characteristics

The experimental input-output characteristics are presented for two idealized modulators. One modulator has 0.500 in. diameter nozzles and the other has 0.125 in. diameter nozzles. Figure 59 shows a schematic of the experimental arrangement. Figure 12 shows the actual emitter nozzle for each experimental modulator. The source nozzle has the same size and shape as the emitter nozzle but the face of the source nozzle also has a flat of about six nozzle diameters. The flow from the source (Q_s) is measured with a rotameter and the emitter and source pressures are measured on inclined manometers or bourdon gages depending on the pressure level. The output pressure is calculated from the flow measurements and Equation (30).

At the beginning of a test, a source pressure is selected and set while the emitter jet is inactive. The flow measured under this condition determines the maximum flow (Q_m). Then, the application of a specific emitter pressure increases the source pressure. After a readjustment of the source pressure to its selected value, the resulting source flow is recorded. The test procedure consists of incrementing the emitter pressure and readjusting the source pressure. Figures 60 and 61 show data taken with the 0.500 in. diameter and 0.125 in. diameter modulators, respectively. Figure 60 shows the empirical and experimental input-output characteristics for nozzle spacings of six and eight diameters. For the 0.500 in. diameter modulator a feedback constant of 0.08 provides the best fit to the experimental results. The data for the 0.125 in. modulator and the model (Figure 61) are in best agreement when there is no feedback ($K_f = 0$). In this latter case

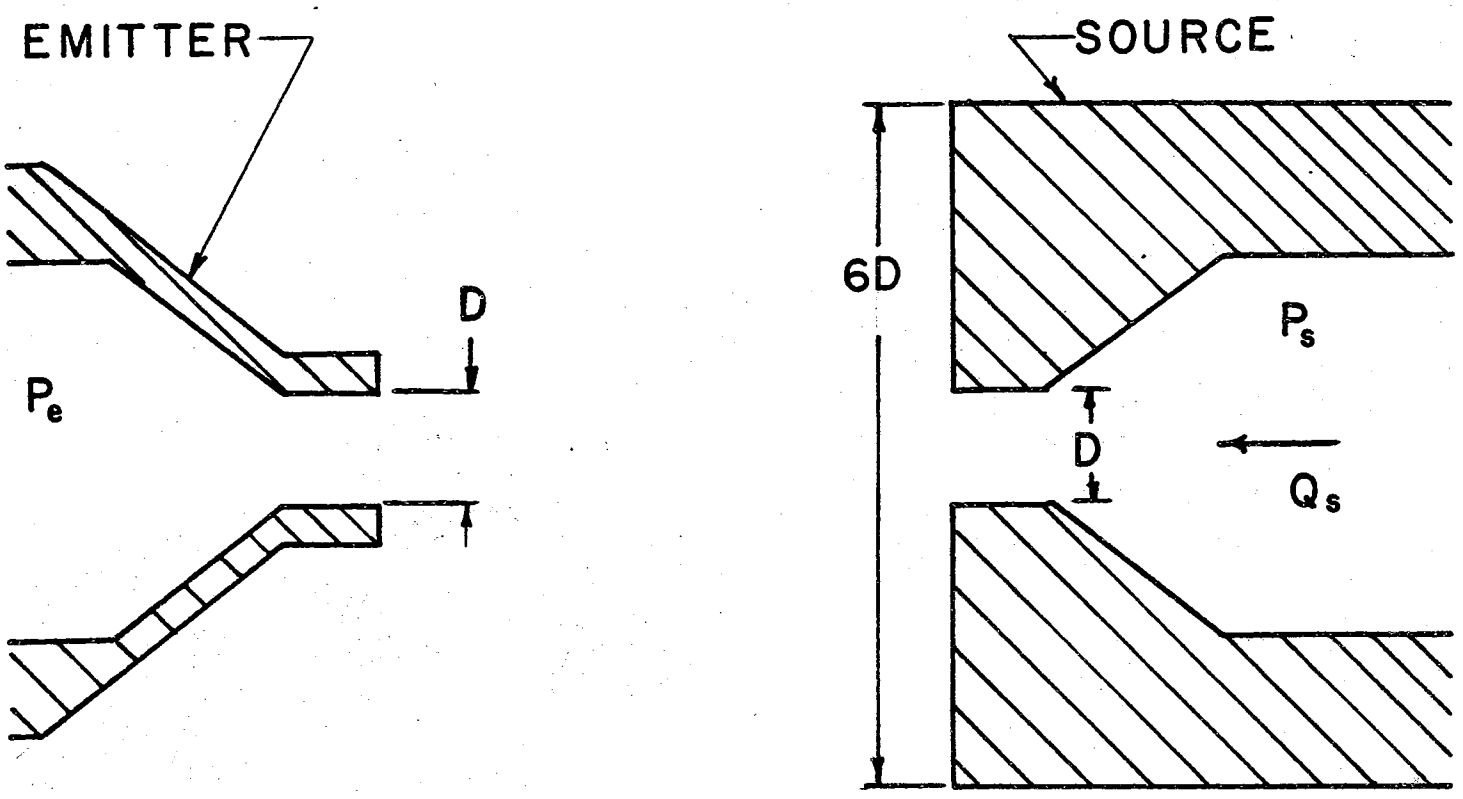

Figure 59. Emitter Modulator Test Arrangement

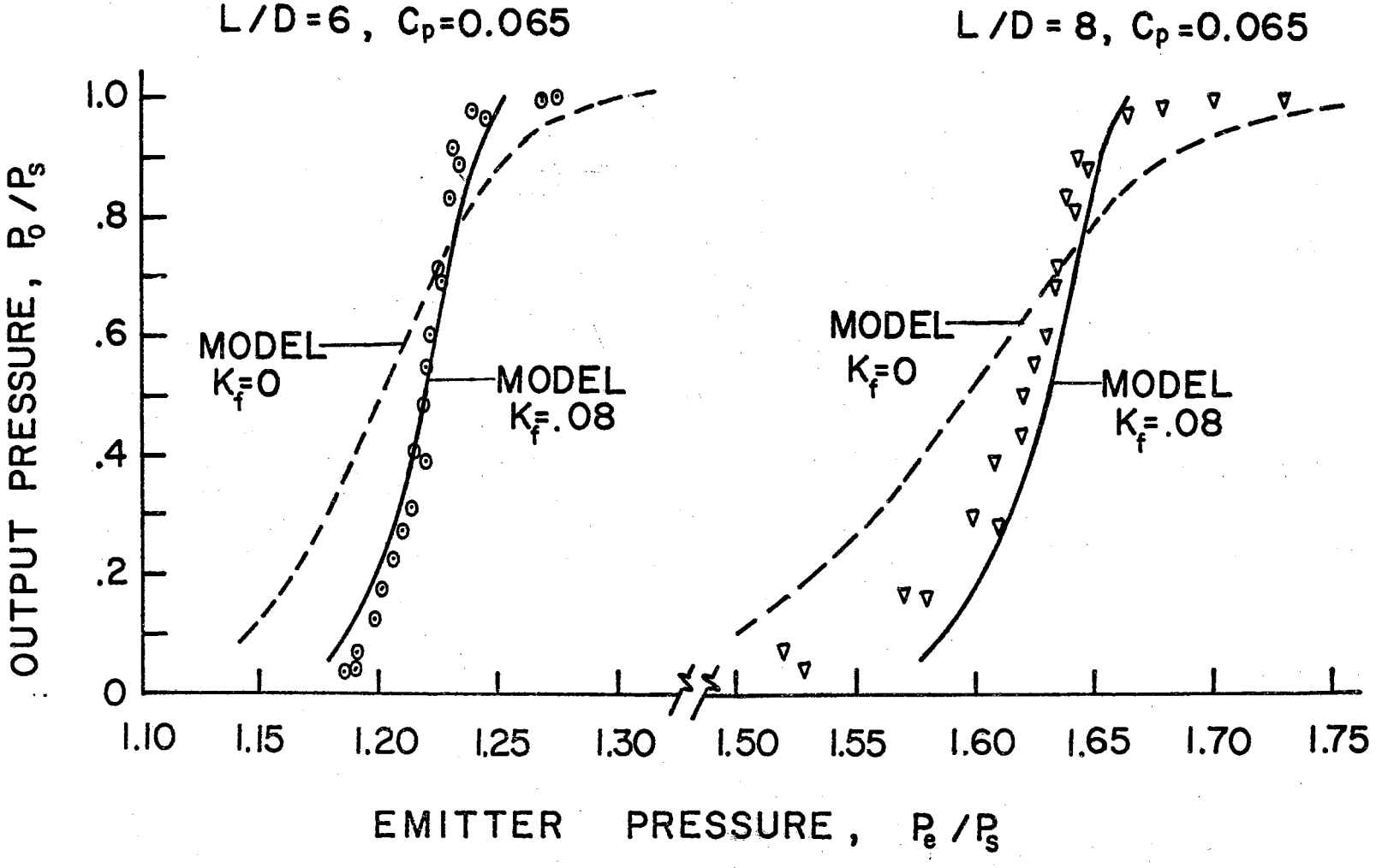

Figure 60. Direct Emitter Modulator Characteristics (0.500 in. unit)

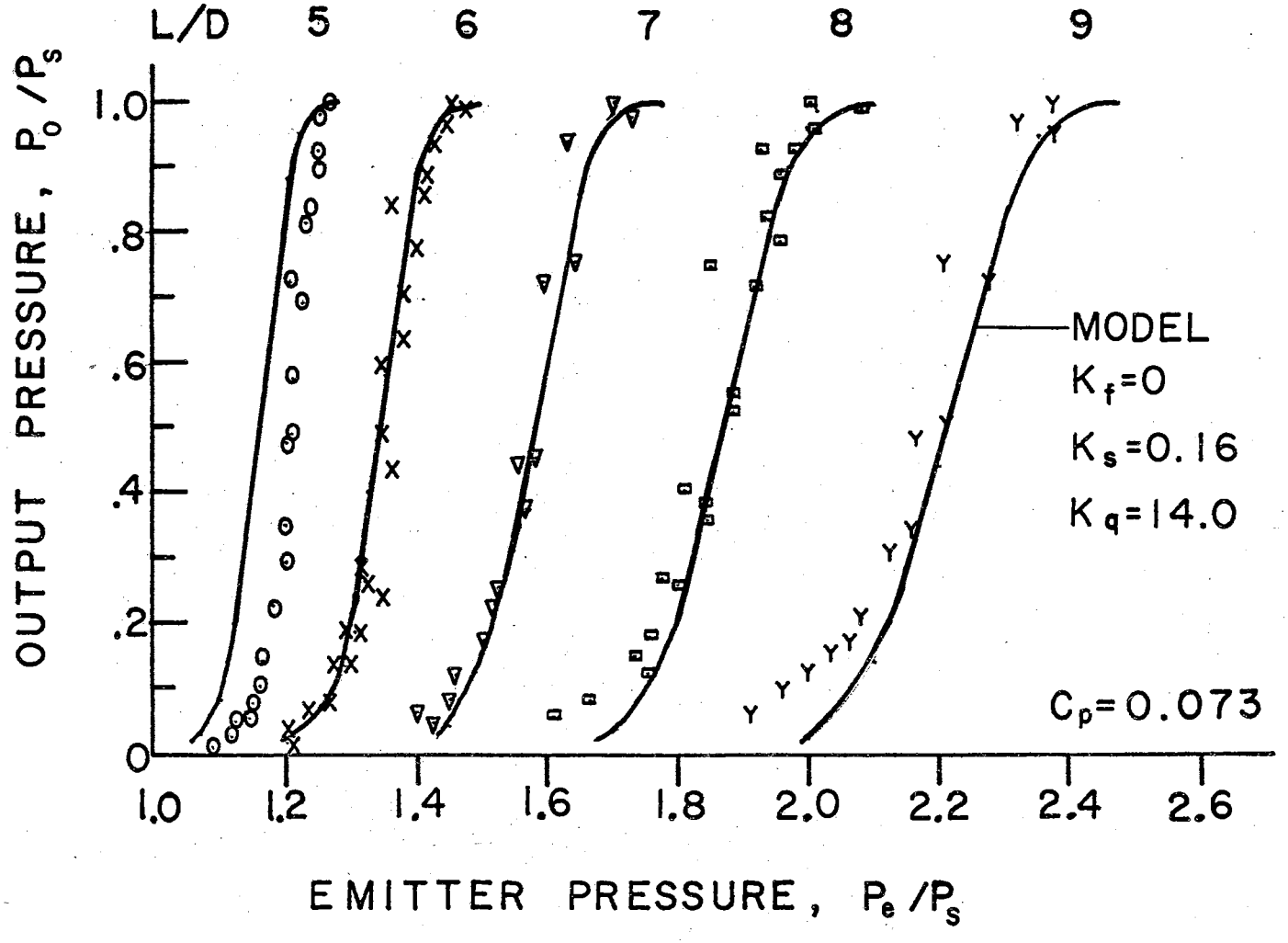

Figure 61. Direct Emitter Modulator Characteristics (0.125 in. unit)

the agreement with the model is good between six and nine nozzle diameters but not as good at five nozzle diameters. The discussion at the end of this chapter considers some possible reasons for the discrepancy between the characteristics of the different size units.

Direct Annular Modulator Characteristics

The experimental annular modulator characteristics are measured on a modulator that has the annular assembly shown in Figure 24b as the emitter side and the source nozzle (0.500 in. diameter, Figure 59) as the source side. The experimental procedure is similar to that of emitter modulation. First, a source pressure is selected. Then the emitter pressure is increased until the balance is close to the beginning of modulation position. Since there is not a clear definition of the beginning modulation, the emitter pressure acts as a bias. Now the application of annular control causes the source pressure to increase. Measurement of the source flow follows the readjustment of source pressure. Figures 62, 63, and 64 present a comparison between experimental results and the conceptual model for nozzle spacings of six, eight and ten diameters, respectively. In this case there is no further determination of the feedback constant. The value of the constant ($K_f = 0.08$) is the same one used in the emitter modulation tests on the 0.500 in. diameter model. To bring the model and test data into correspondence, the initial bias used in the model should be the same bias used in the experiments. However, at the beginning of flow modulation (refer to Figure 44 at $Q_s/Q_m > 0.9$) Equation (29) with $K_q = 14.0$ deviates most from the experimental results. Thus when the magnitude of experimental bias is applied to the model the characteristics derived

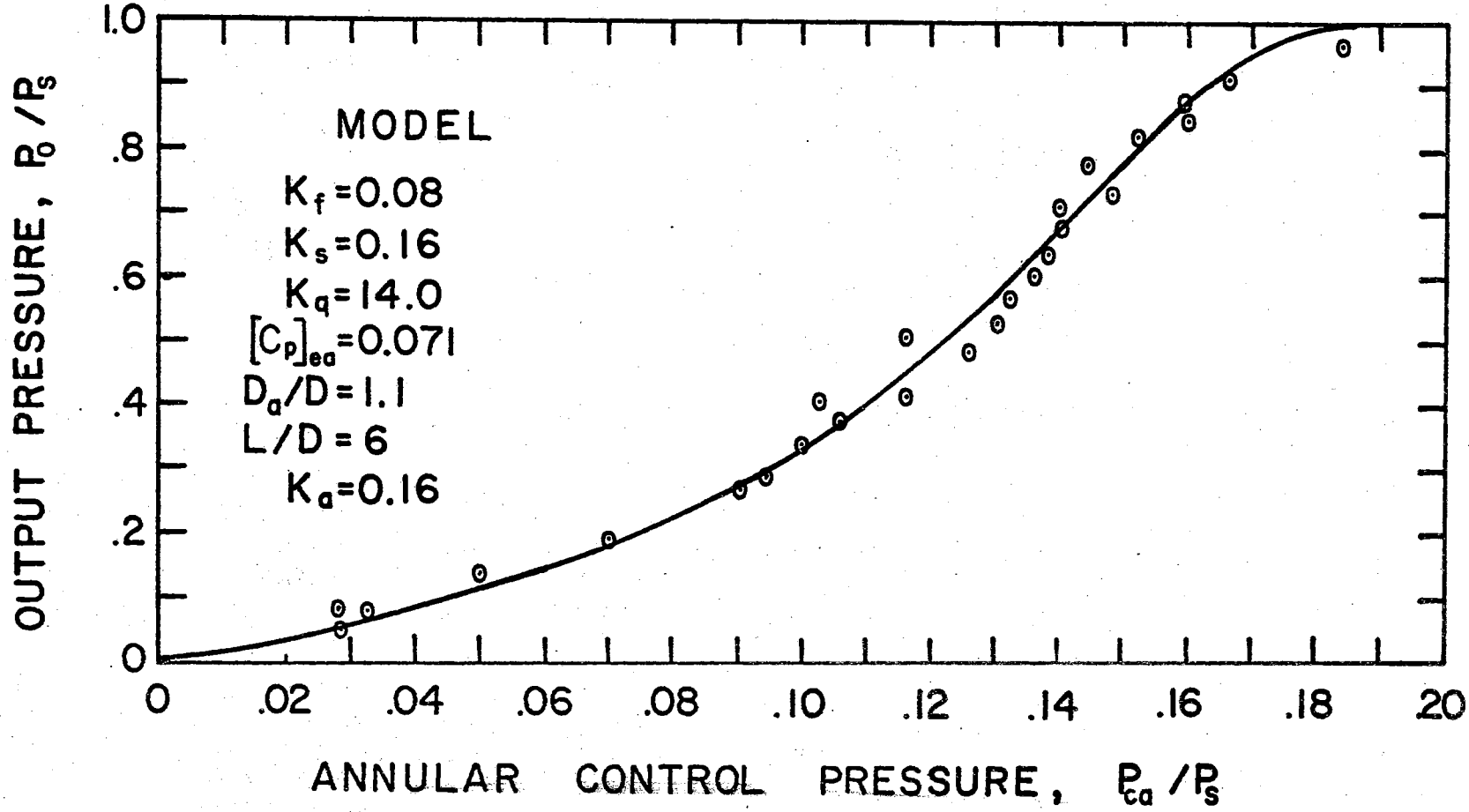

Figure 62. Direct Annular Modulator Characteristics (L/D = 6)

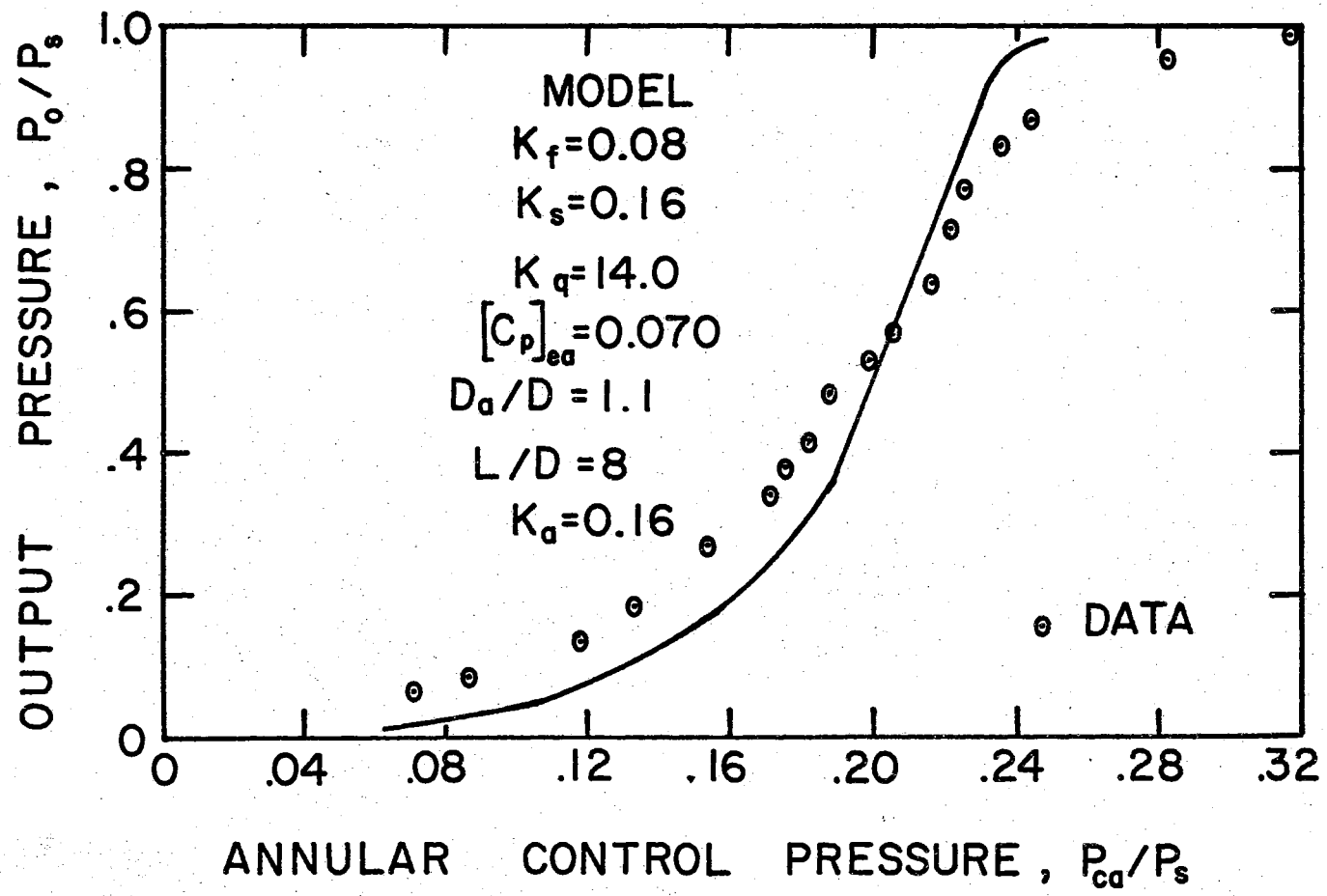

Figure 63. Direct Annular Modulator Characteristics (L/D = 8)

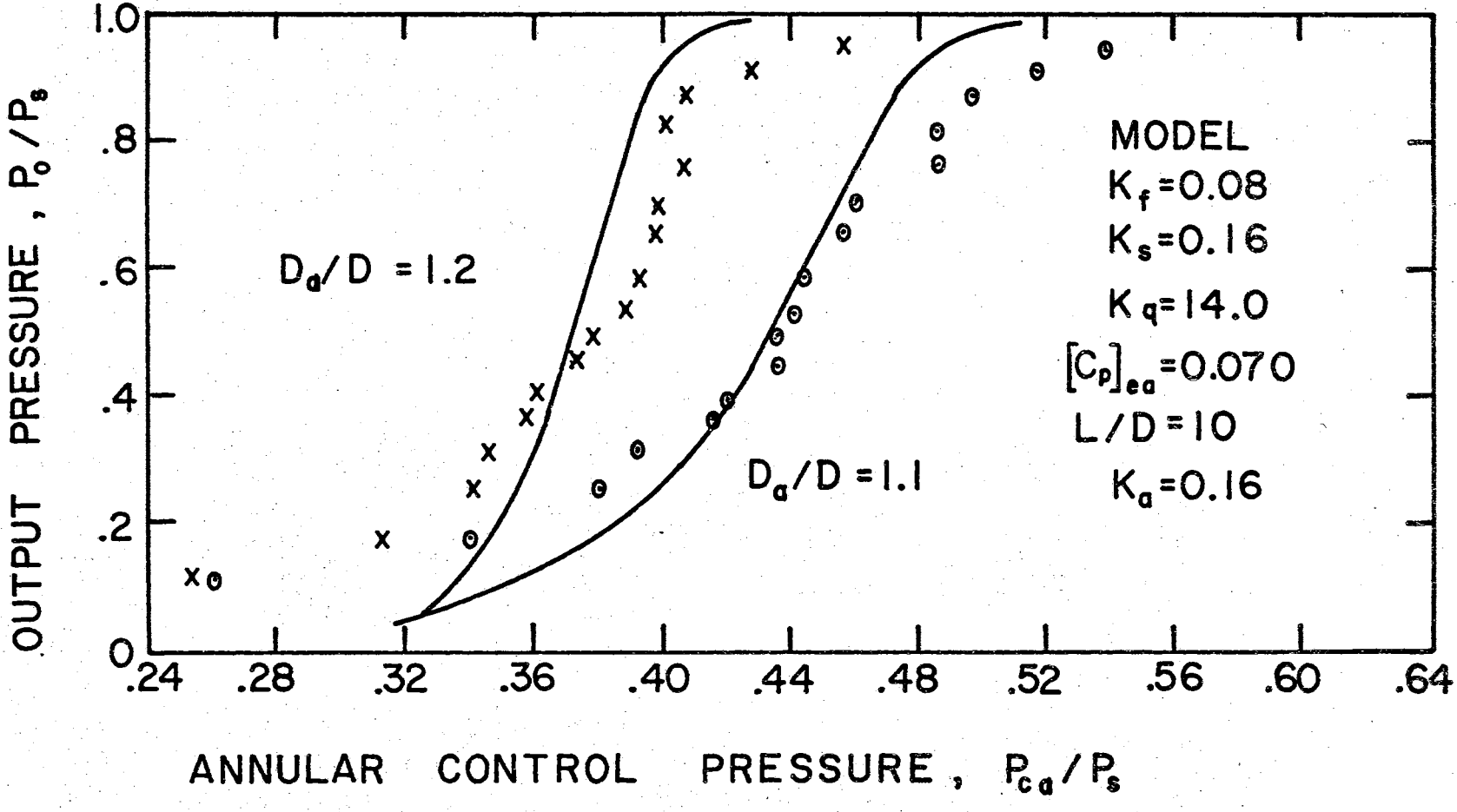

Figure 64. Direct Annular Modulator Characteristics (L/D = 10)

for the model are displaced from the experimental characteristics. To overcome this difficulty the input-output characteristics of the model are calculated with the experimental bias (Q_s/Q_m = 0.99) but the resulting model characteristics are shifted to correspond with the experimental characteristics. This shift has no effect on the shape of input-output characteristics calculated for the model.

At the nozzle spacing of six diameters (Figure 62) the model and the data are in good agreement. There is, however, a slight discrepancy in the vicinity of midrange. For the case of an eight diameter nozzle spacing (Figure 63) the predicted slope of the characteristics is higher than the data below midrange. The correspondence improves at output pressure ratios (P_O/P_s) between 0.6 and 0.8. Figure 64 shows the results at a nozzle spacing of ten diameters with annular control ratios (D_a/D) of 1.1 and 1.2. In general, the experiments confirm the prediction of higher gain for the larger control size. The detailed agreement between model and experiment at D_a/D = 1.2, however, is only fair.

A continued increase in annular control after the modulator reaches cutoff causes the modulation constant (K_a) to change sign (Figure 29). The output pressure then decreases as the control increases. This extended region is not shown on Figures 62, 63, and 64.

Transverse Modulator Characteristics

In the experimental transverse modulator, the nozzles shown in Figure 12a serve as the emitter and transverse control. The source side arrangement is the same one as in the emitter and annular experimental modulator tests (Figure 59). For the transverse modulator experiments an emitter bias pressure brings the balance near the cutoff

position. Then with the emitter pressure held constant, transverse control is applied. This has the effect of lowering source pressure. When the adjusted source pressure reaches its preselected value the flow from the source is measured. In this configuration also, the emitter acts to bias the modulator and to shift the conceptual model characteristics with respect to the experimental characteristics.

Figure 65 shows the results of the transverse modulation at nozzle spacings of four and six nozzle diameters for a control ratio (D_c/D) equal to 0.5. The model and experiment are within 15 per cent when the nozzle spacing is six diameters. However, the experimental modulator has bout twice the gain predicted by the model at a spacing of four nozzle diameters. In general, $L/D = 4$ is not a satisfactory operating condition because of instabilities in the balance position.

Discussion of Experimental Results

The experiments described in the previous sections of this chapter are difficult to perform. Part of the difficulty stems from poor regulation of the chamber pressures. This is especially critical in the 0.500 in. diameter modulators which operate with large flow rates at low pressures. In the annular and transverse modulators the results depend on the constancy of emitter pressure. A slight change causes distortion of the input-output characteristics. An appreciable change in the emitter pressure makes the experimental results meaningless.

During the experiments the emitter pressure requires continual adjustment to maintain its value. Yet it often changes again before the completion of the source pressure readjustment. This problem becomes most acute during tests at nozzle spacings of four and five

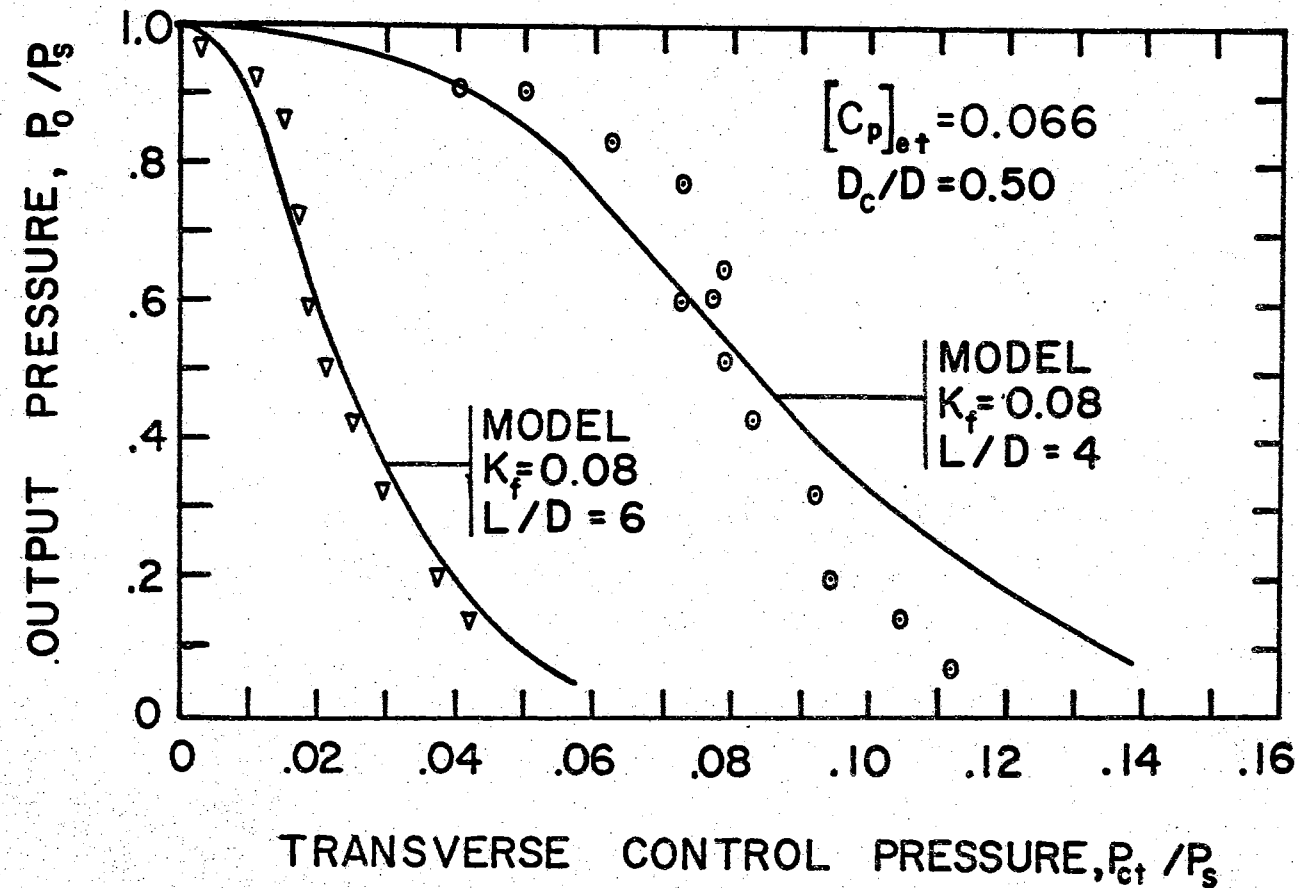

Figure 65. Transverse Modulator Characteristics

nozzle diameters. In these cases, small changes in emitter conditions result in large output pressure changes without any annular or transverse control application.

Another serious difficulty is the high amplitude of random pressure fluctuations produced in the source chamber. These fluctuations are related directly to the turbulence in the emitter jets. To obtain a better indication of source pressure, RC type filters built with passive fluid components, were placed between the output chamber and the manometer. The filters reduce the noise in the pressure reading but create another problem. They increase the response time of the measuring circuit beyond the time that the emitter pressure remains without drift. Eventually a compromise is adopted and an intermediate amount of filtering is used.

The emitter modulator test results show a significant difference between the 0.125 in. unit and the 0.500 in. unit. The emitter pressure gain of the larger unit is about three times that of the smaller unit. Although the measured plate decay factor of the 0.125 in. nozzle is 0.071 and that of the 0.500 in. nozzle is 0.066, this difference is not large enough to account for the observed effect. According to the model, the difference in plate decay factors for the two sizes should produce only a 50 per cent increase in the pressure gain rather than the 300 per cent observed.

To determine the reason for the pressure gain discrepancy, the supply chamber of the smaller nozzle (Figure 12a) is modified. The modification consists of extending the chamber by three inches and introducing the flow through a 0.125 in. tube (at the end of the extension) parallel to the nozzle axis. The measured plate decay factor

on the modified 0.125 in. nozzle is 0.059. Emitter modulation tests are performed with the modified nozzle as the emitter. These tests produce pressure gains that are about two and a half times the gains measured with the unmodified nozzle. The model (without feedback) predicts a doubling of the gain (Figure 48) when the plate decay factors are changed from 0.059 to 0.071. This is reasonably close to the experimental results on the 0.125 in. modulator. According to the model the gain of the modified unit should have exceeded that of the larger unit because of a smaller decay factor (0.059 to 0.066). The fact that the larger unit still has higher gain leads to the conclusion that there is something else besides the plate decay factor that is different about the 0.125 in. and 0.500 in. nozzles. To account for the difference, the nozzles were tested at the same Reynold's number and then at the same exit velocity. The results, however, remain substantially unchanged.

Since the 0.125 in. diameter nozzle is too small to permit streamsurface flow modulation measurements and because the constants associated with these measurements (shape and flow constants) are low in gain sensitivity, a real (rather than assumed) difference between the feedback constants may explain the difference in the pressure gains of the two units. The feedback constant depends upon the centerline pressure stagnated on a streamsurface of varying shape. The difference between probe and flat plate measurements acts as an indication of the effects of streamsurface shape. Figure 19 shows probe-plate pressure differences on both size nozzles. The smaller nozzle presents some experimental difficulty. Originally a 0.031 in. total pressure probe was used to measure the centerline total pressure in the 0.125 in. free jet.

However, the probe cross-sectional area seemed large enough to stagnate an appreciable portion of jet fluid. As a result the measured pressures would be too high. To correct for this possibility the 0.012 in. OD. probe was used for the free jet measurements on the 0.125 in. nozzle. However, the time constant of the smaller probe was about five minutes. Thus, it was very difficult to determine the maximum pressure point of the jet profile with this probe. The probe was finally moved along the geometric centerline and this was assumed to coincide with the jet axis. Therefore, the smaller probe may produce readings that are too low. Then the differences shown in Figure 19 would be too high. Thus the possibility exists that the feedback constant is really smaller in the 0.125 in. modulator than in the 0.500 in. modulator. In Figure 61 the feedback is actually eliminated when the data comes into agreement with the model. At present, it is not known whether this conjecture is correct.

The characteristics presented here are for blocked load (Assumption No. 11). When the output supplies flow to another component, the output static pressure decreases but the output total pressure probably does not change appreciably. The loading of the output and a non-zero source impedance may combine to change the streamsurface position within the modulator. Thus the output pressure-flow characteristics will have a distinctive shape dependent upon the source impedance.

CHAPTER IX

SUMMARY AND CONCLUSIONS

The purposes of this investigation were:

1. To identify the basic fluid flow processes in impact modulators.
2. To indicate the important modulator parameters and their effect on performance.
3. To develop a generalized static model of the modulators.

The investigation began with the separation of the impact modulator into four distinct flow processes. The processes were:

1. Emitter jet modulation.
2. Submerged jet impingement.
3. Source flow modulation.
4. Energy conversion.

The turbulence intensity characteristics of the modulated emitter jet connected process no. 1 to process no. 2. Source flow connected process no. 3 to process no. 4. The interior processes (nos. 2 and 3) associated with each other through the position and shape of a hypothetical barrier, designated as the "dividing streamsurface."

Functional forms were assigned to the processes and to the position and shape of the dividing streamsurface. Then, empirical expressions replaced the functional forms. These expressions, used simultaneously, determined the characteristics of impact modulators.

An analytical formulation, continuous in both transition and fully developed regions, was presented for the axisymmetric turbulent jet with any arbitrary initial velocity profile. The formulation required the determination of a single experimental constant, called "the decay factor." Experimental data agreed well with the analytical formulation.

Annular and transverse auxiliary flows superimposed on a primary jet flow and jet impingement on a flat plate were also considered. In these cases the analytical form derived for the free jet was applied with a modified decay factor.

The introduction of annular control flow altered the turbulence intensity profiles. The profiles at the exit of the annular nozzle, contained two rings of large intensity (referred to as peaks). The relative size of the peaks influenced the magnitude of the decay factor. For annular flows less than one-third of the primary flow, the inner peak exceeded the outer peak and the decay factor decreased. At higher annular flows the outer peak exceeded the inner peak. In this range the decay factor increased as the annular flow increased.

The application of transverse control flow increased the turbulence intensity of the single peak (at the nozzle exit) closer to the control. On the opposite side the turbulence intensity peak remained unchanged. As the turbulence developed, the peaks tended to equalize at a higher level than existed without transverse control. Thus the application of transverse control resulted in an increase in decay factor. At low force ratios (auxiliary to primary force less than 0.08) the change in decay factor for a given change in force ratio was three times larger with transverse flow than with annular flow. However, at higher force ratios the influence of transverse and annular flow was about equal.

When the jet impinged on a flat plate the decay factor, calculated from pressure measurements on the plate, was reduced. This observation suggested an hypothesis that linked the decay factor to the shape of the impingement surface. Concave shapes were assumed to yield smaller decay factors than convex shapes.

The centerline balance position of the dividing streamsurface was calculated from the decay factors for an impinging jet, with and without control flows. Another streamsurface position, the curtain position, was measured along a line parallel to the jet axis but displaced a distance of one nozzle radius. In this investigation only the centerline and curtain positions represented the position and shape of the dividing streamsurface. The shape was a function of the effective decay factor but the effective decay factor depended on the shape. Thus a feedback circuit was required in the model to describe the connection provided by the dividing streamsurface.

The input-output characteristics and the pressure gains of impact modulators depended upon the following eight parameters:

1. Nozzle spacing. In emitter modulation the pressure gain increased when the nozzle spacing decreased. The pressure gain of transverse and annular modulators maximized at a nozzle spacing of from six to eight nozzle diameters.
2. Control size. The blocked load pressure gain increased as control size increased. However the pressure gain for cascaded transverse modulators was larger at $D_c/D = 0.5$ than at $D_c/D = 1.0$.
3. Output pressure. The pressure gains maximized slightly above midrange. However since a small change in slope was

difficult to detect, the characteristics appeared linear from an output pressure ratio (P_O/P_s) of 0.2 to 0.8.

4. Plate decay factor. The plate decay factor was the most critical parameter in the determination of impact modulator pressure gain. The gain increased when the decay factor decreased. The value of the decay factor depended on the geometry of the emitter chamber and nozzle. In general the decay factor decreased when the chamber and nozzle were designed to lower turbulence intensity.

5. Shape constant. The shape constant was associated with the relation between centerline and curtain position and was the least sensitive parameter. No attempts were made to change the shape constant in the experimental apparatus. However, if the emitter and source nozzles were unequal in diameter or were non-aligned, the constant might be changed.

6. Flow constant. The characteristics were more sensitive to the flow constant than to the shape constant. However, the flow constant had only one-third the sensitivity of the decay factor. The flow constant related the nozzle flow to the curtain distance and was analagous to a discharge coefficient. Although the flow constant was not changed in this investigation, the geometric changes suggested for the shape constant or enlargement of the source nozzle face would affect it.

7. Feedback constant. The feedback constant was also a sensitive parameter. It provided a correction to the plate decay factor to account for the changing shape of the impingement surface. In this investigation the magnitude of the constant was

assumed at a value sufficient to bring the model and experimental data into correspondence. Since experiments on emitter modulators with 0.125 in. diameter nozzles had only one-third of the pressure gain of similar experiments on 0.500 in. diameter nozzles, the feedback constant might depend on nozzle size.

8. Modulation constant. The modulation constant represented the effect of control flow on the emitter jet. To increase gain or fan-out for transverse modulators the control should be designated to generate as much turbulence intensity as possible. In annular modulation the constant changed sign at high control pressures. Thus positive or negative gains were possible in annular modulation.

A conceptual model for both direct and transverse impact modulators has been presented. The agreement obtained between the model and the measured characteristics was generally good considering the complexity of the processes involved. Since the experiments were performed on only two idealized impact modulators it was difficult to assess the adequacy of the model. An error or misconception in one of the processes could conceal a compensating error in another process. The problem was further complicated because the feedback process, which had such a large effect on the results, was the one about which the least was known.

Several interesting observations follow from this investigation. First, the impact position is located very close to the source nozzle. Thus the modulators are operated with one jet and one obstructed flow rather than with two impacting jets. Studies on impacting jets, therefore, are unlikely to be useful in describing impact modulators. In

addition, impact modulators are a type of "turbulence amplifier." They do not depend on the transition from laminar to turbulent flow but operate instead by changing the turbulence intensity characteristics of a jet. For this reason the output of an impact modulator may respond to appropriate acoustic signals at the input.

Recommendations for Further Study

1. Streamsurface Shape Measurements. In this investigation the measurement of centerline and curtain distances were made by traversing a pressure probe between the source nozzle and an emitter nozzle with a plate decay factor, C_p, of 0.066. Additional streamsurface measurements to obtain the streamsurface shape for emitter nozzles with different plate decay factors would be valuable.
2. Loading Effects. This investigation considered only blocked loads. The model should be extended to account for the effects of loading.
3. Decay Factor Studies. The parameter with the highest gain sensitivity was the plate decay factor. The model developed here indicated that pressure gain and, therefore, fanout can be increased by reducing the value of the plate decay factor. Studies to determine the emitter nozzle and chamber shapes required to decrease decay factor could lead to improved modulator performance.
4. Jet Impingement on Curved Surface. The model presented here required an hypothesis of the effects of streamsurface shape on the decay of the impinging jet. An additional investigation

is necessary to test the hypothesis on curved surfaces that are representative of dividing streamsurface shapes.

BIBLIOGRAPHY

1. Bjornsen, B. G. "The Impact Modulator." Proceedings of the HDL Fluid Amplification Symposium, Vol. II (May 1964).

2. Lechner, T., Jr., and P. H. Sorenson. "Some Properties and Applications of Direct and Transverse Impact Modulators." Proceedings of the HDL Fluid Amplification Symposium, Vol. II (May 1964).

3. Misevich, K. W. "The Impact of Opposing Axially Symmetric Jets." ASME publication, Advances in Fluidics (May 1967).

4. Katz, S. "Pressure Gain Analysis of an Impacting Jet Amplifier." ASME publication, Advances in Fluidics (May 1967).

5. Desai, P. V., and R. W. McGregor. "Parametric Considerations in the Design of a Fluidic Direct Impact Modulator." ASME paper 69-FLCS-38 (June 1969).

6. Fenger, N. P. "Some Experimental and Theoretical Investigations of the Axial Impingement of Two Axisymmetric Jets." Fourth Cranfield Fluidics Conference, British Hydromechanics Research Association, Paper P-1 (March 1970).

7. Schlicting, H. Boundary Layer Theory. New York: McGraw-Hill Book Company.

8. Albertson, M. S., Y. B. Dai, R. A. Jensen, and H. Rouse. "Diffusion of Submerged Jets." Proceedings ASCE, Vol. 74 (December 1948), p. 571.

9. Alexander, L. G., T. Baron, and E. W. Comings. "Transport of Momentum, Mass and Heat in Turbulent Jets." University of Illinois Engineering Experiment Station, Bulletin No. 413 (1953).

10. Kirshner, J. M. "Jet Flows." Fluidics Quarterly, Vol. I. No. 3.

11. Abramovich, G. N. The Theory of Turbulent Jets. The MIT Press, 1963.

12. Corrsin, S. "Investigation of Flow in an Axially Symmetrical Heated Jet of Air." NACA, WTR W-94 (December 1943).

13. LeClerc, A. "Deviation D'Un Jet Liquide Par Une Plaque Normale A Son Axe." LaHouille Blanche, Vol. 5 (1950), p. 816.

14. Schack, W. "Umlenking Eines Keisformigen Flussigkeitsstrahles An Einer Ebenen Platte Senkrecht Zur Stromungsrichtung." Ingenieur-Archiv (Berlin), Vol. 6 (1936), pp. 51-58.

15. Snedeker, R. S., and C. DuP. Donaldson. "Experiments on Free and Impinging Underexpanded Jets From a Convergent Nozzle." Aeronautical Research Associates, Report No. 63, DDC No. AD 461622 (September 1964).

16. Reid, K. N. "Static and Dynamic Interaction of a Fluid Jet and a Receiver-Diffuser." (Unpub. ScD. Thesis, Massachusetts Institute of Technology, September 1964.)

17. Boyd, M. A., and A. R. Barbin. "Effects of Transverse Secondary Flow on the Laminar-Turbulent Transition of a Free Axisymmetric Jet." ASME publication, Advances in Fluidics (May 1967).

18. Douglas, J. F., and R. S. Neve. "Investigation Into The Behavior of a Jet Deflection Proportional Amplifier." Paper C-3 Second Cranfield Conference (January 1967).

19. Render, A. B. "The Design of Jet Interaction Amplifiers Using Super Critical Pressure Ratios." Paper C-2 Second Cranfield Conference (January 1967).

20. Kirshner, J. M. "Fluerics 1. Basic Principles." HDL TR-1418 (November 1968).

APPENDIX A

ANGULAR DISPLACEMENT OF EMITTER NOZZLE

When a "two-dimensional" jet between plates (confined jet) is deflected by a perpendicular control jet, Douglas and Neve (18), and Render (19) show that the velocity profiles are displaced without an appreciable change in peak velocity (Figure 66a). This pattern continues until the ratio of control jet to primary jet pressure reaches 0.30. For the two dimensional jet, the effect of jet deflection is approximately the same as the effect of a mechanical angular displacement of the jet nozzle. However, when an axisymmetric jet, is deflected by another axisymmetric jet, Kirshner (20) recognizes that the result is an increase in jet spread as well as a displacement of the profile (Figure 66b). This effect was shown experimentally in the test results of Figure 34. For axisymmetric jets, then, the results of jet deflection and mechanical angular displacement are not the same.

To isolate the effect of axisymmetric jet deflection without a change in peak velocity, some experiments are performed with mechanical angular displacements of the nozzle. A schematic drawing of the test set-up for these experiments is shown in Figure 67. Two test arrangements are used. In one, Figure 67a, the axes of the emitter and source nozzles are initially parallel but may be offset. In the other, Figure 67b, the axes are initially oblique. The oblique angle is designated as β. At the beginning of a test with either parallel or

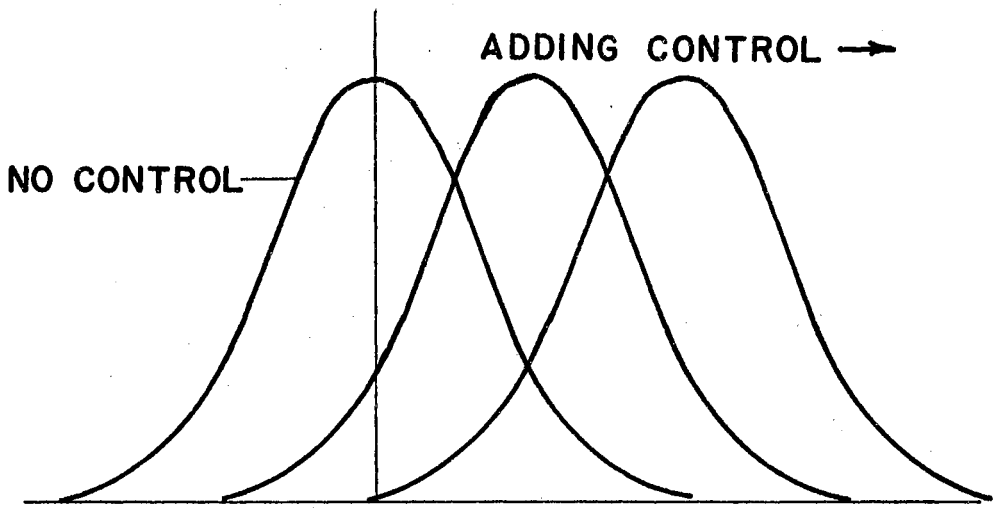

a) TWO DIMENSIONAL

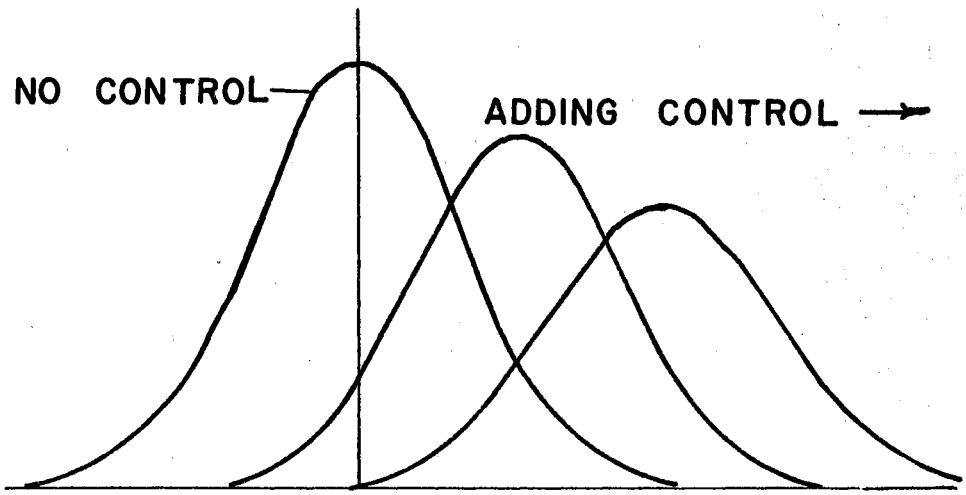

b) AXISYMMETRIC

Figure 66. Velocity Profiles for Two Dimensional and Axisymmetric Jets Subject to Transverse Control

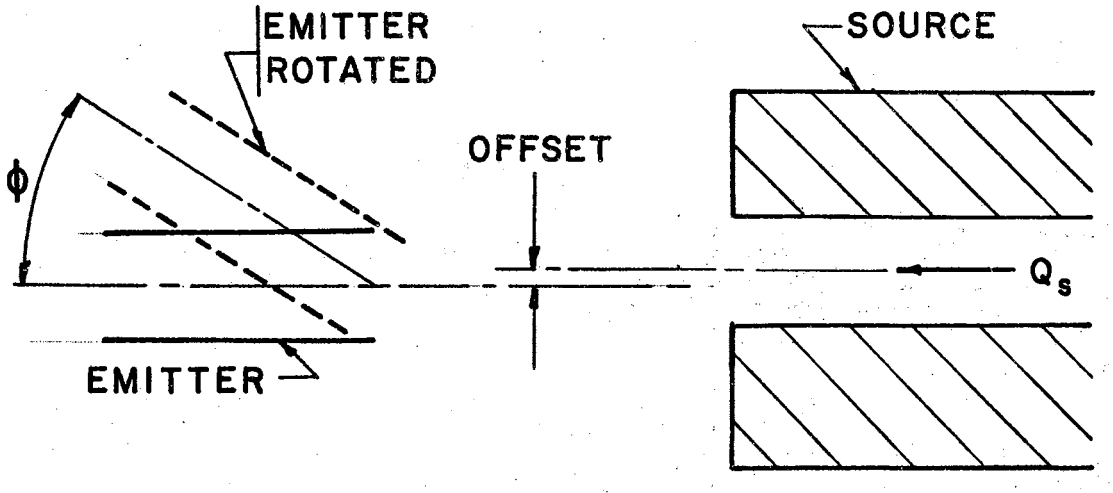

a) PARALLEL AXES

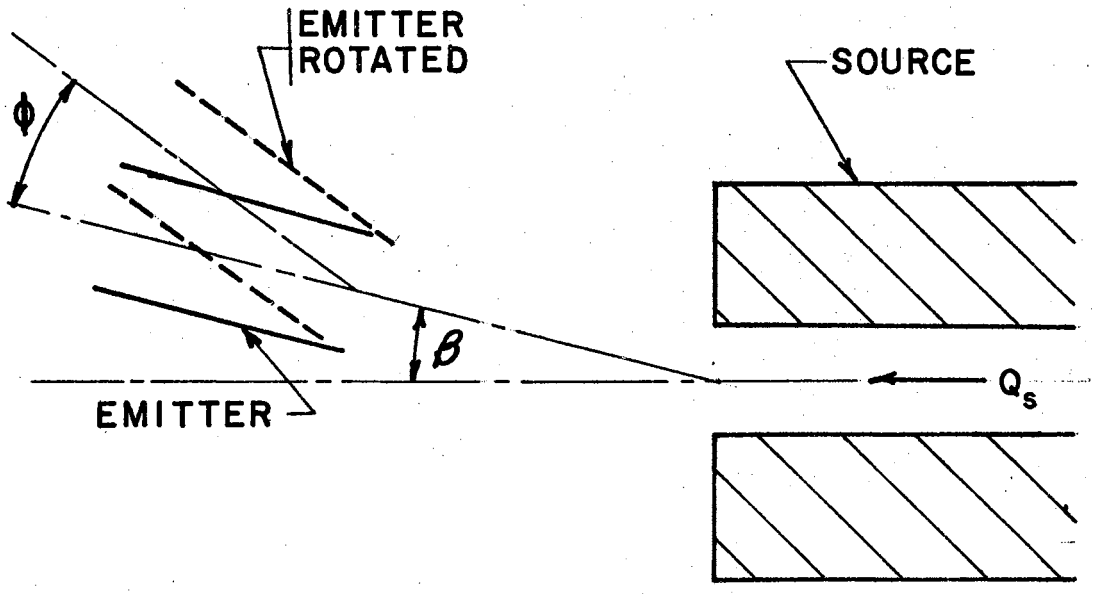

b) OBLIQUE AXES

Figure 67. Test Arrangements for Angular Displacement Experiments

oblique nozzles the angular displacement, φ is zero. The emitter pressure is adjusted until the source flow is cutoff for a preselected source pressure. Then the tests are performed by rotating the emitter nozzle in small angular increments about its initial position. At each increment, the emitter and source pressure are readjusted to their original values and the source flow is measured. An equivalent output pressure is calculated from the source flow by using Equation (30).

Figure 68 shows the relation between output pressure ratio and displacement angle, φ, for various values of nozzle spacing. When the spacing is five nozzle diameters, an angular displacement of three degrees is required to lower the output pressure ratio to 0.99. As the spacing increases the output pressure begins to decrease at smaller angular displacements. In addition the slope of the characteristics at midrange increases as the spacing increases. The output in all cases, however, is relative insensitive to the angular displacement. For example, a displacement angle of about 11 degrees reduces the output pressure ratio to 0.1. However, the jet deflection angle for a transverse modulator is only about two degrees when the output pressure ratio is 0.1.

The characteristics shown in Figure 68 shift if the source and emitter axes are offset. Figure 69 shows the displacement characteristics at a nozzle spacing of five diameters with and without offset. An offset of 0.315 D shifts the characteristic by about three degrees but has no effect on the characteristic shape. Additional pressure gain is attainable when angular displacement is used in conjunction with offset axes. However, the contribution of jet displacement would still be rather small.

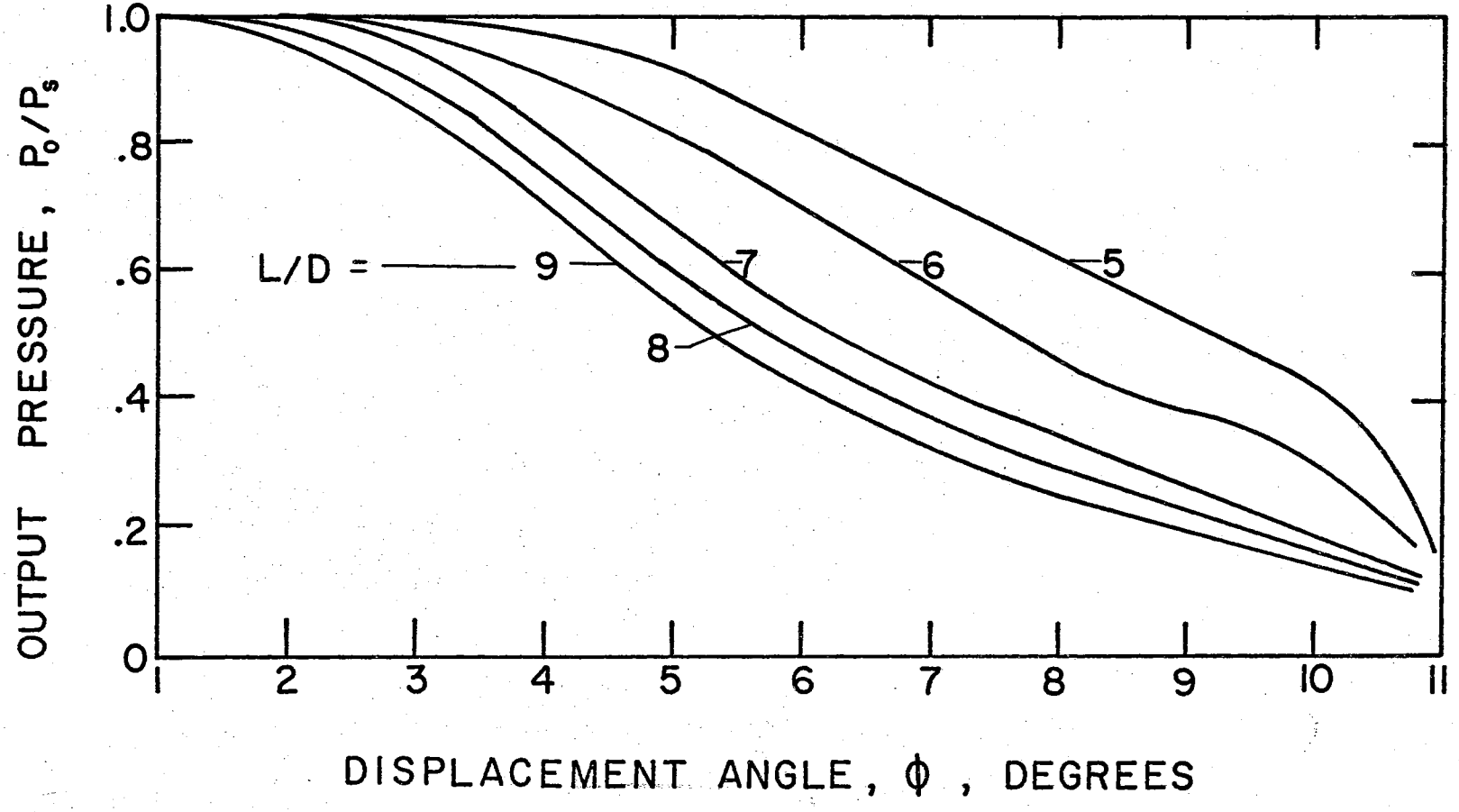

Figure 68. Angular Displacement Characteristics for Various Spacings

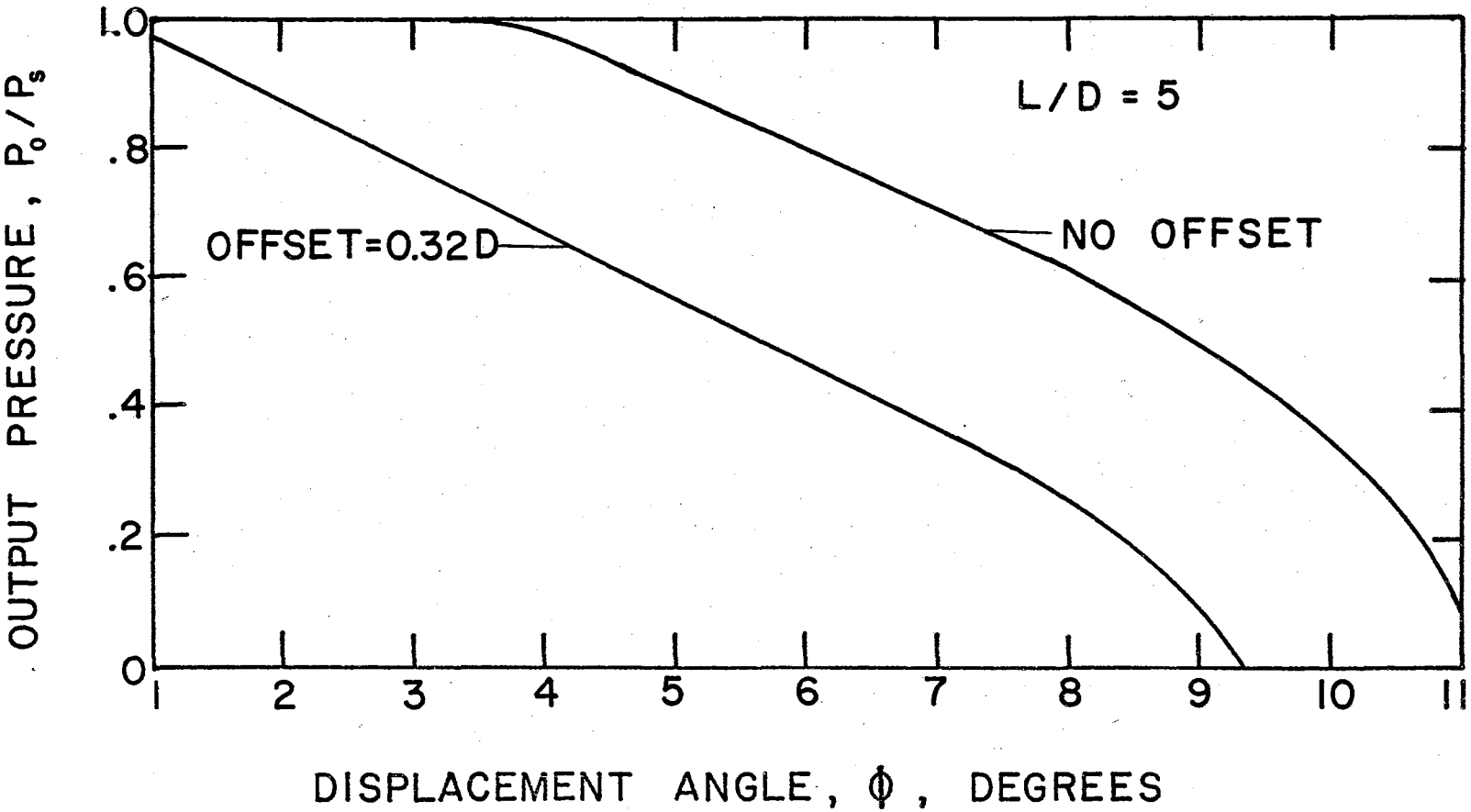

Figure 69. The Effect of Offset on the Angular Displacement Characteristics

The displacement characteristics of oblique jets are shown in Figure 70. For oblique angles greater than about 15 degrees the characteristics are stable. The slope of the characteristics maximizes at about 15 degrees and has twice the slope of the parallel jets ($\beta = 0$). Therefore, transverse modulators with oblique and offset (emitter and source) jets, would have about ten per cent higher pressure gains. At oblique angles less than 15 degrees some bistable effects are produced. These bistabilities are explained with the aide of Figure 71. Figure 71a indicates the rotation of initially aligned jets. The dividing streamsurface distorts with an increase in angular displacement. The streamsurface blocks fluid from one side of the nozzle and allows flow from the other side. When the oblique angle is greater than 15 degrees or thereabouts (Figure 71b) the angular displacement causes the dividing streamsurface to pass flow all around the source nozzle. This is the reason for the increased slope shown in Figure 70 for the oblique cases. Where the initial oblique angle is between 0 and 15 degrees, the characteristic curve follows the aligned characteristic and then suddenly changes to the oblique characteristic. In this case the streamsurface changes from the mode shown in Figure 71a to that shown in Figure 71b.

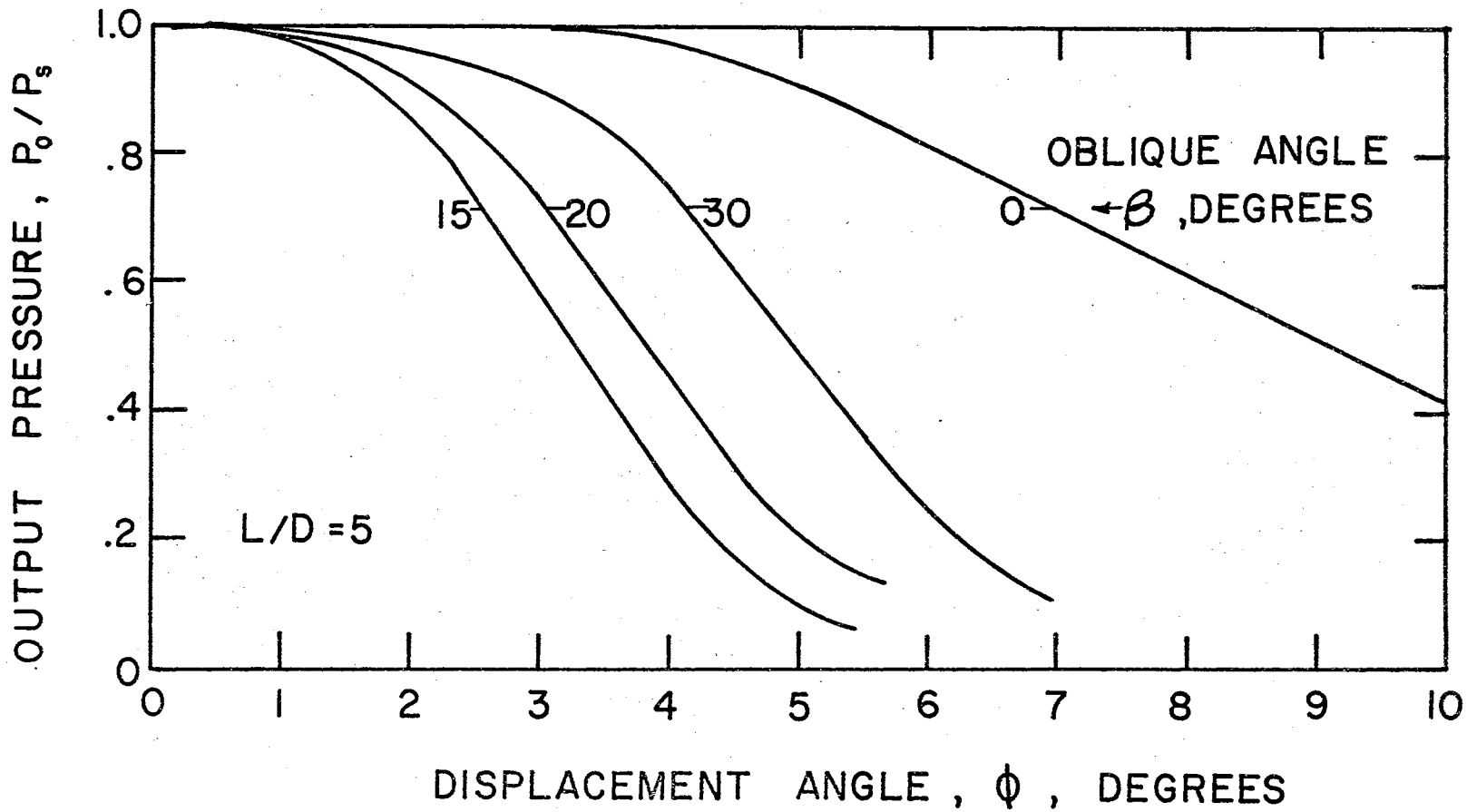

Figure 70. The Effect of Oblique Axes on the Annular Displacement Characteristics

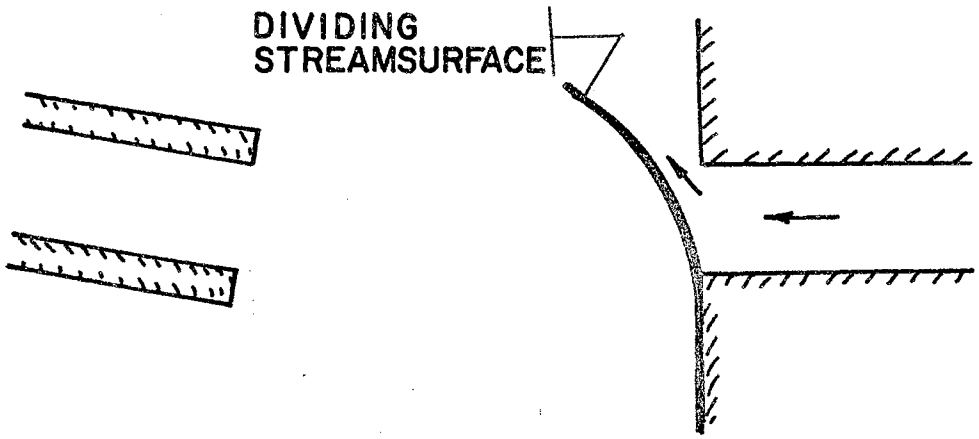

a) PARTIAL BLOCKAGE

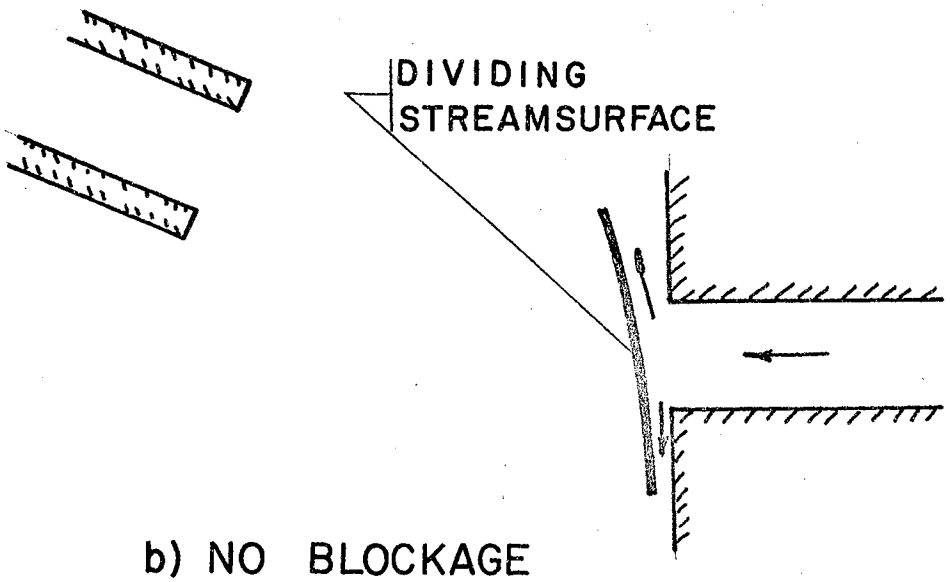

b) NO BLOCKAGE

Figure 71. Modes of Source Flow Discharge

APPENDIX B

DATA

The data presented in this investigation are given in Tables II through XXIV.

TABLE II

FREE JET CENTERLINE TOTAL PRESSURE DISTRIBUTION

	0.125 in. Diameter		0.500 in. Diameter	
X/D	P, in. H_2O	P/P_n	P, in. H_2O	P/P_n
0	10.08	1.000	7.48	1.000
4	9.15	.907	7.05	.943
5	7.89	.783	6.40	.856
6	6.62	.656	5.50	.735
7	5.45	.540	4.58	.612
8	4.50	.446	3.82	.511
9	3.70	.367	3.10	.415
10	3.10	.307	2.63	.352

Source: Figure 13.

TABLE III

FREE JET VELOCITY PROFILES

	X/D = 2		X/D = 6		X/D = 10	
r/D	P, in. H_2O	u/U_o	P, in. H_2O	u/U_o	P, in. H_2O	u/U_o
0	7.49	1.000	5.50	.858	2.60	.588
0.1	7.50	1.000	5.15	.826	2.51	.575
0.2	7.44	.995	4.54	.787	2.33	.557
0.3	7.04	.967	3.77	.710	2.11	.530
0.4	5.59	.862	2.97	.628	1.84	.478
0.5	3.20	.653	2.26	.549	1.57	.458
0.6	1.31	.418	1.64	.467	1.32	.419
0.7	0.38	.226	1.15	.391	1.09	.380
0.8	0.04	.077	0.77	.321	0.89	.345
0.9	0.00	.000	0.50	.247	0.71	.308
1.0	0.00	.000	0.30	.200	0.55	.270
1.1	0.00	.000	0.16	.145	0.43	.238
1.2	0.00	.000	0.09	.110	0.32	.205
1.3	0.00	.000	0.00	.000	0.23	.173
1.4	0.00	.000	0.00	.000	0.16	.145

Source: Figure 14.

TABLE IV

CENTERLINE TOTAL PRESSURE DISTRIBUTION ON FLAT PLATE

	0.125 in. Diameter		0.500 in. Diameter	
X/D	P_p, in. H_2O	P_p/P_n	P_p, in. H_2O	P_p/P_n
0	20.00	1.000	7.48	1.000
4	18.65	.933	7.26	.970
5	17.25	.863	6.84	.914
6	15.22	.761	6.10	.816
7	12.98	.649	5.24	.700
8	10.83	.542	4.39	.587
9	9.08	.454	3.64	.487
10	7.68	.384	3.01	.402

Source: Figures 17 and 18.

TABLE V

THE EFFECT OF EMITTER PRESSURE ON PLATE DECAY FACTOR

	0.125 in. Diameter					0.500 in. Diameter			
	P_e in. H_2O psig					in. H_2O psig			
X/D	4	10	20	1	2	4	10	20	1
0	4.10	10.13	20.00	1.00	1.98	4.09	10.06	20.50	1.00
4	3.92	9.50	18.65	.94	1.88	3.98	9.80	19.55	.98
5	3.63	8.80	17.25	.84	1.76	3.75	9.16	18.26	.93
6	3.18	7.74	15.22	.74	1.55	3.38	8.15	16.20	.82
7	2.69	6.63	12.98	.61	1.29	2.96	7.02	13.95	.68
8	2.28	5.58	10.83	.52	1.09	2.50	5.98	11.75	.57
9	1.93	4.69	9.08	.43	.90	2.15	4.95	9.79	.46
10	1.62	3.97	7.68	.36	.75	1.85	4.25	8.25	.40
C_p	.0696	.0704	.0712	.0738	.0706	.0641	.0664	.0685	.0681

Source: Figure 23.

TABLE VI

HOT WIRE MEASUREMENTS ON ANNULAR NOZZLE

	X/D = 0.125					
	P_{ca} = 0		P_{ca} = 2 in. H_2O		P_{ca} = 4 in. H_2O	
r/D	u, volts	$\sqrt{\overline{u'^2}}$, mv	u, volts	$\sqrt{\overline{u'^2}}$, mv	u, volts	$\sqrt{\overline{u'^2}}$, mv
0	7.05	270	7.00	210	6.96	153
.20	7.13	270	7.16	215	7.06	161
.40	6.85	425	6.50	425	6.35	323
.41	6.75	462	6.32	450	6.20	313
.42	6.58	500	6.12	475	6.15	305
.43	6.35	530	5.85	476	6.05	291
.44	6.20	560	5.70	473	6.07	285
.46	5.65	625	5.35	448	6.00	270
.48	5.10	668	5.00	408	5.90	260
.50	4.10	695	4.60	340	5.75	280
.52	3.30	680	4.35	288	5.60	343
.54	2.62	625	4.18	275	5.38	433
.56	2.00	550	3.94	310	4.90	580
.58	1.48	491	3.55	400	4.22	690
.60	0.88	363	2.63	510	3.82	725
.62	0.48	253	1.55	442	1.65	570
.64	0.24	155	0.63	250	0.69	310
.66	0.00	0	0.22	124	0.28	148

1 volt = 25 ft/sec.

Source: Figures 25 and 26.

TABLE VII

HOT WIRE MEASUREMENTS ON ANNULAR NOZZLE

	X/D = 2.0					
	P_{ca} = 0		P_{ca} = 2 in H_2O		P_{ca} = 4 in. H_2O	
r/D	u, volts	$\sqrt{\overline{u'^2}}$, mv	u, volts	$\sqrt{\overline{u'^2}}$, mv	u, volts	$\sqrt{\overline{u'^2}}$, mv
0	6.85	362	6.92	230	6.95	153
.10	6.88	400	6.95	260	6.95	---
.20	6.70	490	6.80	379	6.95	286
.30	6.15	645	6.10	580	6.57	480
.35	5.72	720	5.70	645	5.78	695
.40	5.08	770	5.08	715	4.65	780
.45	4.43	790	4.45	720	4.16	785
.50	3.69	780	3.72	700	3.60	770
.55	3.03	735	3.20	660	3.20	740
.60	2.39	650	2.50	600	2.70	700
.65	1.78	560	2.06	535	2.20	640
.70	1.25	461	1.55	452	1.75	570
.75	0.86	350	1.15	370	1.35	495
.80	0.54	260	0.70	280	1.00	400
.85	0.32	180	0.45	210	0.65	320
.90	0.16	118	0.25	142	--	---

1 volt = 25 ft/sec

Source: Figure 27.

TABLE VIII

THE EFFECT OF ANNULAR CONTROL ON CENTERLINE PLATE PRESSURE DISTRIBUTION

	D_a = 0.550 in., S = 0.125 in.										
	P_{ca}, in. H_2O										
X/D	0	0.5	1.0	1.5	2.0	2.5	3.0	3.5	4.0	4.5	5.0
0	6.60	6.60	6.60	6.60	6.60	6.60	6.60	6.60	6.60	6.60	6.60
4	6.14	6.21	6.30	6.30	6.31	6.30	6.30	6.28	6.14	6.08	5.86
5	5.76	5.84	6.02	6.07	6.15	6.15	6.11	5.91	5.56	5.24	5.00
6	5.04	5.21	5.43	5.58	5.77	5.82	5.62	5.22	4.74	4.40	4.06
7	4.30	4.42	4.61	4.85	5.11	5.18	5.01	4.45	3.94	3.58	3.26
8	3.54	3.70	3.89	4.17	4.42	4.45	4.24	3.78	3.30	2.90	2.67
9	2.86	2.98	3.22	3.40	3.64	3.64	3.50	3.07	2.75	2.44	2.23
10	2.38	2.50	2.61	2.80	3.03	3.08	2.88	2.54	2.30	2.04	1.88
C_p	.071	.070	.067	.065	.062	.062	.065	.072	.080	.086	.092
	D_a = 0.550 in., S = 0.250 in.										
0	6.60	6.60	6.60	6.60	6.60	6.60	6.60	6.60	6.60	6.60	6.60
4	6.07	6.08	6.15	6.18	6.28	6.33	6.30	6.21	6.00	5.80	5.36
5	5.64	5.68	5.81	5.90	6.02	6.09	6.05	5.68	5.31	4.86	4.40
6	4.92	5.02	5.20	5.32	5.56	5.62	5.50	5.04	4.44	3.91	3.57
7	4.12	4.20	4.42	4.60	4.86	4.96	4.84	4.24	3.68	3.18	2.85
8	3.42	3.52	3.66	3.91	4.12	4.25	4.12	3.54	3.03	2.62	2.34
9	2.84	2.90	3.06	3.22	3.44	3.56	3.46	2.90	2.47	2.16	1.92
10	2.34	2.43	2.52	2.67	2.88	2.99	2.90	2.48	2.10	1.82	1.64
C_p	.073	.073	.070	.068	.065	.064	.066	.075	.084	.094	.103

TABLE VIII (Continued)

	D_a = 0.600 in., S = 0.125 in.										
	P_{ca}, in. H_2O										
X/D	0	0.5	1.0	1.5	2.0	2.5	3.0	3.5	4.0	4.5	5.0
0	6.60	6.60	6.60	6.60	6.60	6.60	6.60	6.60	6.60	6.60	6.60
4	6.05	6.16	6.22	6.29	6.28	6.26	6.14	6.26	6.22		
5	5.69	5.93	6.08	6.11	6.08	5.98	5.90	5.78	5.58		
6	4.97	5.38	5.68	5.74	5.70	5.48	5.30	5.04	4.78		
7	4.13	4.68	5.00	5.14	5.10	4.82	4.57	4.26	3.94		
8	3.40	3.82	4.28	4.46	4.41	4.19	3.85	3.58	3.32		
9	2.79	3.22	3.58	3.71	3.73	3.50	3.20	3.00	2.74		
10	2.30	2.64	2.96	3.16	3.10	2.94	2.71	2.52	2.30		
C_p	.073	.068	.063	.062	.064	.068	.073	.078	.083		

Source: Figures 28 and 29.

TABLE IX

HOT WIRE MEASUREMENTS ON TRANSVERSE NOZZLES

	X/D = 0.250		P = 7.0 in. H_2O			
	P_{ct} = 0		P_{ct} = 1.0 in. H_2O		P_{ct} = 2.0 in. H_2O	
r/D	u, volts	$\sqrt{\bar{u}'^2}$, mv	u, volts	$\sqrt{\bar{u}'^2}$, mv	u, volts	$\sqrt{\bar{u}'^2}$, mv
-.350	7.03	125	6.76	147	6.38	315
-.370	7.03	128	6.75	172	6.30	455
-.390	7.03	133	6.72	238	6.00	670
-.400	7.03	138	6.70	275	5.80	760
-.410	7.00	145	6.65	320	5.55	850
-.420	7.00	155	6.60	385	5.25	930
-.430	7.00	180	6.40	550	4.50	1060
-.440	7.00	220	6.10	690	3.90	1060
-.450	7.00	250	5.75	780	3.35	1020
-.460	6.90	330	5.10	910	2.65	915
-.470	6.75	450	3.90	960	2.10	742
-.480	6.35	600	3.00	910	1.70	600
-.490	5.40	725	2.10	780	1.50	520
-.500	3.85	820	1.45	600	1.38	448
-.510	2.30	730	1.00	437	1.35	410
-.520	1.15	498	0.85	365	1.35	380
-.530	0.50	285	0.80	310	1.48	335
+.450	7.00	220	7.00	212	7.00	200
+.460	7.00	245	7.00	235	7.00	225
+.470	6.85	316	6.90	308	6.92	286
+.480	6.40	502	6.45	485	6.50	455
+.490	5.05	730	5.00	740	5.00	725
+.500	2.55	760	2.55	755	2.70	750
+.510	1.25	560	1.15	530	1.25	540
+.520	0.60	350	0.60	335	0.60	330
+.530	0.20	124	0.20	113	0.20	116

1 volt = 25 ft/sec

Source: Figure 30.

TABLE X

HOT WIRE TRAVERSE ACROSS TRANSVERSE CONTROL (D = .250)

	P_{ct} = 1.0 in. H_2O		P_{ct} = 2.0 in. H_2O	
r/D_c	V, volts	$\sqrt{\bar{v}'^2}$, mv	V, volts	$\sqrt{\bar{v}'^2}$, mv
.486	2.25	94	3.35	135
.491	2.12	103	3.15	151
.494	2.10	113	--	--
.496	2.00	125	2.88	180
.498	1.73	143	2.62	210
.501	0.95	149	1.17	260
.503	0.11	44	0.28	97
.506	0.01	10	0.01	17

Source: Figure 31.

TABLE XI

HOT WIRE TRAVERSE ACROSS PRIMARY NOZZLE
WITH TRANSVERSE CONTROL

X/D = 0.250, P_e = 7.0 in. H_2O

	P_{ct} = 0		P_{ct} = 1.0 in. H_2O		P_{ct} = 2.0 in. H_2O	
r/D	u, volts	$\sqrt{\bar{u}'^2}$, mv.	u, volts	$\sqrt{\bar{u}'^2}$, mv.	u, volts	$\sqrt{\bar{u}'^2}$, mv.
-.78	0.30	225	0.16	76	0.14	66
-.74	0.52	300	0.22	92	0.20	77
-.70	0.76	380	0.22	111	0.20	86
-.66	1.16	510	0.26	155	0.24	104
-.62	1.50	600	0.35	200	0.29	122
-.58	2.30	710	0.49	250	0.32	141
-.54	3.00	795	0.65	340	0.41	174
-.50	3.48	840	0.80	400	0.50	215
-.46	4.50	838	1.25	540	0.62	270
-.42	5.20	835	1.60	640	0.72	325
-.38	5.80	770	2.20	740	1.00	390
-.34	6.40	620	2.70	850	1.20	495
-.30	6.70	530	3.15	910	1.45	565
-.26	6.90	435	3.90	938	1.90	680
-.22	7.00	360	4.70	960	2.35	800
-.18	7.00	310	5.40	895	2.90	900
-.14	7.00	280	6.00	810	3.50	960
-.10	7.00	245	6.35	700	4.10	1000
-.06	7.00	260	6.68	595	4.85	980
-.02	7.00	250	6.90	465	5.50	940
+.02	7.00	248	7.00	400	6.00	850
+.06	7.00	250	7.00	342	6.50	750
+.10	7.00	250	7.00	310	6.70	655

1 volt = 25 ft/sec

Source: Figure 32.

TABLE XII

HOT WIRE TRAVERSE ACROSS PRIMARY NOZZLE
WITH TRANSVERSE CONTROL

	X/D = 4.0, P_e = 7.0 in. H_2O					
	P_{ct} = 0 in. H_2O		P_{ct} = 1.0 in. H_2O		P_{ct} = 2.0 in. H_2O	
r/D	u, volts	$\sqrt{\bar{u}'^2}$, mv.	u, volts	$\sqrt{\bar{u}'^2}$, mv.	u, volts	$\sqrt{\bar{u}'^2}$, mv.
-1.0	0.45	234	0.12	78	0.10	51
-0.9	0.88	346	0.22	132	0.13	77
-0.8	1.42	485	0.40	230	0.25	145
-0.7	2.15	610	0.72	332	0.43	230
-0.6	2.98	730	1.20	445	0.72	325
-0.5	3.95	805	1.70	560	1.10	412
-0.4	4.85	806	2.30	660	1.55	505
-0.3	5.80	700	2.95	750	2.05	605
-0.2	6.501	560	3.65	835	2.55	695
-0.1	6.80	445	4.40	865	3.10	780
0	6.90	400	5.40	852	3.75	860
0.1	6.82	422	6.10	750	4.46	900
0.2	6.65	530	6.50	625	5.10	892
0.3	6.20	635	6.40	608	5.65	835
0.4	5.40	725	5.90	680	5.90	775
0.5	4.50	775	5.12	760	5.65	775
0.6	3.60	750	4.10	780	5.00	810
0.7	----	----	3.10	710	4.20	820
0.8	----	---	2.20	600	3.20	770

1 volt = 25 ft/sec

Source: Figure 33.

TABLE XIII

HORIZONTAL AND VERTICAL TOTAL PRESSURE PROBE TRAVERSES WITH TRANSVERSE CONTROL

	X/D = 6		P_s = 7.5 in. H_2O	
	HORIZONTAL		VERTICAL	
	P_{ct} = 0	P_{ct} = 0.25 in. H_2O	P_{ct} = 0	P_{ct} = 0.25 in. H_2O
r/D	P, in. H_2O	P, in. H_2O	P, in. H_2O	P, in. H_2O
-1.4	--	--	--	0.09
-1.3	--	0.08	--	0.15
-1.2	--	0.16	--	0.26
-1.1	0.22	0.27	0.19	0.40
-1.0	0.39	0.47	0.34	0.62
-0.9	0.61	0.76	0.55	0.94
-0.8	0.94	1.14	0.86	1.25
-0.7	1.37	1.64	1.26	1.75
-0.6	1.91	2.30	1.78	2.22
-0.5	2.60	3.08	2.42	2.68
-0.4	3.35	3.80	3.17	3.19
-0.3	4.13	4.39	3.99	3.72
-0.2	4.86	4.65	4.75	4.14
-0.1	5.34	4.48	5.30	4.44
0	5.44	3.89	5.50	4.62
0.1	5.20	3.32	5.36	4.52
0.2	4.62	2.60	4.90	4.26
0.3	3.90	1.99	4.20	3.85
0.4	3.10	1.48	3.38	3.38
0.5	2.36	1.06	2.60	2.81
0.6	1.73	0.73	1.94	2.28
0.7	1.25	0.48	1.38	1.80
0.8	0.85	0.28	0.95	1.38
0.9	0.55	0.15	0.62	0.98
1.0	0.34	0.06	0.38	0.70
1.1	0.20	0.02	0.22	0.46
1.2	--	--	--	0.30

Source: Figure 34.

TABLE XIV

HOT WIRE TRAVERSE ACROSS PRIMARY NOZZLE
WITH TRANSVERSE CONTROL

	X/D = 6, P_e = 7.0 in. H_2O					
	P_{ct} = 0 in. H_2O		P_{ct} = 0.25 in. H_2O		P_{ct} = 0.9 in. H_2O	
r/D	u, volts	$\sqrt{\bar{u}'^2}$, mv.	u, volts	$\sqrt{\bar{u}'^2}$, mv.	u, volts	$\sqrt{\bar{u}'^2}$, mv.
-1.4	0.22	145	0.35	178	0.65	270
-1.3	0.45	220	0.65	263	1.00	343
-1.2	0.80	305	1.05	352	1.35	438
-1.1	1.20	400	1.42	448	1.85	540
-1.0	1.65	510	2.00	545	2.40	640
-0.9	2.25	605	2.60	652	3.05	735
-0.8	2.95	705	3.29	752	3.75	820
-0.7	3.60	795	4.02	830	4.50	875
-0.6	4.35	860	4.80	895	5.25	906
-0.5	5.10	910	5.60	920	5.80	908
-0.4	5.90	920	6.40	902	6.25	900
-0.3	6.62	900	6.90	862	6.45	885
-0.2	7.22	840	7.20	840	6.30	912
-0.1	7.64	765	7.07	968	6.00	937
0	7.80	730	6.60	926	5.45	938
0.1	7.68	770	6.02	958	4.85	917
0.2	7.25	840	5.35	952	4.25	865
0.3	6.68	905	4.65	905	3.65	803
0.4	6.00	935	4.00	850	3.05	740
0.5	5.22	920	3.37	780	2.43	660
0.6	4.45	880	2.70	695	1.96	580
0.7	3.72	815	2.12	600	1.50	480
0.8	3.00	725	1.60	510	1.05	400
0.9	2.38	625	1.15	422	0.70	312
1.0	1.75	525	0.80	335	0.45	230
1.1	1.25	420	0.50	250	----	---
1.2	0.80	320	0.28	158	----	---
1.3	0.50	225	0.15	110	----	---
1.4	0.25	150	0.10	73	----	---

1 volt = 20 ft/sec

Source: Figure 35.

TABLE XV

PLATE CENTERLINE TOTAL PRESSURES
WITH TRANSVERSE CONTROL

	D = 0.500 in., D_c/D = 0.5, P_e = 7.5 in. H_2O					
P_{ct} =	0	.4	.8	1.2	1.6	2.0 in.H_2O
X/D	P_p	P_p	P_p	P_p	P_p	P_p in.H_2O
4	7.26	7.18	6.88	6.46	6.02	5.62
5	6.84	6.60	6.00	5.38	4.88	4.43
6	6.10	5.71	4.92	4.31	3.86	3.52
7	5.24	4.75	4.08	3.53	3.13	2.84
8	4.39	4.00	3.42	2.97	2.60	2.38
9	3.64	3.36	2.85	2.47	2.21	2.01
10	3.01	2.84	2.42	2.10	1.90	1.77
C_p	.066	.071	.080	.088	.095	.105
	D_c/D = 1.0					
P_{ct} =	0	0.1	0.2	0.3	0.4	0.5 in.H_2O
4	7.26	7.22	7.09	7.00	6.80	6.58
5	6.85	6.74	6.49	6.10	5.70	5.31
6	6.15	5.95	5.50	5.06	4.64	4.28
7	5.22	5.02	4.64	4.20	3.78	3.43
8	4.40	4.16	3.82	3.46	3.12	2.84
9	3.67	3.56	3.19	2.91	2.63	2.39
10	3.05	2.93	2.70	2.44	2.21	2.04
C_p	.067	.069	.074	.079	.084	.090

Source: Figures 36 and 37.

TABLE XVI

PLATE CENTERLINE TOTAL PRESSURES WITH TRANSVERSE CONTROL

	D = 0.125 in.		D_c/D = 1.0	P_e = 4.0 psig
	P_{ct} = 0 in. H_2O	P_{ct} = 2 in. H_2O	P_{ct} = 4 in. H_2O	P_{ct} = 6 in. H_2O
X/D	P_p, psig	P_p, psig	P_p, psig	P_p, psig
4.32	3.66	3.54	3.23	2.90
4.72	3.60	3.40	3.02	2.68
5.04	3.50	3.26	2.81	2.44
5.35	3.41	3.07	2.60	2.23
5.66	3.30	2.89	2.40	2.03
5.98	3.18	2.71	2.20	1.85
6.30	3.01	2.53	2.01	1.67
6.61	2.86	2.36	1.85	1.56
6.93	2.72	2.21	1.71	1.43
7.25	2.56	2.08	1.60	1.32
7.57	2.41	1.92	1.50	1.23
7.88	2.28	1.80	1.40	1.15
8.19	2.15	1.67	1.31	1.09
8.50	2.02	1.57	1.23	1.03
8.82	1.90	1.49	1.15	0.99
9.13	1.79	1.40	1.10	0.92
9.92	1.54	1.21	0.95	0.77
C_p	.071	.080	.092	.105

Source: Figure 38.

TABLE XVII

STREAMSURFACE POSITION

L/D = 5			L/D = 7			L/D = 9		
Q_s/Q_m	Z(R)/D	Z(O)/D	Q_s/Q_m	Z(R)/D	Z(O)/D	Q_s/Q_m	Z(R)/D	Z(O)/D
.326	.040	----	.302	.030	----	.338	.037	----
.458	.042	----	.362	.039	----	.459	.043	----
.543	----	-.065	.413	.043	----	.579	.063	.115
.628	.061	.053	.483	.050	----	.700	.107	.349
.688	.065	----	.543	.057	.033	.820	.127	.418
.748	.090	.191	.604	.065	.131	.870	.150	.525
.808	.108	----	.664	.080	.216	.894	.192	----
.869	.128	.328	.723	.106	.250	.930	.276	----
.917	.186	----	.785	.092	.348	.954	.377	----
.941	.229	----	.845	.149	.427			
.977	.416	----	.907	.222	.584			
			.969	.309	----			

L/D = 6			L/D = 8		
.422	.032	----	.242	.014	----
.483	.039	----	.362	.028	----
.543	.043	-.065	.483	.059	----
.604	.048	.070	.604	.060	.139
.665	.060	.112	.723	.078	.273
.725	.079	----	.785	.117	.309
.787	.106	.250	.845	.128	.427
.845	.121	----	.907	.213	----
.907	.173	.467	.969	.343	----
.969	.263	----			

Source: Figures 40, 42, 44, and 45.

TABLE XVIII

AXIAL PRESSURE TRAVERSE AT r = R

Q_s/Q_m = 0.94		Q_s/Q_m = 0.73		Q_s/Q_m = 0.42	
Z,mm	P, in. H_2O	Z,mm	P, in. H_2O	Z,mm	P, in. H_2O
0.04	-0.55	0.04	2.00	0.04	3.90
0.54	0.20	0.14	2.28	0.14	3.40
1.04	2.30	0.24	3.25	0.24	3.70
1.24	3.40	0.44	4.50	0.29	3.89
1.44	4.10	0.64	5.15	0.34	3.97
1.64	4.56	0.94	5.47	0.39	4.08
1.84	4.80	1.29	5.38	0.44	4.11
2.04	5.10	1.54	5.20	0.49	4.15
2.24	5.35	2.54	3.85	0.54	4.18
2.44	5.55	4.04	2.20	0.59	4.18
2.64	5.65			0.64	4.12
2.84	5.75			0.74	4.10
3.04	5.80			1.04	3.75
3.24	5.75			1.54	3.07
3.44	5.70				
4.04	5.50				

Source: Figure 43.

TABLE XIX

DIRECT EMITTER MODULATION (D = 0.500 in.)

D = 0.500 in., P_s = 4.0 in. H_2O							
L/D = 6				L/D = 8			
P_e, in. H_2O	P_e/P_s	Q_s/Q_m	P_o/P_s	P_e, in. H_2O	P_e/P_s	Q_s/Q_m	P_o/P_s
4.74	1.185	.966	.067	6.08	1.520	.966	.067
4.75	1.188	.976	.047	6.11	1.528	.978	.044
4.79	1.198	.934	.128	6.28	1.570	.913	.166
4.80	1.200	.908	.176	6.32	1.580	.916	.161
4.82	1.205	.883	.220	6.40	1.600	.840	.294
4.84	1.210	.851	.276	6.43	1.608	.782	.389
4.85	1.213	.833	.306	6.44	1.610	.850	.277
4.86	1.215	.771	.406	6.48	1.620	.708	.499
4.87	1.218	.784	.385	6.52	1.630	.633	.599
4.88	1.220	.667	.555	6.53	1.632	.550	.697
4.89	1.223	.633	.599	6.54	1.635	.535	.714
4.90	1.225	.540	.708	6.55	1.638	.417	.826
4.91	1.228	.417	.826	6.56	1.640	.437	.809
4.92	1.230	.283	.920	6.57	1.643	.317	.900
4.93	1.233	.334	.888	6.58	1.645	.345	.881
4.96	1.240	.150	.977	6.65	1.663	.167	.972
4.98	1.245	.178	.968	6.71	1.678	.173	.970
5.08	1.270	0	1.000	6.80	1.700	0	1.000

Source: Figure 60.

TABLE XX

DIRECT EMITTER MODULATION (D = 0.125 in.)

D = 0.125 in., P_s = 2 psig

L/D = 5

P_e, psig	P_e/P_s	Q_s/Q_m	P_o/P_s
2.25	1.13	.976	.048
2.33	1.17	.928	.140
2.30	1.15	.963	.073
2.39	1.20	.842	.292
2.40	1.20	.724	.476
2.41	1.21	.523	.727
2.43	1.22	.325	.895
2.54	1.27	0	1.000
2.50	1.25	.140	.980

L/D = 6

P_e, psig	P_e/P_s	Q_s/Q_m	P_o/P_s
2.20	1.10	.996	.009
2.40	1.20	.989	.022
2.53	1.27	.963	.073
2.58	1.29	.929	.137
2.61	1.31	.903	.185
2.64	1.32	.858	.265
2.69	1.35	.640	.591
2.72	1.36	.401	.839
2.84	1.42	.120	.939
2.90	1.45	0	1.000

L/D = 7

P_e, psig	P_e/P_s	Q_s/Q_m	P_o/P_s
2.66	1.33	1.000	.000
2.72	1.36	.989	.022
2.85	1.43	.976	.048
2.90	1.45	.960	.080
3.01	1.51	.909	.175
3.05	1.53	.863	.255
3.12	1.56	.746	.444
3.18	1.59	.522	.728
3.26	1.63	.248	.939
3.40	1.70	.000	1.000

L/D = 8

P_e, psig	P_e/P_s	Q_s/Q_m	P_o/P_s
3.09	1.55	1.000	.000
3.33	1.67	.959	.081
3.20	1.60	.976	.048
3.51	1.76	.907	.178
3.55	1.78	.856	.268
3.62	1.81	.774	.402
3.70	1.85	.502	.748
3.83	1.92	.268	.928
4.01	2.01	.000	1.000

L/D = 9

P_e, psig	P_e/P_s	Q_s/Q_m	P_o/P_s
3.19	1.60	.906	.008
3.82	1.91	.969	.061
4.01	2.01	.937	.122
4.13	2.07	.907	.177
4.25	2.13	.829	.313
4.33	2.17	.716	.487
4.41	2.21	.493	.757
4.64	2.32	.161	.974
4.74	2.37	.000	1.000

Source: Figure 61.

TABLE XXI

DIRECT EMITTER MODULATION (D = 0.125 in.)

D = 0.125 in., P_s = 4 psig

L/D = 5

P_e, psig	P_e/P_s	Q_s/Q_m	P_o/P_s
4.37	1.09	.997	.006
4.49	1.12	.986	.028
4.55	1.14	.972	.055
4.63	1.16	.948	.101
4.73	1.18	.879	.227
4.851	1.21	.652	.575
4.92	1.23	.429	.816
4.99	1.25	.278	.923

L/D = 6

P_e, psig	P_e/P_s	Q_s/Q_m	P_o/P_s
4.50	1.13	.998	.004
4.82	1.21	.983	.034
4.93	1.23	.969	.061
5.10	1.28	.930	.135
5.16	1.29	.901	.188
5.25	1.31	.848	.281
5.37	1.34	.718	.484
5.51	1.38	.544	.704
5.64	1.41	.367	.865
5.88	1.47	.073	.995

L/D = 7

P_e, psig	P_e/P_s	Q_s/Q_m	P_o/P_s
5.06	1.27	1.000	.000
5.60	1.40	.967	.065
5.85	1.46	.938	.120
6.09	1.52	.876	.233
6.25	1.56	.791	.374
6.32	1.58	.738	.455
6.56	1.64	.493	.757
6.91	1.73	.157	.975

L/D = 8

P_e, psig	P_e/P_s	Q_s/Q_m	P_o/P_s
5.64	1.41	.995	.010
6.44	1.61	.970	.059
6.15	1.54	.982	.036
6.94	1.74	.922	.150
7.19	1.80	.860	.260
7.36	1.84	.783	.387
7.53	1.88	.691	.523
7.82	1.96	.462	.787
8.32	2.08	.105	.989

L/D = 9

P_e, psig	P_e/P_s	Q_s/Q_m	P_o/P_s
6.76	1.69	.987	.026
7.39	1.85	.974	.051
7.85	1.96	.948	.101
8.14	2.04	.917	.159
8.32	2.08	.888	.211
8.62	2.16	.809	.346
8.85	2.21	.702	.507
9.10	2.28	.519	.731
9.50	2.38	.210	.956

Source: Figure 61.

TABLE XXII

DIRECT ANNULAR MODULATION

P_s = 5.0 in. H_2O

L/D = 6, P_e = 6.4 in. H_2O				L/D = 8, P_e = 8.6 in. H_2O			
	D_a/D = 1.1						
P_{ca}, in. H_2O	P_{ca}/P_s	Q_s/Q_m	P_o/P_s	P_{ca}, in. H_2O	P_{ca}/P_s	Q_s/Q_m	P_o/P_s
0	.000	1.000	.000	0	0	1.000	.000
0.14	.028	.957	.085	0.35	.070	.970	.060
0.25	.050	.927	.140	0.43	.086	.957	.085
0.35	.070	.897	.196	0.58	.116	.927	.140
0.45	.090	.856	.268	0.66	.132	.897	.196
0.50	.100	.813	.340	0.76	.152	.856	.268
0.53	.106	.787	.381	0.84	.168	.813	.340
0.58	.116	.767	.412	0.87	.174	.787	.381
0.63	.126	.720	.482	0.90	.180	.767	.412
0.65	.130	.683	.534	0.93	.186	.720	.482
0.66	.132	.658	.567	0.98	.196	.683	.534
0.69	.138	.608	.630	1.02	.204	.658	.567
0.70	.140	.535	.714	1.07	.214	.608	.630
0.72	.144	.478	.772	1.10	.220	.535	.714
0.76	.152	.421	.823	1.12	.224	.478	.772
0.80	.160	.366	.866	1.17	.234	.421	.823
0.83	.166	.311	.903	1.21	.242	.366	.866
0.92	.184	.206	.958	1.40	.280	.206	.958
1.20	.240	.102	.990	1.58	.316	.102	.990
0.16	.032	.957	.085				
0.14	.028	.970	.060				
0.47	.094	.842	.291				
0.51	.102	.774	.401				
0.58	.116	.696	.515				
0.68	.136	.634	.598				
0.70	.140	.571	.674				
0.74	.148	.512	.738				
0.80	.160	.399	.841				

Source: Figures 62, and 63.

TABLE XXIII

DIRECT ANNULAR MODULATION

L/D = 10, P_s = 3.5 in. H_2O, P_a = 8.9 in. H_2O							
D_a/D = 1.1				D_a/D = 1.2			
P_{ca}, in. H_2O	P_{ca}/P_s	Q_s/Q_m	P_o/P_s	P_{ca}, in. H_2O	P_{ca}/P_s	Q_s/Q_m	P_o/P_s
0.60	.171	.971	.056	0.65	.187	.971	.056
0.91	.260	.940	.115	0.89	.254	.940	.115
1.19	.340	.908	.175	1.09	.312	.908	.175
1.33	.380	.864	.255	1.19	.340	.864	.255
1.37	.392	.830	.311	1.21	.346	.830	.311
1.45	.415	.80.	.358	1.25	.358	.801	.358
1.47	.420	.777	.396	1.26	.360	.777	.396
1.52	.435	.745	.445	1.30	.372	.745	.445
1.52	.435	.714	.490	1.32	.378	.714	.490
1.54	.440	.688	.527	1.36	.389	.688	.527
1.55	.443	.646	.583	1.37	.392	.646	.583
1.60	.457	.591	.651	1.38	.395	.591	.651
1.61	.460	.551	.696	1.38	.395	.551	.696
1.70	.486	.486	.764	1.43	.409	.486	.764
1.70	.486	.423	.821	1.40	.400	.423	.821
1.74	.497	.359	.871	1.42	.406	.359	.871
1.80	.515	.297	.912	1.49	.426	.297	.912
1.88	.538	.236	.944	1.60	.457	.236	.944
2.11	.603	.118	.986	1.84	.526	.118	.986

Source: Figure 64.

TABLE XXIV

TRANSVERSE MODULATOR CHARACTERISTICS

P_s = 7.5 in. H_2O, D_c/D = 0.500

L/D = 4, P_e = 7.90 in. H_2O				L/D = 6, P_e = 9.50 in. H_2O			
P_{ct}, in. H_2O	P_{ct}/P_s	Q_s/Q_m	P_o/P_s	P_{ct}, in. H_2O	P_{ct}/P_s	Q_s/Q_m	P_o/P_s
.66	.088	.930	.136	.440	.059	.930	.136
.56	.075	.863	.256	.370	.049	.863	.256
.49	.065	.800	.360	.330	.044	.800	.360
.48	.064	.740	.453	.310	.041	.740	.453
.47	.063	.684	.533	.300	.040	.684	.533
.44	.059	.629	.604	.285	.038	.629	.604
.43	.057	.576	.668	.270	.036	.524	.726
.43	.057	.524	.726	.240	.032	.428	.813
.42	.056	.476	.774	.200	.027	.336	.887
.41	.055	.428	.813	.160	.021	.249	.938
.41	.055	.382	.854	.080	.011	.164	.973
.41	.055	.336	.887				
.37	.049	.249	.938				
.33	.044	.164	.973				
.26	.035	.081	.993				
.17	.023	0	1.000				
.41	.055	.428	.813				
.41	.055	.336	.887				

Source: Figure 65

VITA

Silas Katz

Candidate for the Degree of

Doctor of Philosophy

Thesis: A STATIC MODEL OF DIRECT AND TRANSVERSE IMPACT MODULATORS

Major Field: Engineering

Biographical:

Personal Data: Born in The Bronx, New York, August 20, 1924, the son of Charles and Rose Katz.

Education: Graduated from Erasmus Hall High School, Brooklyn, New York, in January, 1942; received the Bachelor of Mechanical Engineering degree from the City College of New York, January, 1949; received the Master of Science degree from the University of Maryland with a major in Mechanical Engineering in June, 1957; completed requirements for the Doctor of Philosophy degree at Oklahoma State University in July, 1970.

Professional Experience: Aviation Machinist's Mate 3/C, U.S. Navy, 1943-46; Engineering Draftsman, Public Buildings Service, General Services Administration, 1949-52; Mechanical Engineer, National Bureau of Standards, 1952-57; Research Mechanical Engineer, Harry Diamond Laboratories, Army Material Command, 1957-69; Research Associate in Mechanical Engineering, Oklahoma State University, 1969-70.

Professional Organizations: Associate Member American Society of Mechanical Engineers, Phi Kappa Phi.